ABSTRACT

PRITCHARD, EWAN GARETH DAVID. Torque Converter Interactions in a Parallel Post Transmission Hybrid Driveline. (Under the direction of Dr. Richard Gould and Dr. Richard R. Johnson).

Based on the work of both NC State University and independent non-profit Advanced Energy, a group of 15 plug-in hybrid school buses were constructed to determine basic performance characteristics and improve upon the design. This project was a joint effort with the IC Bus division of Navistar and the many school districts participating in the program. The buses have been in operation for up to four years as of the writing of this paper. The performance of the buses is better than traditional buses in terms of fuel economy and emissions, but not as favorable as originally predicted in ADVISOR modeling.

There are a variety of reasons for this discrepancy in the performance, some of which were addressed in subsequent design iterations of the buses, such as decreasing final drive ratios and adjusting the capture of regenerative energy. Some other discrepancies remain unexplained. The basic design of the buses uses a parallel post transmission hybrid system. This design has been proposed in a number of retrofit situations and therefore has application across a wide variety of platforms. The current work looks at the energy lost to drag in the torque converter by extending existing models to a more general case and adding models of the overrunning regime. In this study, a majority of the emphasis is on creating an adequate model of the performance of a torque converter

in the negative torque state without the application of lookup tables, which require specific torque converter testing.

An automatic transmission has a hydraulic torque converter with a complex flow that aids the vehicle by multiplying torque at low speed from the combustion engine and facilitates idling of the engine while the vehicle is not moving. From 1960 to 1990, the torque converter was studied and modeled in great detail, but in each case, no modeling was conducted in the overrunning regime, where the speed of the turbine exceeds the speed of the impeller. Throughout the late 1990s and 2000's, several drivelines have been built which use a parallel post transmission hybrid system. There is a high percentage of time where the electric motor is the prime mover of the vehicle and in this case, the speed of the motor will cause the torque converter to overrun. Vehicle computer models such as DOE's ADVISOR and PSAT utilize lookup tables for this purpose. The modeling approach developed here allows the user to generate an accurate model for the torque, speed, flow and losses for the torque converter from two independent performance variables and the geometric parameters of the specific torque converter in question.

The torque converter model is compared in DOE ADVISOR 2002 with a similar torque converter model which uses a lookup table. The performance results for the positive torque state show strong correlation with the results of the lookup table version in both a macro (drive cycle) scale as well as in specific performance results against real world data and short duration events; however, the model shows that the overall energy losses

of the converter can be 19 times greater than the traditional lookup table predicts. This is an important new finding that helps explain the losses in the torque converter when the vehicle is being driven by an electric motor downstream of the torque converter.

Torque Converter Interactions in a Parallel Post Transmission Hybrid Driveline.

by
Ewan Gareth David Pritchard

A dissertation submitted to the Graduate Faculty of
North Carolina State University
in partial fulfillment of the
requirements for the degree of
Doctor of Philosophy

Mechanical Engineering

Raleigh, North Carolina

October 27th, 2010

APPROVED BY:

_____   _____

Dr Richard D. Gould   Dr Richard R. Johnson
Committee Chair

_____   _____

Dr Tiegang Fang   Dr Nagui Rouphail

UMI Number: 3442692

UMI®
Dissertation Publishing

ProQuest®

ProQuest LLC
789 East Eisenhower Parkway
P.O. Box 1346
Ann Arbor, MI 48106-1346

DEDICATION

This work is dedicated to my family, especially Lora, Kira and Ellie who have all been
extraordinarily patient in the logarithmic path towards finishing this work.

BIOGRAPHY

Ewan Pritchard was born in Bedford, England in 1973. In 1977, his parents Gail and David and sisters Sera and Vicky, moved to Cary, North Carolina in the United States.

From hiking in England and the mountains of North Carolina, to working in the garden, Ewan loves to spend time in the outdoors. As a child, Ewan developed allergies and asthma and needed to use an inhaler before exercise. A likely cause of the asthma and allergies are from the pollution problems seen in the Research Triangle area in the early 1980s. This condition, while not critical, caused Ewan to be more aware of the effects of transportation on the environment.

Ewan attended Enloe High School in Raleigh, North Carolina and was fortunate enough to have the opportunity to take an engineering class under the leadership of Mr. Tom Blanford. Mr. Blanford enabled the students to learn engineering in a creative way. As part of the class, Ewan worked on a project designing a model solar powered car. During the course of this project Ewan realized that he wanted to dedicate his career to investigating and promoting the use of alternate-fueled vehicles.

Ewan attended NC State University and received a degree in Mechanical Engineering in 1997. In his senior year at NC State University, he met his future wife, Lora Neel, then a

sophomore in Mechanical Engineering. After graduation, he found an internship at Advanced Energy Corporation, a non-profit energy consulting company. He later accepted a full engineering position back at Advanced Energy in late 1997, where he was given the opportunity to attend graduate school and follow his passion in electric vehicles while he worked on Centennial Campus of NCSU.

Ewan began graduate school at NCSU on a part time basis in the spring of 1998. Ewan and Lora were married a year later in the summer of 1999. In November of 2003, their first child, Kira was born. Shortly after Kira's birth, Ewan received his Master's degree from NC State University in Spring of 2004. Kira had the honor of being one of the first children in the world to ride on a plug-in hybrid school bus.

Immediately following the Master's Degree, Ewan began working towards a PhD in Mechanical Engineering from North Carolina State University. In 2008, North Carolina State University formed the Advanced Transportation Energy Center (ATEC) along with the State of North Carolina and the electric utilities Duke Energy and Progress Energy to help focus on the development of electric drive technologies, such as the school buses described here. In the Fall of 2009, Ewan accepted the position to become the Program Manager of the ATEC. Also that Fall, Ewan and Lora welcomed their second daughter Ellie to the world. Ellie has proven to be a very curious and determined young lady, like her father.

ACKNOWLEDGMENTS

I recognize that I have not reached this point alone, a lot of my advisors, coworkers, colleagues, mentors, friends and family have worked hard to get me here. I thank all of you for believing in me enough to help me get here.

I would also like to acknowledge the hard work and trust provided to me by the school bus districts and manufacturers throughout this program. I acknowledge that a lot of work has been put in by a lot of people and we have a lot more to do.

I would like to thank Mr. Maynard Harding of Covington Detroit Diesel/Allison for providing me with ongoing guidance throughout this process and access to a cutaway torque converter to analyze.

Together we can all have clean, sustainable, and inexpensive transportation. Let's get to work.

TABLE OF CONTENTS

LIST OF TABLES

LIST OF FIGURES

NOMENCLATURE

Symbol	Description (Assumed value where applicable)	Units
α_{ie}	impeller entry angle in positive flow	rad
α_{ix}	impeller exit angle in positive flow	rad
α_{te}	turbine entry angle in positive flow	rad
α_{tx}	turbine exit angle in positive flow	rad
α_{se}	stator entry angle in positive flow	rad
α_{sx}	stator exit angle in positive flow	rad
$\alpha_{i\acute{e}}$	impeller entry angle in negative flow	rad
$\alpha_{i\acute{x}}$	impeller exit angle in negative flow	rad
$\alpha_{t\acute{e}}$	turbine entry angle in negative flow	rad
$\alpha_{t\acute{x}}$	turbine exit angle in negative flow	rad
$\alpha_{s\acute{e}}$	stator entry angle in negative flow	rad
$\alpha_{s\acute{x}}$	stator exit angle in negative flow	rad
τ_i	impeller torque (engine)	N-m
τ_s	stator torque	N-m
τ_t	turbine torque (transmission)	N-m
ω_i	impeller angular speed	rad/s
ω_t	turbine angular speed	rad/s

Symbol	Description (Assumed value where applicable)	Units
ω_s	stator angular speed	rad/s
A_{ie}	impeller entry area in positive flow	m^2
A_{ix}	impeller exit area in positive flow	m^2
A_{te}	turbine entry area in positive flow	m^2
A_{tx}	turbine exit area in positive flow	m^2
A_{se}	stator entry area in positive flow	m^2
A_{sx}	stator exit area in positive flow	m^2
$\acute{A}_{ie}$	impeller entry area in negative flow	m^2
$\acute{A}_{ix}$	impeller exit area in negative flow	m^2
$\acute{A}_{te}$	turbine entry area in negative flow	m^2
$\acute{A}_{tx}$	turbine exit area in negative flow	m^2
$\acute{A}_{se}$	stator entry area in negative flow	m^2
$\acute{A}_{sx}$	stator exit area in negative flow	m^2
C_f	friction coefficient (0.5)	-
C_p	Battery Capacity	A-h
k	Peukert Coefficient	-
ρ	transmission fluid density (Dextron, 844.3 kg/m^3)	kg/m^3
Q	torque converter secondary flow rate	m^3/s
r_{ie}	impeller entry radius in positive flow	m

Symbol	Description (Assumed value where applicable)	Units
r_{ix}	impeller exit radius in positive flow	m
r_{te}	turbine entry radius in positive flow	m
r_{tx}	turbine exit radius in positive flow	m
r_{se}	stator entry radius in positive flow	m
r_{sx}	stator exit radius in positive flow	m
$\acute{r}_{ie}$	impeller entry radius in negative flow	m
$\acute{r}_{ix}$	impeller exit radius in negative flow	m
$\acute{r}_{te}$	turbine entry radius in negative flow	m
$\acute{r}_{tx}$	turbine exit radius in negative flow	m
$\acute{r}_{se}$	stator entry radius in negative flow	m
$\acute{r}_{sx}$	stator exit radius in negative flow	m
SR	speed ratio	-
TR	torque ratio	-
$\dot{L}_{ix}$	angular momentum change leaving the impeller	kg-m^2/s^2
$\dot{L}_{tx}$	angular momentum change leaving the turbine	kg-m^2/s^2
$\dot{L}_{sx}$	angular momentum change leaving the stator	kg-m^2/s^2

1. Introduction

The current generation of plug-in hybrid electric school buses achieves significant economic advantages though a simple approach to integration. The current system utilizes an 80 kW post transmission parallel hybrid electric system designed by Enova Corporation. This system is coupled with a traditional school bus from Navistar. While the existing buses do provide certified fuel economy gains, these gains are not as significant as originally anticipated. This paper investigates the significant interplay between the electric motor and the transmission and engine that contributes to losses in the overall system efficiency. The primary targets for these losses are in the torque converter of the transmission and engine braking. These losses are opportunities for significant improvement in the driveline efficiency and can provide insight into some of the benefits of providing engine off operation in future generations of buses.
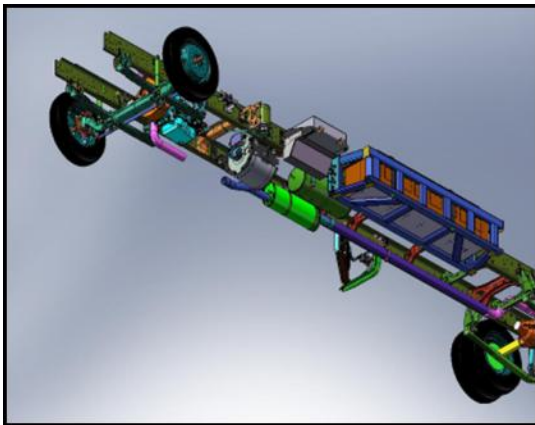

Figure 1-1, Post Transmission Hybrid Driveline

The plug-in hybrid electric school buses have been in operation for nearly four years and while all buses show some fuel economy improvements, these results are highly mixed. Increases in fuel economy as seen in day to day operation of the buses range between five and 50 percent improvement. This improvement is most specifically based on the distance travelled between charging, indicating many buses return at the end of the day in charge sustaining mode. Significant improvements have been made in the programming of the buses, but electric consumption during charge depleting mode remains high, meaning the buses enter this sustaining mode faster than anticipated. Vehicle modeling and experience with many all electric vehicles of a similar weight imply that the bus should show an electric consumption of approximately 1 kWh per mile. While this is the published expected electric performance of these buses (Pritchard and Johnson), actual data show this performance to be more on the order of 1.5 kWh per mile. This research is an investigation into the possible causes for this unexpected 50% increase in energy consumption.

1.1. Dynamometer Performance

The model for the buses was created to help optimize the system and establish the benefits of engine-off operation and all-electric range validation of this model is accomplished by comparison with both chassis dynamometer data and real world reported usage. Real world usage has been collected on 15 of these buses located around the country. Due to the varying environmental and route conditions of these buses, the performance of these fleets the data is useful for general performance, but less useful for the specific second by second performance

2

seen in this study. In addition to the real operation of the buses, several nationally recognized laboratories have conducted dynamometer testing of these buses as listed below:

California Truck Testing Services (CaTTS): In February 2008, the 2006 Engine buses for Florida were not performing as expected. In response IC corporation and Enova conducted dynamometer testing at CaTTS to validate the performance. CaTTS data presented here are WVUSub cycle in depleting mode from this study. The WVUSub Cycle was determined in previous publications to be the most appropriate drive cycle for typical school bus operation (Pritchard and Johnson). The total fuel economy over this route was on the order of 16 MPG although three different measurement methods were used and each provided a very different value. The original ADVISOR model predicted a lower fuel economy of 11.8 MPG (Pritchard and Johnson). These fuel consumption data do not include electricity consumption. Unfortunately only hybrid system data is available, roller energy data is not available at this time.

In order to provide continuity with earlier analyses using the WVU-Sub Cycle (Pritchard and Johnson), Testing Cycle at California Truck Testing Services or (CaTTS) was selected for many comparisons in this study. shows that there is little difference between the lab driven and modeled cycles.

3
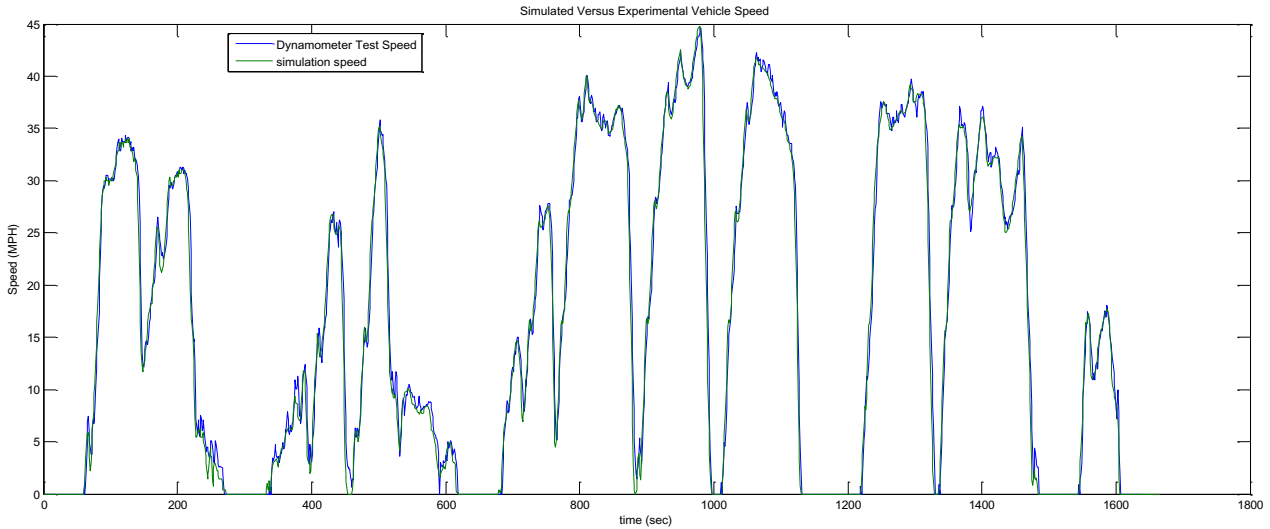
Figure 1-2, Experimental Versus Model Cycle Speeds

Southwestern Research Institute (SwRI): In May 2008, IC Bus contracted SwRI to test for California emission certification of the buses to receive low emission hybrid tax credits. All data presented here are UDDS Heavy Vehicle cycle in charge depleting mode. In this test, the total fuel economy reported by SwRI was approximately 10 MPG. Fortunately, the SWRI data includes tire force, emission and fuel flow data on a second by second basis. While these data could provide the basis for energy flow mapping, A series of inconsistencies in the data have caused concern for the use of this data without adequate knowledge of the systems taking the data and these data have not been used for this study.

National Renewable Energy Laboratories (NREL): In August 2009, NCSU Worked with NREL to determine some of the testing criteria for these tests. As a result the hybrid system data and summarized dynamometer roll data were made available. These tests run were UDDS, OCTA, and a school bus cycle. The UDDS-HV Cycle reported 8.8 MPG

4

1.2. Efficiency Losses

The Parallel Post-Transmission Hybrid Plug-In Driveline is shown in Figure 1-3. As mentioned in section 1.1, earlier modeling shows lower losses that real world data. The true nature of the vehicle losses are not completely known, but there are several key areas implicated as a beginning of investigation such as losses in the torque converter and engine braking creating a drag on the electric motor.
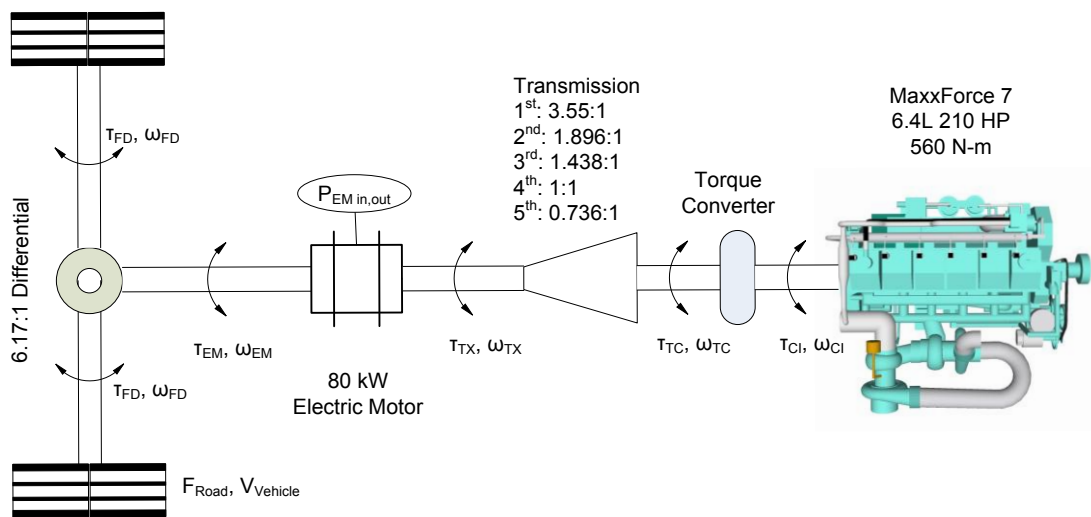
Figure 1-3, Parallel Post Transmission Driveline

To evaluate overall performance and help determine the source of these losses, a series of data was acquired from the hybrid system while the vehicle was tested at California Truck Testing Services in California in addition to the basic dynamometer data. The tests were run on a known drive cycle and on a vehicle with a 2006 emissions package (emissions prior to the incorporation of particulate traps).

5

1.3. Losses in the torque converter

A torque converter is intended to act as a mediator between the engine and the automatic transmission. Torque conversion relies on fluid pressure and centrifugal force to allow for slip between the engine rotational speed and the transmission rotational speed, the effect is much like a clutch on a conventional transmission. In this case, however, torque from the electric motor is able to travel backwards through the transmission and into the torque converter. This happens in all vehicles as the vehicle is slowing down, and allows for engine braking to occur. In the post
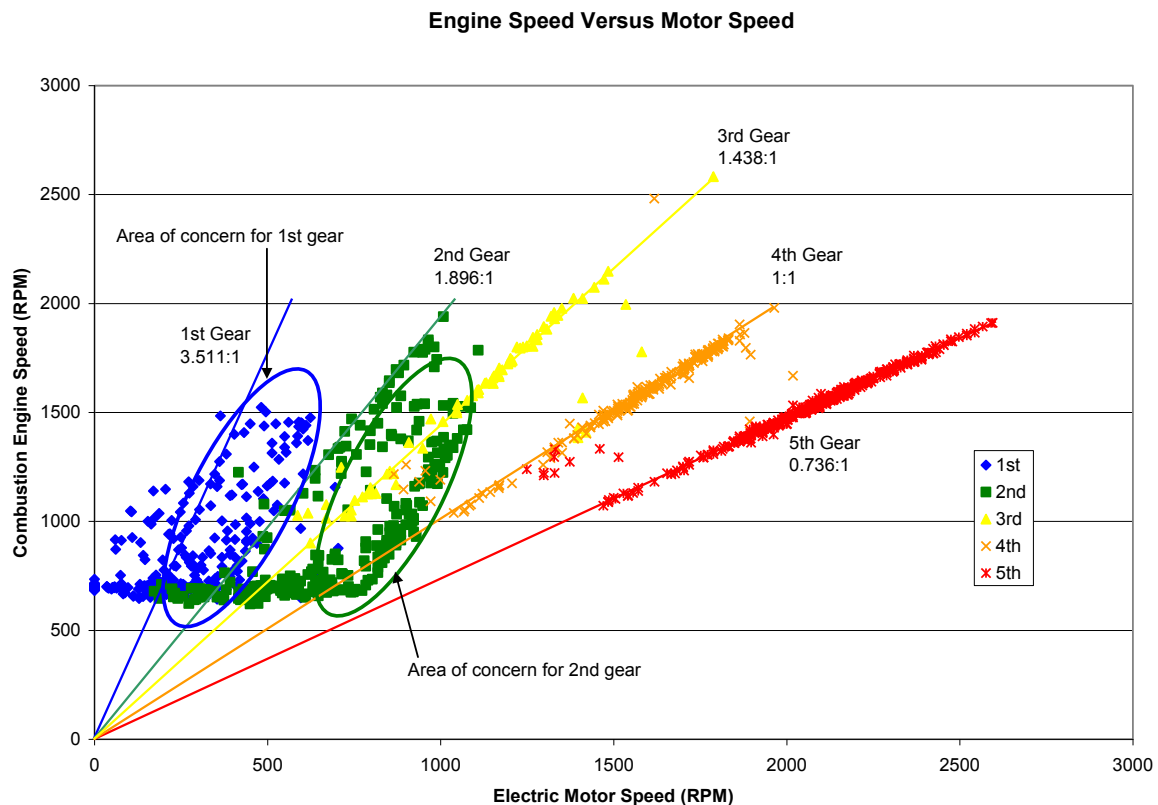
Figure 1-4, CaTTS Hybrid System Data: Likely Torque Converter Slip Areas

transmission hybrid, the torque may have been supplied by the electric motor to drive the vehicle but resulted in opposing torques and loss of energy to either heat in the torque converter or

engine. Losses in the torque converter will appear when the engine speed does not match the output speed at one of the exact gearing ratios set by the transmission. As is seen in Figure 1-4, there are two clear areas of concern for further investigation in the specific route file. These areas of concern show up in both first and second gears. If the vehicle were at a stop, the data points would occur at approximately 700 RPM for the engine, but 0 RPM for the motor.

1.4. Engine braking causing a drag on the electric motor

This power consumption is much more difficult to observe, and showed up in early data as a secondary curve on the motor performance maps. The control system has been modified to correct this early problem, but this secondary curve still appears in the data.
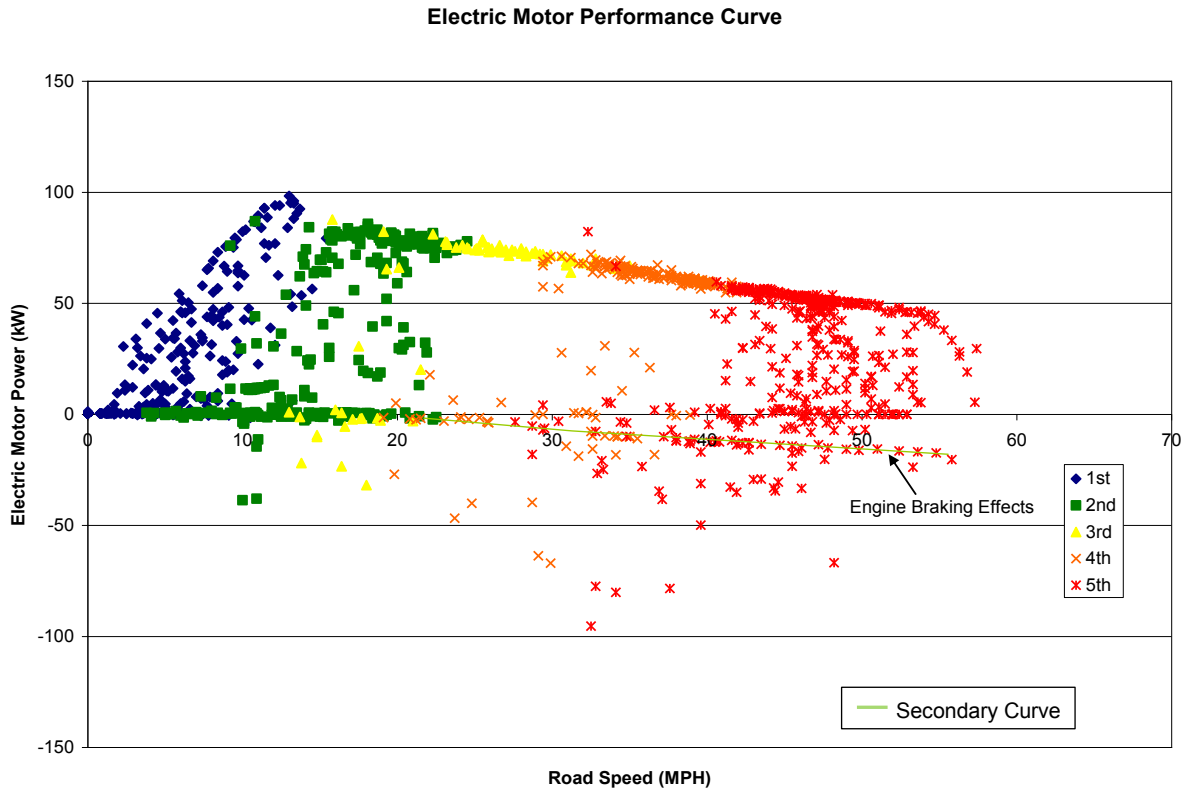
Figure 1-5, Electric Motor Performance Curve with Engine Braking Effects

The performance shown in Figure 1-5 collected from the CATTS Hybrid system data demonstrates that very little energy is being regenerated in the current system. In addition to the relatively low level of regeneration, the engine retarder still show clearly as a secondary curve in the data.

1.5. Evaluation

It is apparent that each of these problems: torque converter losses, and engine braking could be causing some level of poor performance based on the evidence and through literature surveys. It is also clear that little is known about the performance of a torque converter in the overrunning mode. As a result, the remainder of this study will focus on this characteristic and the determination of a model adequate enough to predict the performance of such a system using only the base geometry of the torque converter.

8

2. Torque Converter

The primary focus of this study is in the operation of the torque converter. Torque converters are commonly used as a mediator between a combustion engine and an automatic transmission. This torque is transferred through a complex flow of transmission fluid located inside of the converter. Initially when automatic transmissions were developed in the late 1930's fluid couplings were used. This coupling allowed torque to be transferred to the wheels, but also allowed for the vehicle to be stationary while the engine was running.

2.1. Torque Coupling

The torque coupling is a much simpler design and useful in understanding the operation of the torque converter. A torque coupling has two components which rotate with one imparting its torque on the other like two fans placed face to face. These components are each one half of a toroid as shown in Figure 2-1.

9
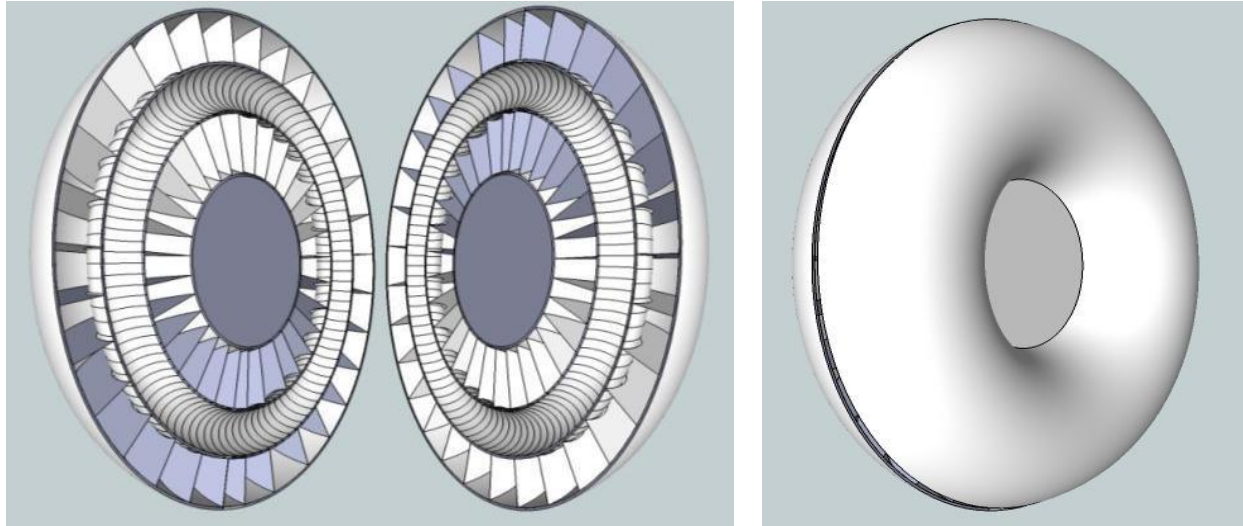
Figure 2-1, Torque Coupling: Cut Open (Left), Assembled (Right)

Fluid flows in a complex pattern within the coupling; the entire unit spins upon its primary axis. The two halves of the torque coupling are typically called the impeller and the turbine. These names appropriately describe the role of each. The impeller is connected to the engine and acts as a pump driving fluid from the inner ring of the impeller to the outer ring. A guide ring serves to help ensure fluid flow around the area. This is done by both the centrifugal force of the fluid as the impeller spins as well as the use of specially engineered fins to guide the fluid outward, imparting as much of the energy from the impeller to the fluid as possible.
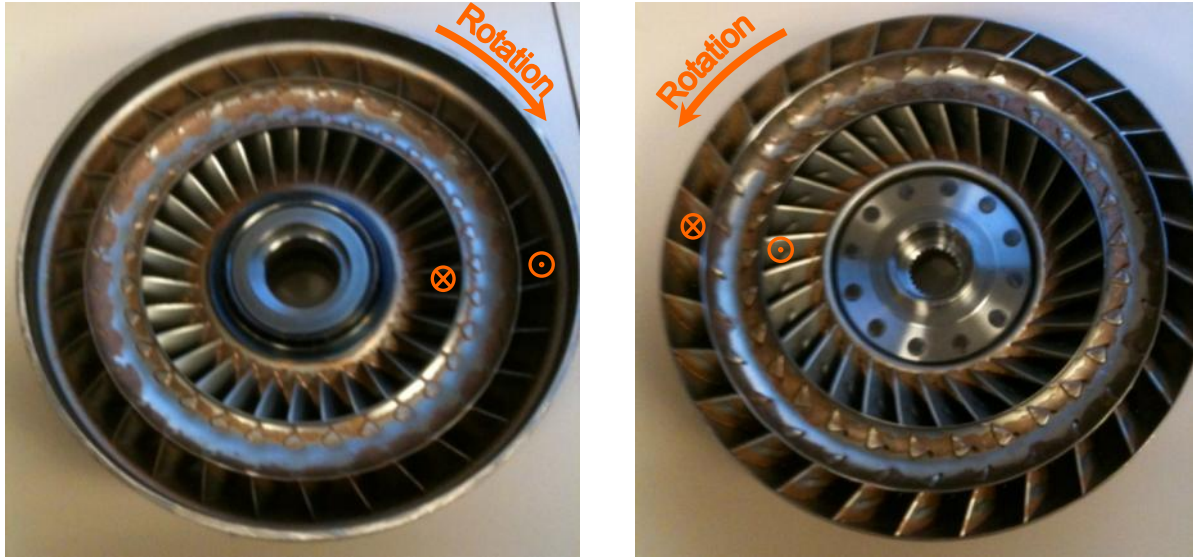
Figure 2-2, Impeller (left) and Turbine (right)

As the fluid leaves the impeller, it enters the second half of the chamber, the turbine. Like the impeller, the turbine also has radial fins, but these are designed for the opposite purpose. These fins are designed to impart the maximum amount of energy from the fluid into the turbine. Figure 2-2 shows the direction of rotation for a vehicle when it is moving forward. The figure also shows a circle with an X which is the fluid entry point and a circle with a dot to show the fluid exit point for the normal regime where the engine is providing power to the wheels. Energy is transformed in the torque coupling in the form of torque and speed as shown in Figure 2-3.

11
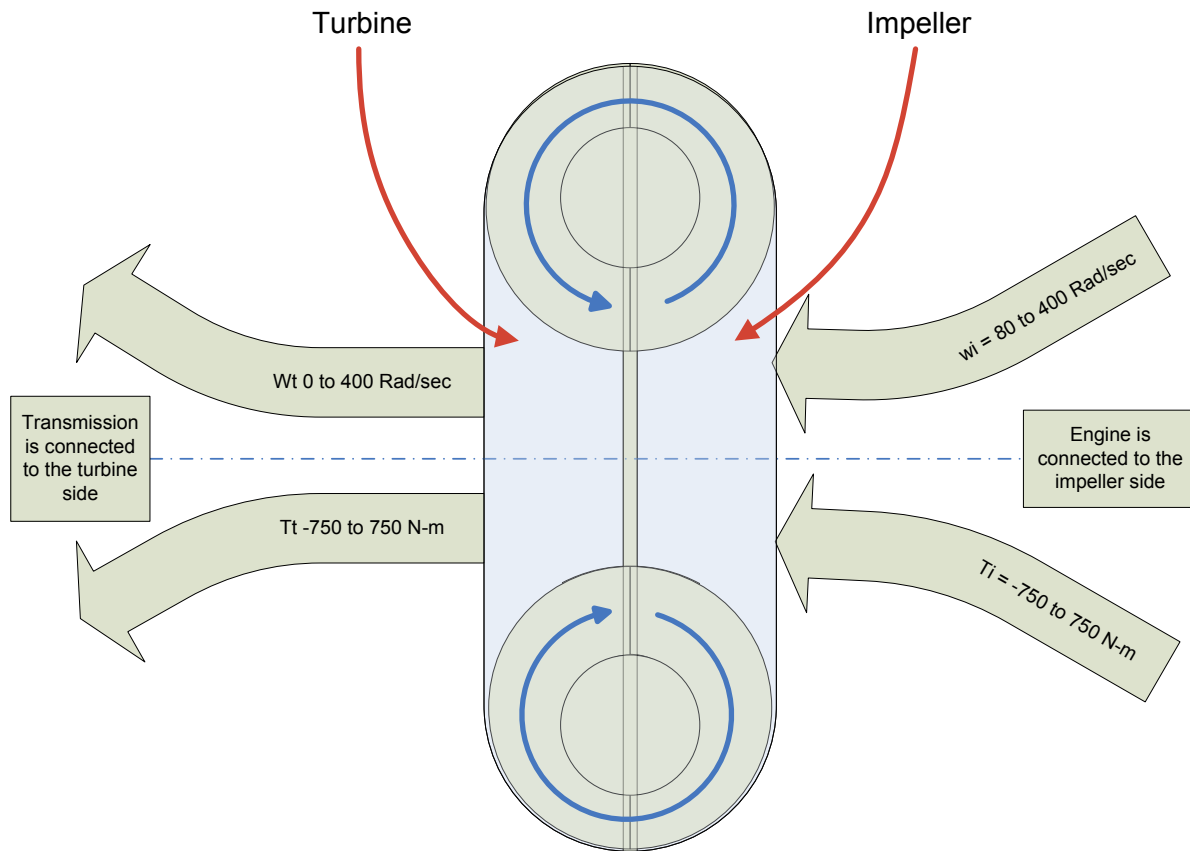
Figure 2-3, Torque Converter Inputs and Outputs

In a torque coupling, the torque leaving the coupling is always the same as the torque entering the coupling. This is often expressed as the torque ratio of one, where torque ratio (TR) is the ratio of the turbine torque (τ_t) to the impeller torque (τ_i) as shown in Equation 2.1.

$$TR = \frac{\tau_t}{\tau_i} \tag{2.1}$$

All power loss and inefficiency occurs in the torque coupling through a speed differential, where the level of slip between the two sides results in a similar expression called the speed ratio (SR) which is simply the ratio of turbine speed (ω_t) to the impeller speed (ω_i) All power loss and inefficiency occurs in the torque coupling through a speed differential, where the level of slip

between the two sides results in a similar expression called the speed ratio (SR) which is simply

the ratio of turbine speed (ω_t) to the impeller speed (ω_i)

$$SR = \frac{\omega_t}{\omega_i} \hspace{6cm} (2.2)$$

In the case of a SR of less than one, the engine is driving the vehicle. In the case the SR is greater

than one, the torque coupling is overrunning as is the case when coasting down hills or slowing

down. A typical plot of the performance of a torque converter shows TR versus SR as found in

Marks Handbook for Mechanical Engineers (Avallone et al.) and shown in Figure 2-4. It is worth

noting that the SR on this plot does not exceed 1.0.
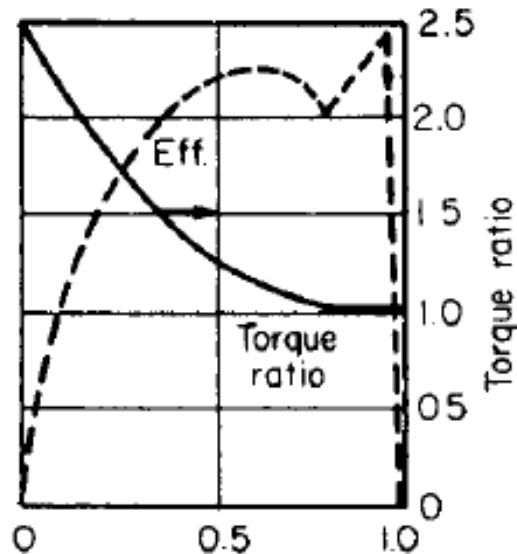
Figure 2-4, Torque Ratio Versus Speed Ratio excerpt from Marks Handbook(Avallone et al.)

The speed ratio bears a lot of influence over the fluid dynamics within the torque coupling.

Figure 2-5 shows how the fluid flows within a torque coupling. The primary flow is caused by

the normal rotation of components as the fluid inside tries to keep pace with its donut shaped

vessel. The secondary flow is a much more complex flow that changes as a function of the speed

13

ratio. At speed ratios below one, the vortex flow is as shown in Figure 2-5, and considered positive in this study. As the speeds of both components become equal, the centrifugal forces of both sides cancel each other out, and the vortex flow goes to zero. Finally, as the speed of the turbine begins to exceed that of the impeller, this flow reverses and flows in the opposite direction (negative value of Q in this study), imparting energy from the turbine to the impeller.

Primary flow is caused by any of the components rotating

Secondary flow is caused by the differential speeds of the impeller and turbine

Vortex flow is the result of the combined primary and secondary flows
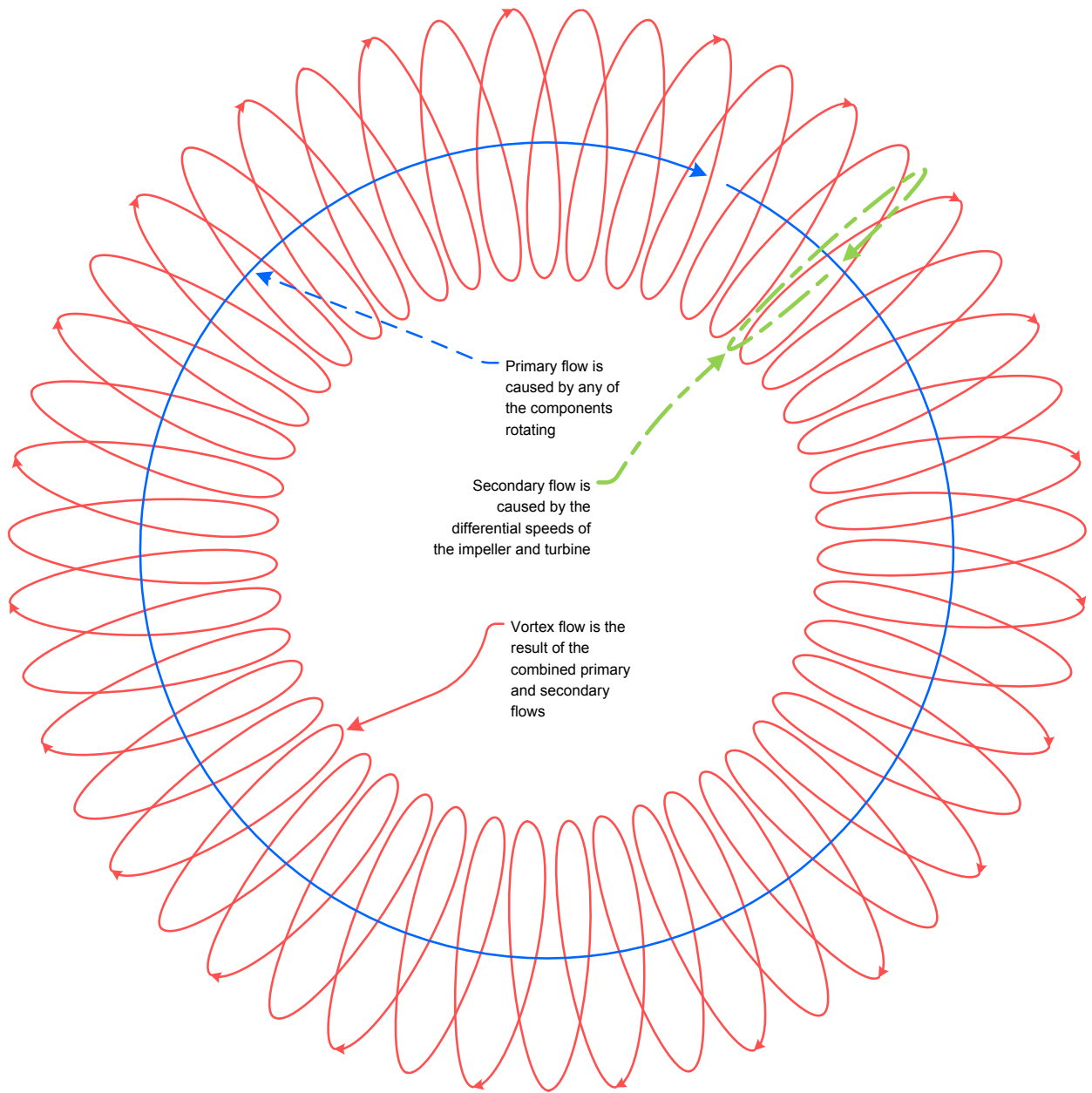
Figure 2-5, Torque Coupling Fluid Flow at SR<1

2.2. Torque Converter

The torque converter was introduced into vehicles in the 1940s as a solution to issues posed by the torque coupling. A torque coupling has the problem that at low speed ratios, the output torque is very low. This poor output torque at low speeds makes the vehicle sluggish on starting. The torque converter was introduced to overcome this problem. The addition of another component to the system, the stator, ensures that the fluid returning from the turbine to the impeller is redirected upward and forward, preparing it for the trip back through the impeller. The stator is attached to a one way clutch, ensuring that when fluid flows back from the turbine to the impeller, the stator is held fixed and used as a lever to force the fluid in a new direction. This allows the torque converter to have a multiplying effect on the incoming torque at low input speeds.

16
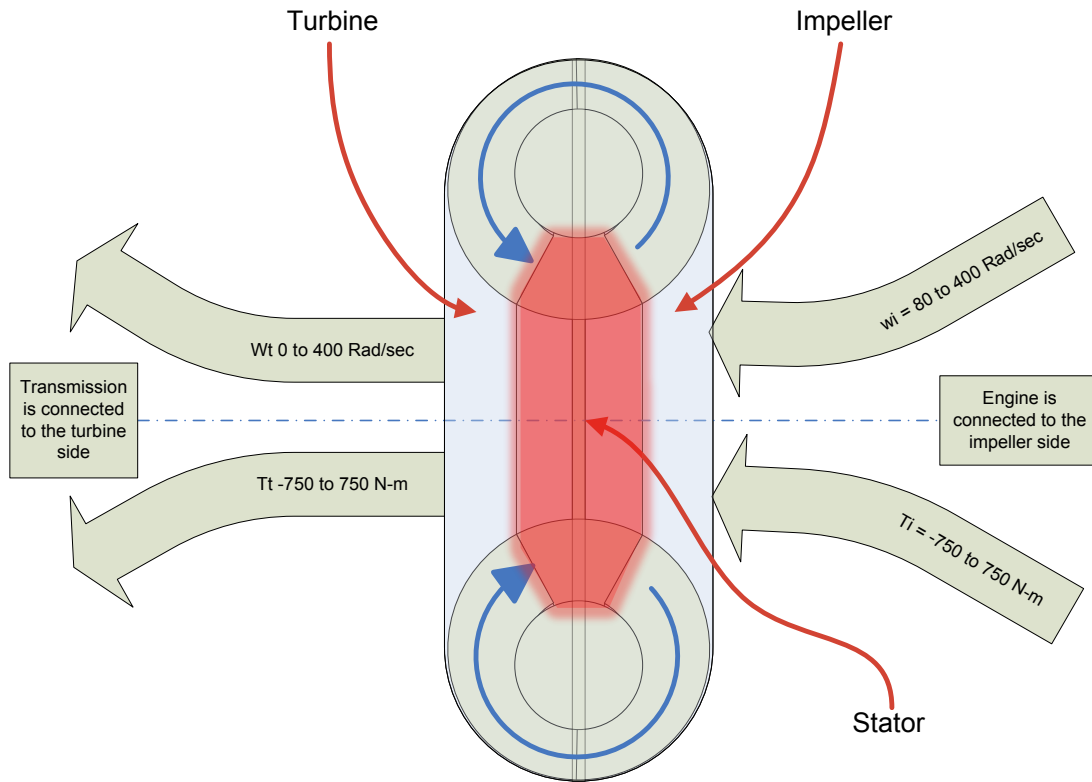
Figure 2-6, Torque Converter with Added Stator

Figure 2-6 shows the torque converter including the stator which intercepts and redirects the returning flow between the turbine and the impeller. Because of the one way clutch, the torque converter will behave like a torque coupling when the flow is reversed because the stator is free to rotate in this direction. As a result of this phenomenon, the torque converter has three distinct operating regimes as follows:

- Regime 1: This is where the secondary flow rate (Q) is positive (flowing from impeller to turbine) and the torque converter is multiplying torque. In this regime the stator is locked

due to the flow of the fluid around the converter, this locked stator enables torque multiplication. This is seen in speed ratios of 0 up to approximately 90% depending on the design of the specific converter (Avallone et al.). This point where the shift occurs is termed the "coupling" point.

- Regime 2: Above the coupling point, the secondary flow rate (Q) is still positive, but the flow rate becomes small enough for the net resulting torque to be zero. At the point the reaction on the stator becomes zero and further reductions actually lead the stator to turn. The speed ratios in this regime are above the coupling point but still below one.

- Regime 3: In this regime, the torque is flowing from the turbine to the impeller, and the speed ratio is greater than one. This results in a negative secondary flow rate (Q).

These three operating regimes will be discussed in further detail later but each has very distinct behavior. To better understand this behavior, we must first explore the various calculations on which these behaviors are based.

2.3. Torque Coupling Flow Calculations

The primary nature of the torque converter is based on the exchange of angular momentum between fluid elements and the motion of the component containing the fluid. Mathematically, this means that the fluid angular momentum flowing out of a component minus the amount flowing in is equal to the torque applied to that element. A highly simplified case of this is seen in a torque coupling with flat blades.

18
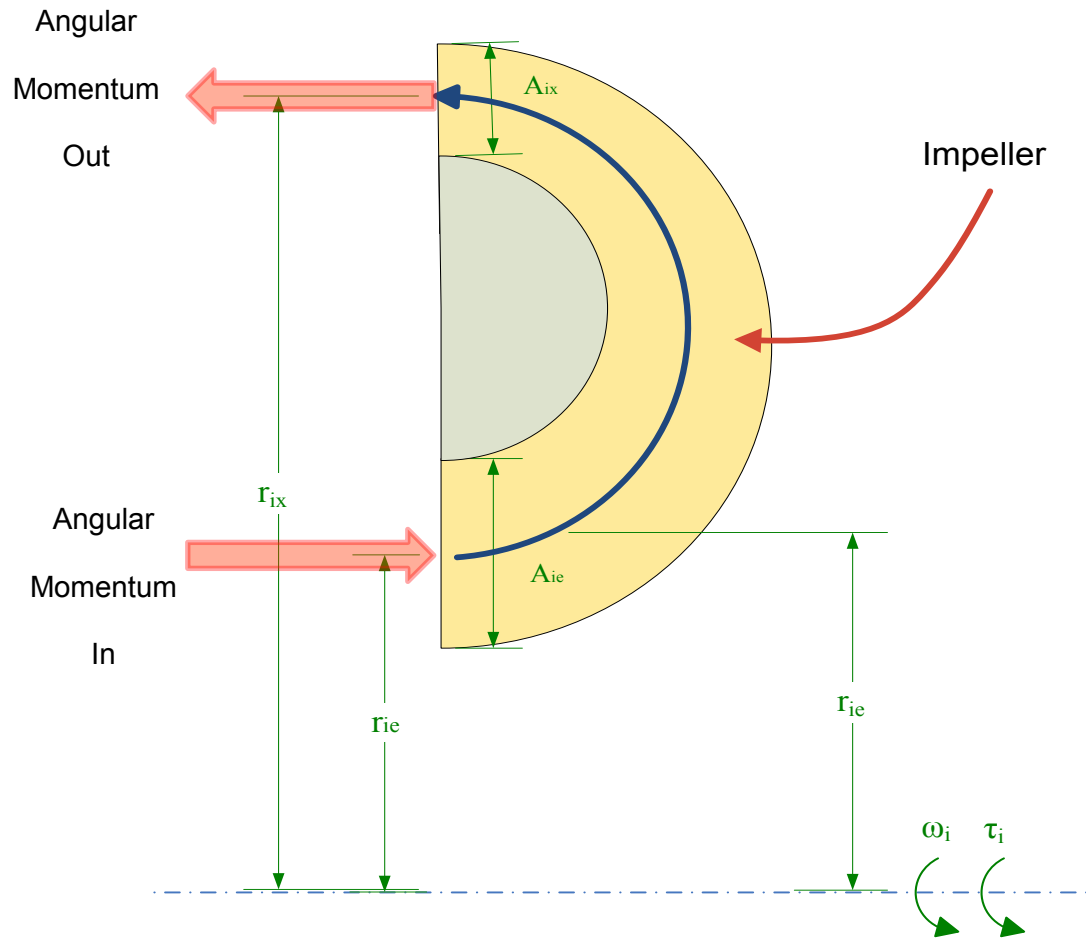
In this case, the change in angular momentum of the flow would be the following:

$$\dot{L}_{ix} = \rho Q r_{ix}^2 \omega_i \tag{2.3}$$

The same is true for the turbine.

$$\dot{L}_{tx} = \rho Q r_{tx}^2 \omega_t \tag{2.4}$$

Because the secondary angular momentum flow rate is the same exiting the impeller as it is entering the turbine, the resulting torque is the difference in these changes in angular momentum in the turbine.

$$\tau_t = \dot{L}_{tx} - \dot{L}_{ix} = \rho Q (r_{tx}^2 \omega_t - r_{ix}^2 \omega_i) \tag{2.5}$$

Following the same logic, the torque in the impeller is equal and opposite in the fluid coupling:

$$\tau_i = -\tau_t = \dot{L}_{ix} - \dot{L}_{tx} = \rho Q (r_{ix}^2 \omega_i - r_{tx}^2 \omega_t) \tag{2.6}$$

To convert each of these torques to power we multiply by the speed.

$$P_t = \rho Q \omega_t (r_{tx}^2 \omega_t - r_{ix}^2 \omega_i) \tag{2.7}$$

and

$$P_i = \rho Q \omega_i (r_{ix}^2 \omega_i - r_{tx}^2 \omega_t) \tag{2.8}$$

Finally, the power equations can be used to determine the power losses of the entire converter

$$P_i + P_t = \rho Q \omega_i (r_{ix}^2 \omega_i - r_{tx}^2 \omega_t) + \rho Q \omega_t (r_{tx}^2 \omega_t - r_{ix}^2 \omega_i) \tag{2.9}$$

or

$$P_i + P_t = \rho Q (r_{ix}^2 \omega_i^2 - r_{tx}^2 \omega_t \omega_i + r_{tx}^2 \omega_t^2 - r_{ix}^2 \omega_t \omega_i) \tag{2.10}$$

Because fluid losses are typically described in terms of pressure, Equation 2.10 can also be expressed as:

$$\Delta p_i + \Delta p_t = \rho (r_{ix}^2 \omega_i^2 - r_{tx}^2 \omega_t \omega_i + r_{tx}^2 \omega_t^2 - r_{ix}^2 \omega_t \omega_i) \tag{2.11}$$

This relationship is important, because the losses in the coupling can also be expressed by the two sources of the losses, fluid friction (Δp_f) and shock losses (Δp_{sl}). Fluid friction is based on the square of the volume flow rate:

$$\Delta p_f = \frac{1}{2}\rho C_f Q^2 \tag{2.12}$$

Shock losses describe the effect of fluid flowing from one component to the next and the irreversibility that occurs as a result of this sudden change of direction. In the torque coupling, there are two of these transitions and are therefore quantified as:

$$\Delta p_{sl} = \frac{1}{2}\rho r_{ix}^2(\omega_i - \omega_t)^2 + \frac{1}{2}\rho r_{tx}^2(\omega_t - \omega_i)^2 \tag{2.13}$$

Setting the fluid losses calculated in Equation 2.11 equal to the sum of the friction and shock losses provides a compatibility equation:

$$\rho(r_{ix}^2\omega_i^2 - r_{tx}^2\omega_t\omega_i + r_{tx}^2\omega_t^2 - r_{ix}^2\omega_t\omega_i)$$
$$= \frac{1}{2}\rho C_f Q^2 + \frac{1}{2}\rho(r_{ix}^2 + r_{tx}^2)(\omega_i - \omega_t)^2 \tag{2.14}$$

or

$$Q = \left(\frac{r_{ix}^2 - r_{tx}^2}{C_f}\right)^{1/2}(\omega_i^2 - \omega_t^2)^{1/2} \tag{2.15}$$

This can then be substituted into the torque expressions 2.5 and 2.6 to establish the relationship between velocities and torques.

21

A true torque converter is more challenging to handle as a result of the stator and the angled fins. The addition of the stator also allows for torque multiplication by eliminating the flow of angular momentum term to be subtracted at the turbine as shown above because stator speed is equal to 0. The resulting impeller torque is as follows:

$$\tau_i = \dot{L}_{ix} - \dot{L}_{sx} = \rho r_{ix} \omega_i Q + \rho \left(\frac{r_{ix} \tan \alpha_{ix}}{A_{ix}} - \frac{r_{sx} \tan \alpha_{sx}}{A_{sx}} \right) Q^2 \qquad (2.16)$$

The first part of 2.16 is due to angular momentum change in the tangential velocity of the fluid increasing to the speed of the impeller at the radius of the impeller exit. The second part comes from the change in the tangential component of the velocity resulting from blade angles. Both velocities are multiplied by the fluid flow rate and the fluid density.

3. Model Development

In order to fully understand the performance of the torque converter in all modes of operation, it is necessary to formulate a mathematical model that can be used to predict torque and speed inputs, outputs and losses. In this section the guiding equations are developed and a series of methodologies are developed to easily determine the output based on specific inputs.

3.1. Previous Torque Converter Work

As innovation has waned in the advancement of torque converter design and modeling over the past 20 years, so has much of the research on the modeling and performance of them. Throughout the 1940's and 1950's a large amount of work was done on developing steady state models of the performance of torque converters at speed ratios below one. In 1966, Ishihara and Emori(Ishihara and Emori 501) developed a simple and effective model for transient characteristics. The relationships developed in the Ishihara and Emori(Ishihara and Emori 501) paper formed the basis of several more general models developed by Kotwicki(Kotwicki 1982) and Hrovat and Tobler(Hrovat 1985). Kotwicki(Kotwicki 1982) developed a clear set of steady state relations in his paper in 1982 which clearly describes the tie between the input torque and speed and the output torque and speed. In 1985 Hrovat and Tobler(Hrovat 1985) developed computer simulations and bond graphs to predict the performance of torque converters. Hrovat and Tobler(Hrovat 1985) developed a set of four first order nonlinear equations describing torque converter dynamics. In their paper, they begin to develop some of the relations for torque

ratios greater than one in their appendix, but do not develop simplified relationships. Figure 3-1 shows an excerpt from Kotwicki(Kotwicki 1982) along with the current thinking, limiting the relevant SR to one and below.
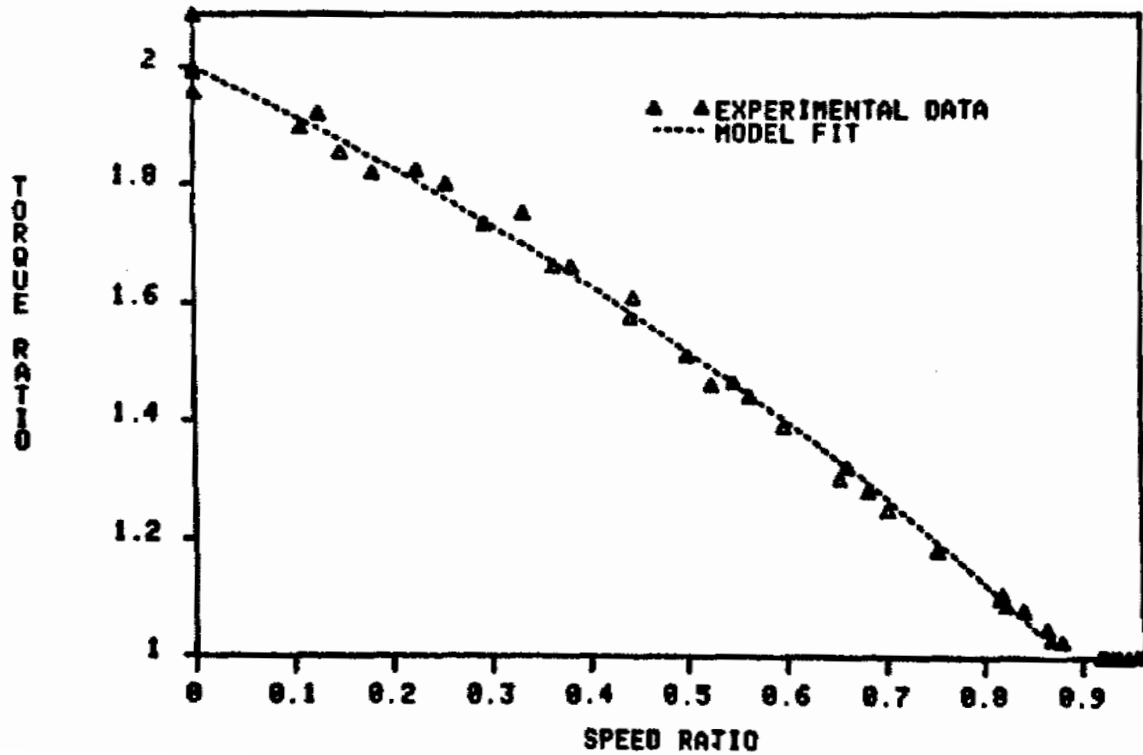
Figure 3-1, TR versus SR Plot Excerpt from Kotwicki(Kotwicki 1982)

Published results on torque converter modeling indicate that steady state models are appropriate for speeds exceeding 60 Hz (Kotwicki 1982) or more succinctly if the frequency of the disturbance is below one pulse per two impeller revolutions (Ishihara and Emori 501). As discussed in the previous section, the basis for these calculations is by developing the torque relationships through conservation of angular momentum. Once the torque values are found, these values can be used to develop a compatibility equation by equating the generated pressure

24

changes and the pressure losses. This equation can then be solved for Q to determine the flow rate in a given situation. These solutions must be found for each of the three modes described earlier as follows:

- Regime 1: A speed ratio below the coupling point where the stator is held in place due to the one way clutch.

- Regime 2: The speed ratio has reached the coupling point and is still below one. The torque reaction on the stator causes the stator to spin (freewheel) at this point but the flow rate is still positive.

- Regime 3: A speed ratio exceeding one, the stator is now spinning (freewheeling) and the secondary flow rate is in a negative rotation causing the stator to spin freely and torque to be transferred from the turbine to the impeller.

3.2. Torque Converter Mathematical Model

The purpose of this study is to extend the current models of torque converters, and include the ability to reasonably predict the performance of a specific converter from a series of parameters in both the coupled and uncoupled state to include the overrunning regime. The first two models are redeveloped here and using a similar methodology, the overrunning regime is also added.

In the regimes we are focused on, two of the following variables are known, while the other two are not: ω_i, ω_t, τ_i, and τ_t. In addition to the desired variables, another variable, Q is important for use here. The evaluation of these relations comes from the development of torque as a function of the other variables. The determination of torque comes from the exchange of angular

momentum as shown in Chapter 2; however the addition of the stator and fins makes this derivation a little more challenging. There are now three components to calculate torque as well as three component transitions which create shock loss. The fins also add a tangential component to the primary flow, as the fins convert this flow to secondary flow as shown in Figure 3-2.
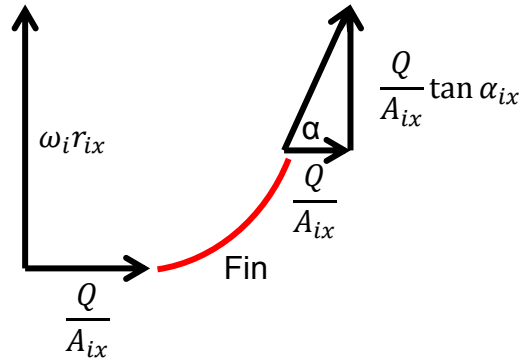
Recreated from Kotwicki(Kotwicki

Figure 3-2, Effect of Fin Angle on Velocity

An example of the modified calculation for the angular momentum leaving the impeller using the geometry described in Figure 3-3 is given in Equation 3.1

$$\dot{L}_{ix} = \rho Q r_{ix} \left(\frac{Q}{A_{ix}} \tan \alpha_{ix} + r_{ix} \omega_i \right) \tag{3.1}$$

The resulting torque is the difference in the angular momentum flow entering the component and the flow leaving it.

3.2.1. Regime 1: Below the Coupling Point ($\omega_s=0$)

$$\tau_i = \rho Q (r_{ix}^2 \omega_i - r_{sx}^2 \omega_s) + \rho Q^2 \left(\frac{r_{ix} \tan \alpha_{ix}}{A_{ix}} - \frac{r_{sx} \tan \alpha_{sx}}{A_{sx}} \right) \tag{3.2}$$

$$\tau_t = - \left(\rho Q (r_{tx}^2 \omega_t - r_{ix}^2 \omega_i) + \rho Q^2 \left(\frac{r_{tx} \tan \alpha_{tx}}{A_{tx}} - \frac{r_{ix} \tan \alpha_{ix}}{A_{ix}} \right) \right) \tag{3.3}$$

$$\tau_s = \rho Q (r_{sx}^2 \omega_s - r_{tx}^2 \omega_t) + \rho Q^2 \left(\frac{r_{sx} \tan \alpha_{sx}}{A_{sx}} - \frac{r_{tx} \tan \alpha_{tx}}{A_{tx}} \right) \tag{3.4}$$

For speed ratios below one, the flow rate of the fluid is in the normal "positive" direction. This means that the impeller forces the fluid to the outside of the unit, the turbine absorbs the energy in the fluid, and finally, the stator redirects the fluid to begin the operation again. Using the modified momentum equations in a similar methodology to that used in Chapter 2, torque equations 3.2 – 3.4 for each component of the system are developed.

The negative sign on the turbine torque equation is due to the sign convention of outgoing torque being positive. Due to the one way clutch in the stator, the stator will not spin until the flow rate slows to the point where the reaction force on the stator becomes zero, called coupling. This mode is considered to be below the coupling point.
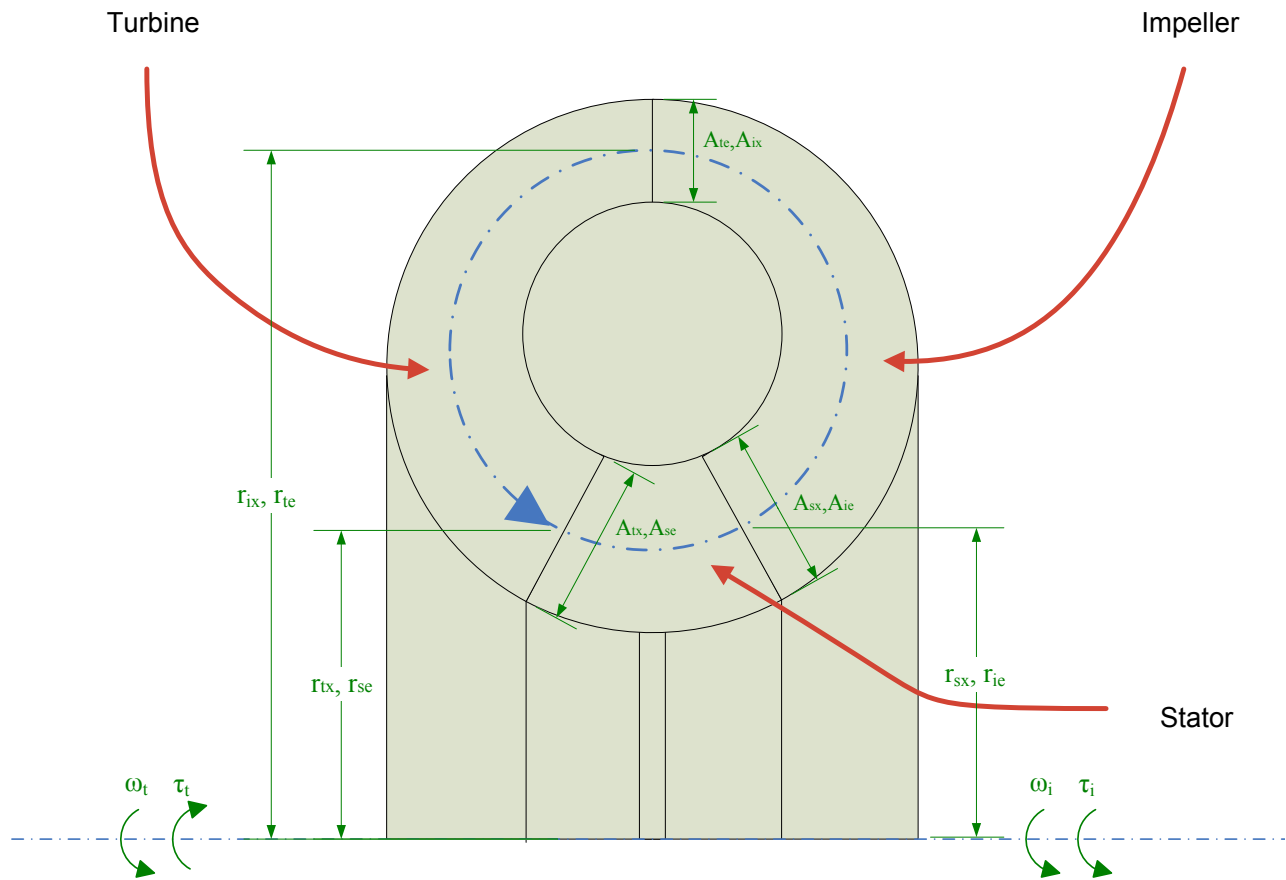
Figure 3-3, Positive Flow Dimensions

Below the coupling point, the positive flow equations include a stator speed. Eliminating terms that contain this value yield the following.

$$\tau_i = \rho Q (r_{ix}^2 \omega_i) + \rho Q^2 \left(\frac{r_{ix}\tan\alpha_{ix}}{A_{ix}} - \frac{r_{sx}\tan\alpha_{sx}}{A_{sx}} \right) \tag{3.5}$$

$$\tau_t = -\left(\rho Q (r_{tx}^2 \omega_t - r_{ix}^2 \omega_i) + \rho Q^2 \left(\frac{r_{tx}\tan\alpha_{tx}}{A_{tx}} - \frac{r_{ix}\tan\alpha_{ix}}{A_{ix}} \right) \right) \tag{3.6}$$

28

$$\tau_s = \rho Q^2 \left(\frac{r_{sx} \tan \alpha_{sx}}{A_{sx}} - \frac{r_{tx} \tan \alpha_{tx}}{A_{tx}} \right) - \rho Q r_{tx}^2 \omega_t \tag{3.7}$$

Similar to the method described in Chapter 2, each of the torques is converted to a pressure change as shown below.

$$\Delta p_i = \rho \omega_i (r_{ix}^2 \omega_i) + \rho \omega_i Q \left(\frac{r_{ix} \tan \alpha_{ix}}{A_{ix}} - \frac{r_{sx} \tan \alpha_{sx}}{A_{sx}} \right) \tag{3.8}$$

$$\Delta p_t = - \left(\rho \omega_t (r_{tx}^2 \omega_t - r_{ix}^2 \omega_i) + \rho \omega_t Q \left(\frac{r_{tx} \tan \alpha_{tx}}{A_{tx}} - \frac{r_{ix} \tan \alpha_{ix}}{A_{ix}} \right) \right) \tag{3.9}$$

$$\Delta p_s = \rho \omega_s Q \left(\frac{r_{sx} \tan \alpha_{sx}}{A_{sx}} - \frac{r_{tx} \tan \alpha_{tx}}{A_{tx}} \right) - \rho \omega_s r_{tx}^2 \omega_t = 0 \tag{3.10}$$

Because the stator speed is zero, the resulting pressure change is also zero. Each of these pressures must now be equated to the determined pressure losses of flow and shock losses as shown below.

$$\Delta p_{sl\,i-t} = \frac{1}{2} \rho \left[Q \left(\frac{\tan \alpha_{ix}}{A_{ix}} - \frac{\tan \alpha_{te}}{A_{te}} \right) + r_{ix} \omega_i - r_{te} \omega_t \right]^2 \tag{3.11}$$

$$\Delta p_{sl\,t-s} = \frac{1}{2} \rho \left[Q \left(\frac{\tan \alpha_{tx}}{A_{tx}} - \frac{\tan \alpha_{se}}{A_{se}} \right) + r_{tx} \omega_t - r_{se} \omega_s \right]^2 \tag{3.12}$$

$$\Delta p_{sl\,s-i} = \frac{1}{2} \rho \left[Q \left(\frac{\tan \alpha_{sx}}{A_{sx}} - \frac{\tan \alpha_{ie}}{A_{ie}} \right) + r_{sx} \omega_s - r_{ie} \omega_i \right]^2 \tag{3.13}$$

$$\Delta p_f = \frac{1}{2} \rho C_f Q^2 \tag{3.14}$$

The resulting compatibility equation is therefore the following:

$$\Delta p_t + \Delta p_i + \Delta p_s = \Delta p_{sl\ i-t} + \Delta p_{sl\ t-s} + \Delta p_{sl\ s-i} + \Delta p_f \tag{3.15}$$

or

$$
\begin{aligned}
0 = & \left[\frac{1}{2}\, \rho \left(\frac{\tan(\alpha_{tx})}{A_{tx}} - \frac{\tan(\alpha_{se})}{A_{se}} \right)^2 + \frac{1}{2}\, \rho \left(\frac{\tan(\alpha_{ix})}{A_{ix}} - \frac{\tan(\alpha_{te})}{A_{te}} \right)^2 \right. \\
& + \frac{1}{2}\, \rho \left(\frac{\tan(\alpha_{sx})}{A_{sx}} - \frac{\tan(\alpha_{ie})}{A_{ie}} \right)^2 + \frac{1}{2}\, \rho\, cf \left] Q^2 + \left(\rho \left(\varpi_i\, r_{ix} \right. \right. \right. \\
& \left. - \varpi_t\, r_{te} \right) \left(\frac{\tan(\alpha_{ix})}{A_{ix}} - \frac{\tan(\alpha_{te})}{A_{te}} \right) + \rho \left(\frac{r_{tx} \tan(\alpha_{tx})}{A_{tx}} - \frac{r_{ix} \tan(\alpha_{ix})}{A_{ix}} \right) \varpi \\
& - \rho\, \varpi_i\, r_{ie} \left(\frac{\tan(\alpha_{sx})}{A_{sx}} - \frac{\tan(\alpha_{ie})}{A_{ie}} \right) + \rho\, \varpi_t\, r_{tx} \left(\frac{\tan(\alpha_{tx})}{A_{tx}} - \frac{\tan(\alpha_{se})}{A_{se}} \right) \\
& \left. - \rho \left(\frac{r_{ix} \tan(\alpha_{ix})}{A_{ix}} - \frac{r_{sx} \tan(\alpha_{sx})}{A_{sx}} \right) \varpi_i \right) Q + \frac{1}{2}\, \rho \left(\varpi_i\, r_{ix} - \varpi_t\, r_{te} \right)^2 \\
& + \frac{1}{2}\, \rho\, \varpi_i^2\, r_{ie}^2 + \frac{1}{2}\, \rho\, \varpi_t^2\, r_{tx}^2 + \rho \left(\varpi_t\, r_{tx}^2 - \varpi_i\, r_{ix}^2 \right) \varpi_t - \rho\, \varpi_i^2\, r_{ix}^2
\end{aligned}
\tag{3.16}
$$

By gathering like terms and substituting the equal radii we can gather the different powers of Q to arrive at equation 3.17. For more details on this simplification see Appendix A.

$$0 = \frac{1}{2}\rho\left[\left(\frac{\tan\alpha_{ix}}{A_{ix}} - \frac{\tan\alpha_{te}}{A_{te}}\right)^2 + \left(\frac{\tan\alpha_{tx}}{A_{tx}} - \frac{\tan\alpha_{se}}{A_{se}}\right)^2\right.$$
$$\left. + \left(\frac{\tan\alpha_{sx}}{A_{sx}} - \frac{\tan\alpha_{ie}}{A_{ie}}\right)^2 + cf\right]Q^2$$
$$+ \left(\rho\omega_t\left(\frac{r_{te}\tan\alpha_{te}}{A_{te}} - \frac{r_{tx}\tan\alpha_{se}}{A_{se}}\right)\right.$$
$$\left. - \rho\omega_i\left(\frac{r_{ix}\tan\alpha_{te}}{A_{te}} - \frac{r_{ie}\tan\alpha_{ie}}{A_{ie}}\right)\right)Q$$
$$+ \frac{1}{2}\rho\left((r_{ix}^2 - r_{ie}^2)\omega_i^2 + (r_{tx}^2 - r_{te}^2)\omega_t^2\right) \tag{3.17}$$

Making the following substitutions for the coefficients of Q results in a simpler equation

$$A_1 = \frac{1}{2}\rho\left[\left(\frac{tan(\alpha_{ix})}{A_{ix}} - \frac{tan(\alpha_{te})}{A_{te}}\right)^2 + \left(\frac{tan(\alpha_{tx})}{A_{tx}} - \frac{tan(\alpha_{se})}{A_{se}}\right)^2\right.$$
$$\left. + \left(\frac{tan(\alpha_{sx})}{A_{sx}} - \frac{tan(\alpha_{ie})}{A_{ie}}\right)^2 + cf\right] \tag{3.18}$$

$$B_1 = \rho\omega_t\left(\frac{r_{te}\tan\alpha_{te}}{A_{te}} - \frac{r_{tx}\tan\alpha_{se}}{A_{se}}\right) - \rho\omega_i\left(\frac{r_{ix}\tan\alpha_{te}}{A_{te}} - \frac{r_{ie}\tan\alpha_{ie}}{A_{ie}}\right) \tag{3.19}$$

$$C_1 = \frac{1}{2}\rho\left((r_{ix}^2 - r_{ie}^2)\omega_i^2 + (r_{tx}^2 - r_{te}^2)\omega_t^2\right) \tag{3.20}$$

Equation 2.19 now becomes a simple quadratic formula:

$$A_1 Q^2 + B_1 Q + C_1 = 0 \qquad (3.21)$$

With the solution for Q of:

$$Q = \frac{-B_1 + \sqrt{B_1^2 - 4A_1 C_1}}{2A_1} \qquad (3.22)$$

This overall flow rate calculation correlates with the published torque converter models determined by Kotwicki(Kotwicki 1982) if radii and areas were assumed equal and Hrovat and Tobler(Hrovat 1985) if the equations were considered steady state. These equations provide a more general set of equations than those provided by Kotwicki (Kotwicki 1982)

3.2.2. Regime 2: Above the Coupling Point (τ$_s$=0,SR<1)

When the calculated impeller torque is equal to or greater than the calculated turbine torque, the torque reaction on the stator must be either zero or less than zero. Because of the one way clutch mounted on the stator, the stator will begin to turn as soon as the torque reaction is applied in this negative direction and the converter will begin to behave as a coupling with an extra element. The effect of this eliminates the stator multiplication effects in the torque equation. Above the coupling point, the stator torque is zero, but the rotational speed is no longer zero. Eliminating terms that contain this value yield the following.

$$\tau_i = \rho Q(r_{ix}^2 \omega_i - r_{sx}^2 \omega_s) + \rho Q^2 \left(\frac{r_{ix} \tan \alpha_{ix}}{A_{ix}} - \frac{r_{sx} \tan \alpha_{sx}}{A_{sx}} \right) \tag{3.23}$$

$$\tau_t = - \left(\rho Q(r_{tx}^2 \omega_t - r_{ix}^2 \omega_i) + \rho Q^2 \left(\frac{r_{tx} \tan \alpha_{tx}}{A_{tx}} - \frac{r_{ix} \tan \alpha_{ix}}{A_{ix}} \right) \right) \tag{3.24}$$

$$\tau_s = 0 = \rho Q(r_{sx}^2 \omega_s - r_{tx}^2 \omega_t) + \rho Q^2 \left(\frac{r_{sx} \tan \alpha_{sx}}{A_{sx}} - \frac{r_{tx} \tan \alpha_{tx}}{A_{tx}} \right) \tag{3.25}$$

Taking advantage of the stator condition provides a substitute for the stator speed

$$\omega_s = \frac{Q \left(\frac{r_{tx} \tan \alpha_{tx}}{A_{tx}} - \frac{r_{sx} \tan \alpha_{sx}}{A_{sx}} \right) + r_{tx}^2 \omega_t}{r_{sx}^2} \tag{3.26}$$

Which can then be placed back into the impeller torque

$$\tau_i = \rho Q(r_{ix}^2 \omega_i - r_{tx}^2 \omega_t) + \rho Q^2 \left(\frac{r_{ix} \tan \alpha_{ix}}{A_{ix}} - \frac{r_{tx} \tan \alpha_{tx}}{A_{tx}} \right) \tag{3.27}$$

Similar to the method used in the below coupling regime, each of the torques is converted to a pressure change as shown below.

$$\Delta p_t = -\left(\rho\omega_t(r_{tx}^2\omega_t - r_{ix}^2\omega_i) + \rho\omega_t Q \left(\frac{r_{tx}\tan\alpha_{tx}}{A_{tx}} - \frac{r_{ix}\tan\alpha_{ix}}{A_{ix}} \right) \right) \tag{3.28}$$

$$\Delta p_i = \rho\omega_i(r_{ix}^2\omega_i - r_{tx}^2\omega_t) + \rho\omega_i Q \left(\frac{r_{ix}\tan\alpha_{ix}}{A_{ix}} - \frac{r_{tx}\tan\alpha_{tx}}{A_{tx}} \right) \tag{3.29}$$

Both of these pressures must now be equated to the determined pressure losses of flow and shock losses as shown in Equations $3.30 - 3.33$. While the stator dropped out of the torque equations, the stator fluid transitions will still be a part of the calculation of the shock loss.

$$\Delta p_{sl\,i-t} = \frac{1}{2}\rho \left[Q\left(\frac{\tan\alpha_{ix}}{A_{ix}} - \frac{\tan\alpha_{te}}{A_{te}} \right) + r_{ix}\omega_i - r_{te}\omega_t \right]^2 \tag{3.30}$$

$$\Delta p_{sl\,t-s} = \frac{1}{2}\rho \left[Q\left(\frac{\tan\alpha_{tx}}{A_{tx}} - \frac{\tan\alpha_{se}}{A_{se}} \right) + r_{tx}\omega_t - r_{se}\omega_s \right]^2 \tag{3.31}$$

$$\Delta p_{sl\,s-i} = \frac{1}{2}\rho \left[Q\left(\frac{\tan\alpha_{sx}}{A_{sx}} - \frac{\tan\alpha_{ie}}{A_{ie}} \right) + r_{sx}\omega_s - r_{ie}\omega_i \right]^2 \tag{3.32}$$

$$\Delta p_f = \frac{1}{2}\rho C_f Q^2 \tag{3.33}$$

The resulting compatibility equation is found in Equation 3.34

$$\rho\omega_t(r_{ix}^2\omega_i - r_{tx}^2\omega_t) + \rho\omega_t Q\left(\frac{r_{ix}\tan\alpha_{ix}}{A_{ix}} - \frac{r_{tx}\tan\alpha_{tx}}{A_{tx}}\right)$$

$$+ \rho\omega_i(r_{ix}^2\omega_i - r_{tx}^2\omega_t) + \rho\omega_i Q\left(\frac{r_{ix}\tan\alpha_{ix}}{A_{ix}} - \frac{r_{tx}\tan\alpha_{tx}}{A_{tx}}\right)$$

$$= \frac{1}{2}\rho\left[Q\left(\frac{\tan\alpha_{ix}}{A_{ix}} - \frac{\tan\alpha_{te}}{A_{te}}\right) + r_{ix}\omega_i - r_{te}\omega_t\right]^2 \qquad (3.34)$$

$$+ \frac{1}{2}\rho\left[Q\left(\frac{\tan\alpha_{tx}}{A_{tx}} - \frac{\tan\alpha_{se}}{A_{se}}\right) + r_{tx}\omega_t - r_{se}\omega_s\right]^2$$

$$+ \frac{1}{2}\rho\left[Q\left(\frac{\tan\alpha_{sx}}{A_{sx}} - \frac{\tan\alpha_{ie}}{A_{ie}}\right) + r_{sx}\omega_s - r_{ie}\omega_i\right]^2 + \frac{1}{2}\rho C_f Q^2$$

Equation 3.34 can be manipulated using mathematical manipulation software such as Maple to determine the flow rate subscripts in this regime as shown in Appendix 1 to find the subscripts for Q as shown in Equation 3.35

$$0 = \frac{1}{2}\rho\left[\left(\frac{tan(\alpha_{ix})}{A_{ix}} - \frac{tan(\alpha_{te})}{A_{te}}\right)^2 + \left(\frac{tan(\alpha_{sx})}{A_{sx}} - \frac{tan(\alpha_{se})}{A_{se}}\right)^2\right.$$

$$\left. + \left(\frac{tan(\alpha_{ie})}{A_{ie}} - \frac{tan(\alpha_{tx})}{A_{tx}}\right)^2 + cf\right]Q^2$$

$$+ \left(\rho\omega_t\left(\frac{r_{te}\tan\alpha_{te}}{A_{te}} - \frac{r_{ie}\tan\alpha_{ie}}{A_{ie}}\right)\right. \qquad (3.35)$$

$$\left. - \rho\omega_i\left(\frac{r_{te}\tan\alpha_{te}}{A_{te}} - \frac{r_{ie}\tan\alpha_{ie}}{A_{ie}}\right)\right)Q$$

$$+ \frac{1}{2}\rho\left((r_{ix}^2 - r_{ie}^2)\omega_i^2 + (r_{tx}^2 - r_{te}^2)\omega_t^2\right)$$

Extracting coefficients from the compatibility equation gives Equations 3.36-3.38

$$A_2 = \frac{1}{2}\rho\left[\left(\frac{tan(\alpha_{ix})}{A_{ix}} - \frac{tan(\alpha_{te})}{A_{te}}\right)^2 + \left(\frac{tan(\alpha_{sx})}{A_{sx}} - \frac{tan(\alpha_{se})}{A_{se}}\right)^2\right.$$
$$\left.+ \left(\frac{tan(\alpha_{ie})}{A_{ie}} - \frac{tan(\alpha_{tx})}{A_{tx}}\right)^2 + cf\right]$$

(3.36)

$$B_2 = \rho\omega_t\left(\frac{r_{te}\tan\alpha_{te}}{A_{te}} - \frac{r_{ie}\tan\alpha_{ie}}{A_{ie}}\right) - \rho\omega_i\left(\frac{r_{te}\tan\alpha_{te}}{A_{te}} - \frac{r_{ie}\tan\alpha_{ie}}{A_{ie}}\right)$$

(3.37)

$$C_2 = \frac{1}{2}\rho\left((r_{ix}^2 - r_{ie}^2)\omega_i^2 + (r_{tx}^2 - r_{te}^2)\omega_t^2\right)$$

(3.38)

Equation 3.35 also becomes a simple quadratic formula:

$$A_2 Q^2 + B_2 Q + C_2 = 0$$

(3.39)

With the solution for Q of:

$$Q = \frac{-B_2 + \sqrt{B_2^2 - 4A_2 C_2}}{2A_2}$$

(3.40)

The relationships between Q, ω_i, ω_t,τ_i, and τ_t are now determined for the conditions beyond the coupling point, the converter is characterized for all conditions up to a speed ratio of 1. Again these values also correlate exactly with those found by both Kotwicki(Kotwicki 1982) and Hrovat and Tobler(Hrovat 1985). For speed ratios above 1, we must use a new set of conditions which are highlighted in the following section.

3.2.3. Regime 3: Overrunning Regime with Negative Flow (SR>1)

In the case of the turbine overrunning the impeller, the fluid flow is reversed from the designed direction, or negative. Using a similar approach to the one used for the positive regime, but with new exit and entrance values a new set of equations can be established that are used to develop this relationship. It is important to recognize that with a negative flow, or speed ratio greater than one, the converter will behave as a coupling. Behaving as a torque coupling also means that turbine torque will equal impeller torque or more succinctly have a torque ratio of one. As shown in Figure 3-4, the flow is reversed in this regime.
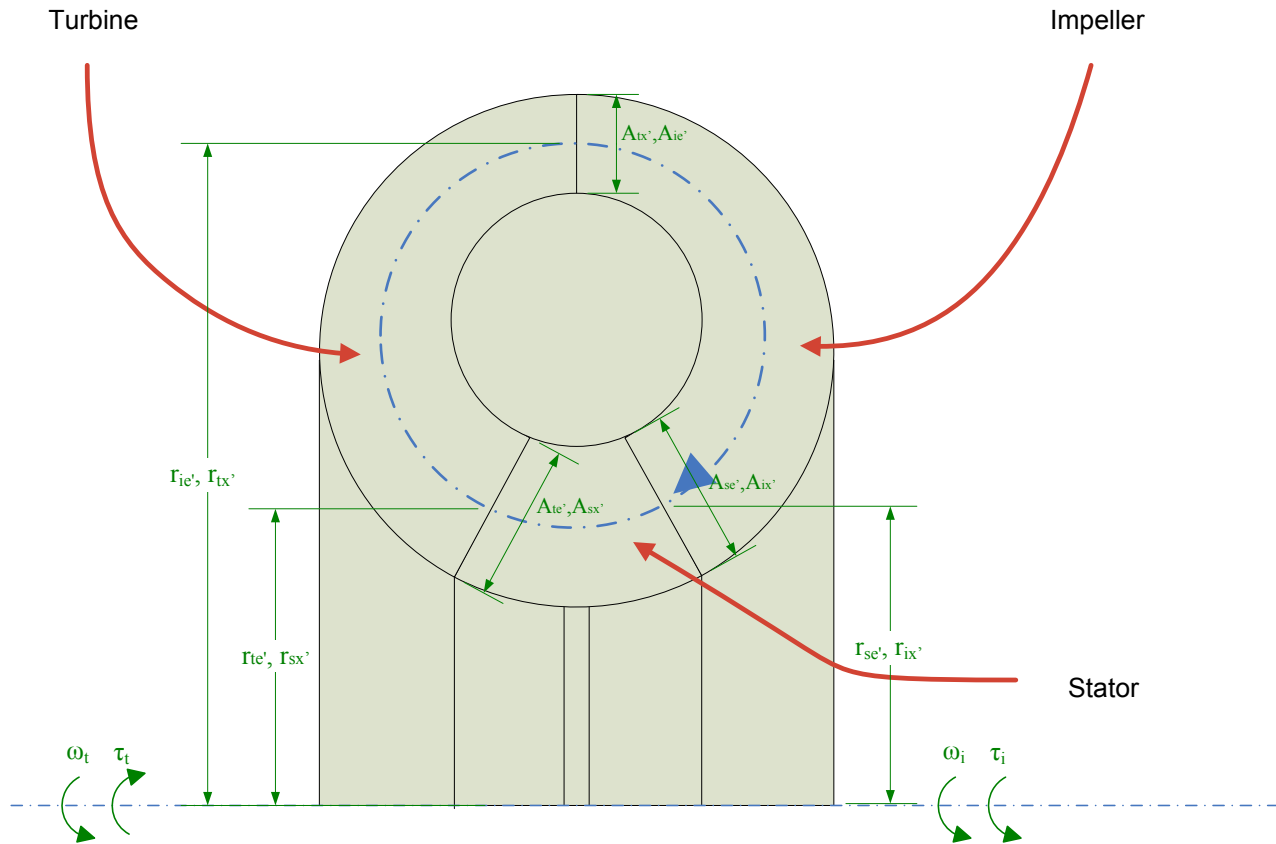

Figure 3-4, Negative Flow Geometry

As a result, values that were once entrance values become exit values and so forth. Not only do the angles on the blades change from entrance to exit, but the side of the blade the fluid first approaches changes also. For this reason, the angles may not simply be inverted as was done in modeling by Hrovat and Tobler(Hrovat 1985). This is a unique contribution.

Using a similar method to that used for the positive regimes but using the flow direction and variables shown in Figure 3-4, we arrive at the following relations for torque and flow:

$$\tau_i = \rho Q(\omega_i r'^2_{ix} - \omega_t r'^2_{tx}) + \rho Q^2 \left(\frac{r'_{ix} \tan \alpha'_{ix}}{A_{ix}} - \frac{r'_{tx} \tan \alpha'_{tx}}{A_{tx}} \right) \tag{3.41}$$

$$\tau_t = - \left(\rho Q(\omega_t r'^2_{tx} - \omega_s r'^2_{sx}) + \rho Q^2 \left(\frac{r'_{tx} \tan \alpha'_{tx}}{A'_{tx}} - \frac{r_{sx} \tan \alpha'_{sx}}{A'_{sx}} \right) \right) \tag{3.42}$$

$$\tau_s = \rho Q(\omega_s r'^2_{sx} - \omega_i r'^2_{ix}) + \rho Q^2 \left(\frac{r'_{sx} \tan \alpha'_{sx}}{A'_{sx}} - \frac{r'_{ix} \tan \alpha'_{ix}}{A'_{ix}} \right) = 0 \tag{3.43}$$

Taking advantage of the stator torque being zero provides a substitute for the stator speed.

$$\omega_s = \frac{Q \left(\frac{r'_{ix} \tan \alpha'_{ix}}{A'_{ix}} + \frac{r'_{sx} \tan \alpha'_{sx}}{A'_{sx}} \right) + \omega_i r'^2_{ix}}{r'^2_{sx}} \tag{3.44}$$

Equation 3.44 can then be placed back into the turbine torque and simplified to become Equation 3.45 and 3.46.

$$\tau_t = \rho Q \left(\omega_t r'^2_{tx} - \frac{Q \left(\frac{r'_{ix} \tan \alpha'_{ix}}{A_{ix}} + \frac{r'_{sx} \tan \alpha'_{sx}}{A_{sx}} \right) + \omega_i r'^2_{ix}}{r'^2_{sx}} r'^2_{sx} \right)$$
$$+ \rho Q^2 \left(\frac{r'_{tx} \tan \alpha'_{tx}}{A'_{tx}} - \frac{r'_{sx} \tan \alpha'_{sx}}{A'_{sx}} \right) \tag{3.45}$$

or

$$\tau_t = \rho Q(\omega_t r'^2_{tx} - \omega_i r'^2_{ix}) + \rho Q^2 \left(\frac{r'_{tx} \tan \alpha'_{tx}}{A'_{tx}} - \frac{r'_{ix} \tan \alpha'_{ix}}{A'_{ix}} \right) \tag{3.46}$$

Based on the known performance of torque converters above the coupling point, this validates the result, as a torque converter is known to behave as a torque coupling at speeds above the coupling point(Avallone et al.). Note that the torque of the impeller is equal to the torque of the turbine. Similar to the method used in the prior regimes, each of the torques is converted to a pressure change as shown in Equations 3.47 and 3.48.

$$\Delta p_t = \rho \omega_t (\omega_t r'^2_{tx} + \omega_i r'^2_{ix}) + \rho \omega_t Q \left(\frac{r'_{tx} \tan \alpha'_{tx}}{A_{tx}} - \frac{r'_{ix} \tan \alpha'_{ix}}{A_{ix}} \right) \tag{3.47}$$

$$\Delta p_i = - \left(\rho \omega_i (\omega_i r'^2_{ix} - \omega_t r'^2_{tx}) + \rho \omega_i Q \left(\frac{r'_{ix} \tan \alpha'_{ix}}{A'_{ix}} - \frac{r'_{tx} \tan \alpha'_{tx}}{A'_{tx}} \right) \right) \tag{3.48}$$

Each of these pressures must now be equated to the determined pressure losses of flow and shock losses as shown below.

$$\Delta p_{sl\ t-i} = \frac{1}{2} \rho \left[Q \left(\frac{\tan \alpha'_{tx}}{A'_{tx}} - \frac{\tan \alpha'_{ie}}{A'_{ie}} \right) + r'_{tx} \omega_t - r'_{ie} \omega_i \right]^2 \tag{3.49}$$

$$\Delta p_{sl\ i-s} = \frac{1}{2} \rho \left[Q \left(\frac{\tan \alpha'_{ix}}{A'_{ix}} - \frac{\tan \alpha'_{se}}{A'_{se}} \right) + r'_{ix} \omega_i - r'_{se} \omega_s \right]^2 \tag{3.50}$$

$$\Delta p_{sl\ s-t} = \frac{1}{2} \rho \left[Q \left(\frac{\tan \alpha'_{sx}}{A'_{sx}} - \frac{\tan \alpha'_{te}}{A'_{te}} \right) + r'_{sx} \omega_s - r'_{te} \omega_t \right]^2 \tag{3.51}$$

39

$$\Delta p_f = \frac{1}{2}\rho C_f Q^2 \tag{3.52}$$

The resulting compatibility equation is therefore the following:

$$\rho\omega_t(r'^2_{tx}\omega_t - r'^2_{ix}\omega_i) + \rho\omega_t Q\left(\frac{r'_{tx}\tan\alpha'_{tx}}{A'_{tx}} - \frac{r'_{ix}\tan\alpha'_{ix}}{A'_{ix}}\right) - \rho\omega_i(r'^2_{ix}\omega_i - $$

$$r'^2_{tx}\omega_t) - \rho\omega_i Q\left(\frac{r'_{ix}\tan\alpha'_{ix}}{A'_{ix}} - \frac{r'_{tx}\tan\alpha'_{tx}}{A'_{tx}}\right) = \frac{1}{2}\rho\left[Q\left(\frac{\tan\alpha'_{tx}}{A'_{tx}} - \frac{\tan\alpha'_{ie}}{A'_{ie}}\right) + \right.$$

$$\left. r'_{tx}\omega_t - r'_{ie}\omega_i\right]^2 + \frac{1}{2}\rho\left[Q\left(\frac{\tan\alpha'_{ix}}{A'_{ix}} - \frac{\tan\alpha'_{se}}{A'_{se}}\right) + r'_{ix}\omega_i - r'_{se}\omega_s\right]^2 + \tag{3.53}$$

$$\frac{1}{2}\rho\left[Q\left(\frac{\tan\alpha'_{sx}}{A'_{sx}} - \frac{\tan\alpha'_{te}}{A'_{te}}\right) + r'_{sx}\omega_s - r'_{te}\omega_t\right]^2 + \frac{1}{2}\rho C_f Q^2$$

Which can be manipulated using a mathematical package such as Maple in this regime. The Maple session is included in Appendix A, to find the subscripts for Q as shown in Equation 3.54. Note that all angles, radii and areas refer to the negative regimes although not noted.

$$\left(\frac{1}{2}\, \rho \left(\frac{\tan\left(\alpha_{ix}\right)}{A_{ix}} - \frac{\tan\left(\alpha_{se}\right)}{A_{se}} - \frac{\left(\frac{r_{ix}\tan\left(\alpha_{ix}\right)}{A_{ix}} - \frac{r_{sx}\tan\left(\alpha_{sx}\right)}{A_{sx}} \right) r_{se}}{r_{sx}^2} \right)^2 \right.$$

$$+ \frac{1}{2}\, \rho \left(\frac{\tan\left(\alpha_{tx}\right)}{A_{tx}} - \frac{\tan\left(\alpha_{ie}\right)}{A_{ie}} \right)^2 + \frac{1}{2}\, \rho \left(\frac{\tan\left(\alpha_{sx}\right)}{A_{sx}} - \frac{\tan\left(\alpha_{te}\right)}{A_{te}} \right.$$

$$\left. + \frac{\frac{r_{ix}\tan\left(\alpha_{ix}\right)}{A_{ix}} - \frac{r_{sx}\tan\left(\alpha_{sx}\right)}{A_{sx}}}{r_{sx}} \right)^2 \left. + \frac{1}{2}\, \rho\, cf \right] Q^2 + \left(\rho \left(\varpi_t\, r_{tx} \right. \right.$$

$$- \varpi_i\, r_{ie} \right) \left(\frac{\tan\left(\alpha_{tx}\right)}{A_{tx}} - \frac{\tan\left(\alpha_{ie}\right)}{A_{ie}} \right) - \rho \left(\frac{r_{tx}\tan\left(\alpha_{tx}\right)}{A_{tx}} - \frac{r_{ix}\tan\left(\alpha_{ix}\right)}{A_{ix}} \right) \varpi$$

$$+ \rho \left(\frac{\varpi_i\, r_{ix}^2}{r_{sx}} - \varpi_t\, r_{te} \right) \left(\frac{\tan\left(\alpha_{sx}\right)}{A_{sx}} - \frac{\tan\left(\alpha_{te}\right)}{A_{te}} \right. \qquad (3.54)$$

$$\left. + \frac{\frac{r_{ix}\tan\left(\alpha_{ix}\right)}{A_{ix}} - \frac{r_{sx}\tan\left(\alpha_{sx}\right)}{A_{sx}}}{r_{sx}} \right) + \rho \left(\varpi_i\, r_{ix} - \frac{\varpi_i\, r_{ix}^2\, r_{se}}{r_{sx}^2} \right) \left(\frac{\tan\left(\alpha_{ix}\right)}{A_{ix}} \right.$$

$$\left. - \frac{\tan\left(\alpha_{se}\right)}{A_{se}} - \frac{\left(\frac{r_{ix}\tan\left(\alpha_{ix}\right)}{A_{ix}} - \frac{r_{sx}\tan\left(\alpha_{sx}\right)}{A_{sx}} \right) r_{se}}{r_{sx}^2} \right) + \rho \left(\frac{r_{ix}\tan\left(\alpha_{ix}\right)}{A_{ix}} \right.$$

$$\left. \left. - \frac{r_{tx}\tan\left(\alpha_{tx}\right)}{A_{tx}} \right) \varpi_i \right) Q + \frac{1}{2}\, \rho \left(\varpi_t\, r_{tx} - \varpi_i\, r_{ie} \right)^2 + \frac{1}{2}\, \rho \left(\frac{\varpi_i\, r_{ix}^2}{r_{sx}} \right.$$

$$\left. - \varpi_t\, r_{te} \right)^2 + \frac{1}{2}\, \rho \left(\varpi_i\, r_{ix} - \frac{\varpi_i\, r_{ix}^2\, r_{se}}{r_{sx}^2} \right)^2 - \rho \left(\varpi_t\, r_{tx}^2 - \varpi_i\, r_{ix}^2 \right) \varpi_t$$

$$+ \rho \left(\varpi_i\, r_{ix}^2 - \varpi_t\, r_{tx}^2 \right) \varpi_i$$

Extracting coefficients from the compatibility equation gives:

$$A_3 = \frac{1}{2}\,\rho\left(\frac{\tan(\alpha_{ix})}{A_{ix}} - \frac{\tan(\alpha_{se})}{A_{se}} - \frac{\left(\dfrac{r_{ix}\tan(\alpha_{ix})}{A_{ix}} - \dfrac{r_{sx}\tan(\alpha_{sx})}{A_{sx}}\right)r_{se}}{r_{sx}^2}\right)^2$$

$$+ \frac{1}{2}\,\rho\left(\frac{\tan(\alpha_{tx})}{A_{tx}} - \frac{\tan(\alpha_{ie})}{A_{ie}}\right)^2 + \frac{1}{2}\,\rho\left(\frac{\tan(\alpha_{sx})}{A_{sx}} - \frac{\tan(\alpha_{te})}{A_{te}}\right.$$

$$\left. + \frac{\dfrac{r_{ix}\tan(\alpha_{ix})}{A_{ix}} - \dfrac{r_{sx}\tan(\alpha_{sx})}{A_{sx}}}{r_{sx}}\right)^2 + \frac{1}{2}\,\rho\,cf \tag{3.55}$$

$$B_3 = \rho\left(\varpi_t\,r_{tx} - \varpi_i\,r_{ie}\right)\left(\frac{\tan(\alpha_{tx})}{A_{tx}} - \frac{\tan(\alpha_{ie})}{A_{ie}}\right) - \rho\left(\frac{r_{tx}\tan(\alpha_{tx})}{A_{tx}}\right.$$

$$\left. - \frac{r_{ix}\tan(\alpha_{ix})}{A_{ix}}\right)\varpi_t + \rho\left(\frac{\varpi_i\,r_{ix}^2}{r_{sx}} - \varpi_t\,r_{te}\right)\left(\frac{\tan(\alpha_{sx})}{A_{sx}} - \frac{\tan(\alpha_{te})}{A_{te}}\right.$$

$$\left. + \frac{\dfrac{r_{ix}\tan(\alpha_{ix})}{A_{ix}} - \dfrac{r_{sx}\tan(\alpha_{sx})}{A_{sx}}}{r_{sx}}\right) + \rho\left(\varpi_i\,r_{ix} - \frac{\varpi_i\,r_{ix}^2\,r_{se}}{r_{sx}^2}\right)\left(\frac{\tan(\alpha_{ix})}{A_{ix}}\right.$$

$$\left. - \frac{\tan(\alpha_{se})}{A_{se}} - \frac{\left(\dfrac{r_{ix}\tan(\alpha_{ix})}{A_{ix}} - \dfrac{r_{sx}\tan(\alpha_{sx})}{A_{sx}}\right)r_{se}}{r_{sx}^2}\right) + \rho\left(\frac{r_{ix}\tan(\alpha_{ix})}{A_{ix}}\right.$$

$$\left. - \frac{r_{tx}\tan(\alpha_{tx})}{A_{tx}}\right)\varpi_i \tag{3.56}$$

$$C_3 = \frac{1}{2}\,\rho\left(\varpi_t\,r_{tx} - \varpi_i\,r_{ie}\right)^2 + \frac{1}{2}\,\rho\left(\frac{\varpi_i\,r_{ix}^2}{r_{sx}} - \varpi_t\,r_{te}\right)^2 + \frac{1}{2}\,\rho\left(\varpi_i\,r_{ix}\right.$$

$$\left. - \frac{\varpi_i\,r_{ix}^2\,r_{se}}{r_{sx}^2}\right)^2 - \rho\left(\varpi_t\,r_{tx}^2 - \varpi_i\,r_{ix}^2\right)\varpi_t + \rho\left(\varpi_i\,r_{ix}^2 - \varpi_t\,r_{tx}^2\right)\varpi_i \tag{3.57}$$

After substitution Equation 3.53 represents itself as a simple quadratic equation:

$$A_3 Q^2 + B_3 Q + C_3 = 0 \tag{3.58}$$

With the solution for Q of:

42

$$Q = \frac{-B_3 + \sqrt{B_3^2 - 4A_3 C_3}}{2A_3}$$
(3.59)

At this point, all three regimes are developed as a system of three equations (Q, τ_i, and τ_t) and of five variables (Q, τ_i, τ_t, ω_i, and ω_t) and can be fully characterized, albeit with fairly complex relations. In the next section, we will develop relationships that are more useful in modeling.

3.3. Model Application

Complex relationships of ω_i, ω_t, τ_i, and τ_t were developed in the previous section. These results can now be recast to establish a means whereby knowing any two of the values, the others can be found and used in control algorithms or vehicle modeling. As discussed in the previous section, there are three distinct regimes of flow within the torque converter. The three regimes are as follows:

- Regime 1: This is where the secondary flow rate is normal (flowing from impeller to turbine) and the torque converter is multiplying torque. In this regime the stator is locked due to the flow of the fluid around the converter, this locked stator enables torque multiplication. This is seen in speed ratios of 0 up to approximately 90% depending on the design of the specific converter. This point where the shift occurs is termed the "coupling" point.

- Regime 2: Above the coupling point, the secondary flow rate is still positive, but the flow rate becomes small enough for the net resulting torque to be zero. As the point the reaction on the stator becomes zero and further reductions actually lead the stator to turn. The speed ratios in this regime are above the coupling point but still below one.

- Regime 3: In this regime, the torque is flowing from the turbine to the impeller, and the speed ratio is greater than one. This results in a negative secondary flow rate (Q).

A convenient way to understand the nature of these three modes is in a plot of the torque ratio as a function of speed ratio as shown in Figure 3-5.

While in the previous section the relationships between flow, torque and speed were developed, none of these relationships is of a form that can be readily used in modeling or control, since they are still deeply intertwined. In this specific example, we are seeking to determine the losses in the converter when a bus is driven on a particular cycle.
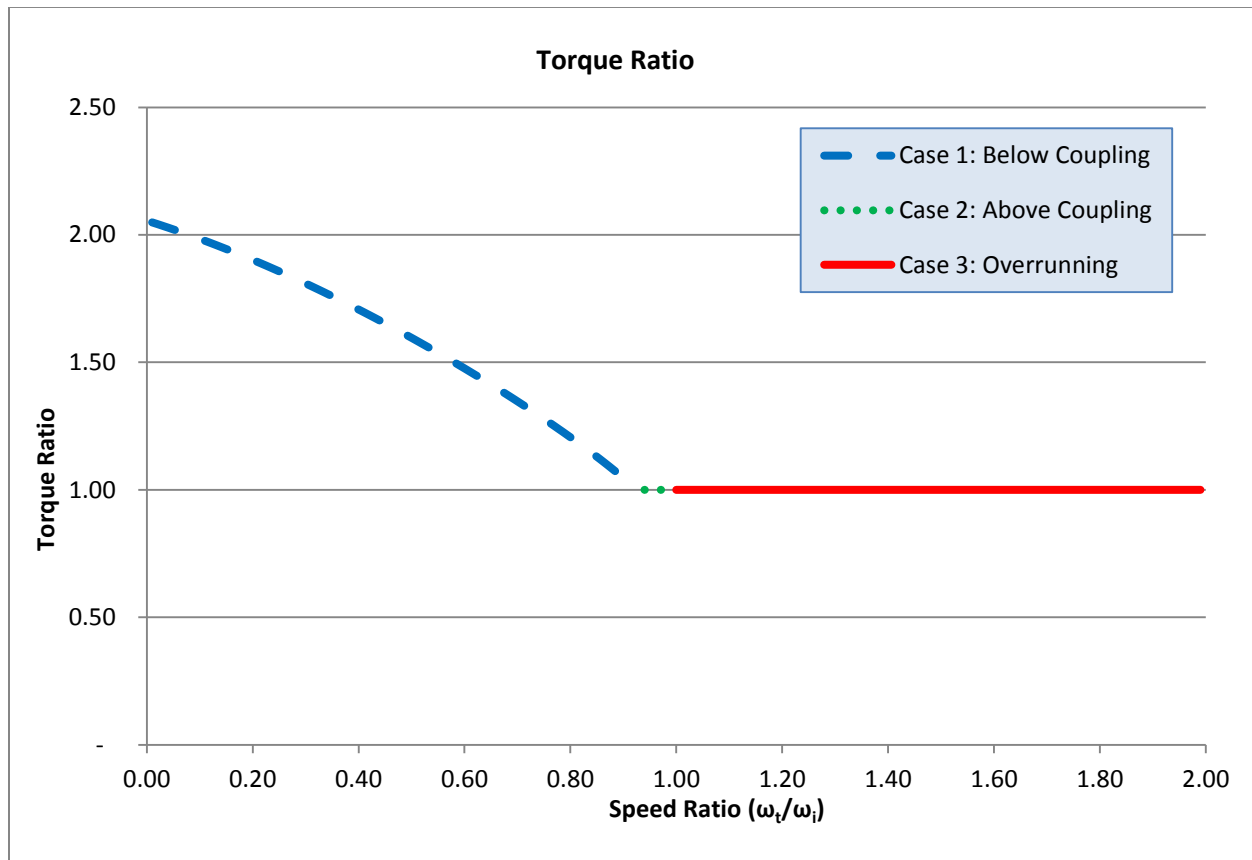

Figure 3-5, Torque and Speed Ratio of the Three Distinct Modes

The modeling used in this case is ADVISOR, which is a backwards facing model where the torque and speed of the turbine is known and the torque and speed of the impeller is needed. Another is the case of a forward facing model such as PSAT, where the torque and speed of the

engine is known, and the torque and speed of the turbine, or transmission is needed. Finally there are the cases of low cost instrumentation and control where speed is known for both sides but the torque is not. Table 3-1 shows the four distinct models possible.

Table 3-1, Torque Converter Models

Model	Knowns	Unknowns	Possible Application
1	τ_t, ω_t	$Q, \tau_i, \omega_i,$	Backward Facing Model (ADVISOR)
2	τ_i, ω_i	Q, τ_t, ω_t	Forward Facing Model (PSAT)
3	ω_i, ω_t	$Q, \tau_i, \tau_t,$	Low Cost Controls
4	τ_i, τ_t	Q, ω_i, ω_t	Experimentation

Based on each of the first three cases, a different set of steps can be used to determine the needed unknowns. In the fourth case, the determination of speeds from torque, the singular nature of the torque ratio makes this evaluation impossible.

Another relevant feature of Figure 3-5 is the torque ratio value at the intersection of the y-axis. This point is called the stall ratio. Published data on the Allison TC-210(Allison Transmission 1) indicates that this value is 2.05. The calculated value of this ratio is 2.0546, as shown in trf_c in Table 3-3, which provides a high validation of the geometry used in this study.

This relationship of torque and speed is strongly dependent on the flow rate and direction of the fluid flowing in secondary rotation about the torque converter. From the previous section, we established clear relationships where this flow rate can be established for all speed ratios based entirely on the torque converter geometry. A detailed survey of the geometry and measurements

was conducted on the Allison TC-210 torque converter by taking measurements from a disassembled unit to determine the data presented in **Error! Reference source not found.**.

Table 3-2, Allison Transmission TC-210 Torque Converter Geometry

Variable	Value	Variable	Value	Variable	Value
α_{ie}	0°	r_{ie}	0.0778 m	A_{ie}	0.019 m^2
α_{ix}	38°	r_{ix}	0.1365 m	A_{ix}	0.022 m^2
α_{te}	45°	r_{te}	0.1365 m	A_{te}	0.022 m^2
α_{tx}	-45°	r_{tx}	0.0778 m	A_{tx}	0.019 m^2
α_{se}	43°	r_{se}	0.0778 m	A_{se}	0.019 m^2
α_{sx}	75°	r_{sx}	0.0778 m	A_{sx}	0.019 m^2
$\acute{\alpha}_{ie}$	38°	$\acute{r}_{ie}$	0.1365 m	$\acute{A}_{ie}$	0.022 m^2
$\acute{\alpha}_{ix}$	0°	$\acute{r}_{ix}$	0.0778 m	$\acute{A}_{ix}$	0.019 m^2
$\acute{\alpha}_{te}$	-45°	$\acute{r}_{te}$	0.0778 m	$\acute{A}_{te}$	0.019 m^2
$\acute{\alpha}_{tx}$	45°	$\acute{r}_{tx}$	0.1365 m	$\acute{A}_{tx}$	0.022 m^2
$\acute{\alpha}_{se}$	75°	$\acute{r}_{se}$	0.0778 m	$\acute{A}_{se}$	0.019 m^2
$\acute{\alpha}_{sx}$	10°	$\acute{r}_{sx}$	0.0778 m	$\acute{A}_{sx}$	0.019 m^2

The intent of this work is to more fully understand the conditions that occur in the post transmission hybrid system in the plug-in hybrid electric school buses. In this case, the specific variables from the torque converter used in the Allison 2000 PTS transmission has the geometry listed in . In this study, all calculations of regime three refer to the prime values shown in the table because of the negative flow rate.

Figure 3-6 shows the resulting flow rate as a function of speed ratio. While the torque ratio versus speed ratio presents a singularity at all speed ratios above the coupling point, the flow rate

is distinct across all speed ratios. The three regimes show a smooth transition from positive to negative, although the calculations are undefined at the speed ratio of 1.
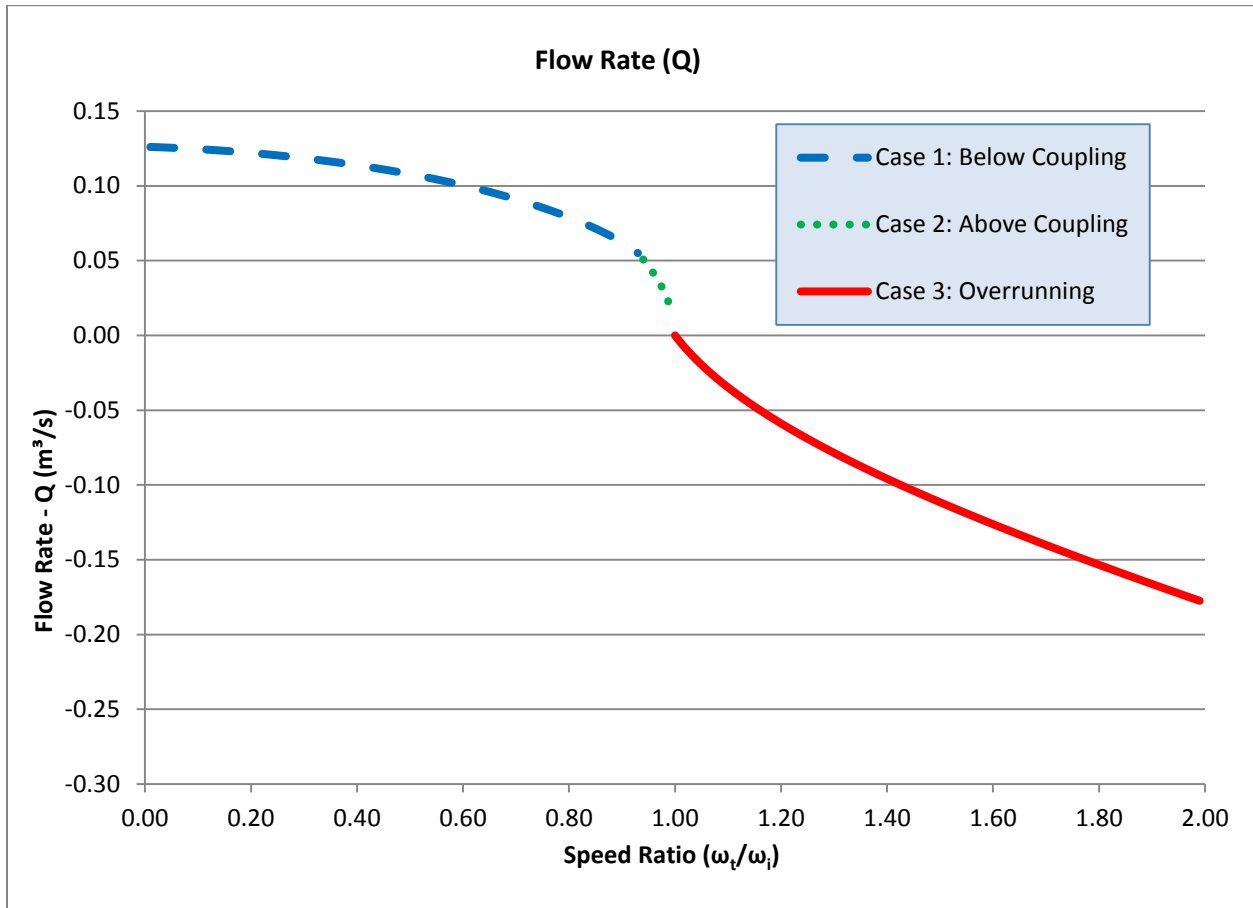

Figure 3-6, Flow Rate versus Speed Ratio for Torque Converter

3.3.2. Known Turbine Conditions (backwards facing models)

In modeling of a vehicle there are several different model approaches. A backward facing model begins with a vehicle velocity trace and determines the needed torque and speed at the wheels, which in turn dictates the needed torque and speed at the axles and final drive. The model of a torque converter in this case will require that ω_t, τ_t are known and we need to develop relations for ω_i and τ_i. In this case, we can partially nondimensionalize the converter by establishing the performance of each mode as a function of SR and τ_t/ω_i^2 using the equations developed earlier. In this case each of these curves is a polynomial relationship of the characteristic form show in Equation 3.60 and individual polynomial curve fits can be determined for each mode where x is either 1, 2, or 3 depending on the mode.

$$\frac{\tau_i}{\omega_i^2} = k_{xa}SR^2 + k_{xb}SR + k_{xc} \tag{3.60}$$

These resulting curves are shown in Figure 3-7 for the specific torque converter selected in this study.
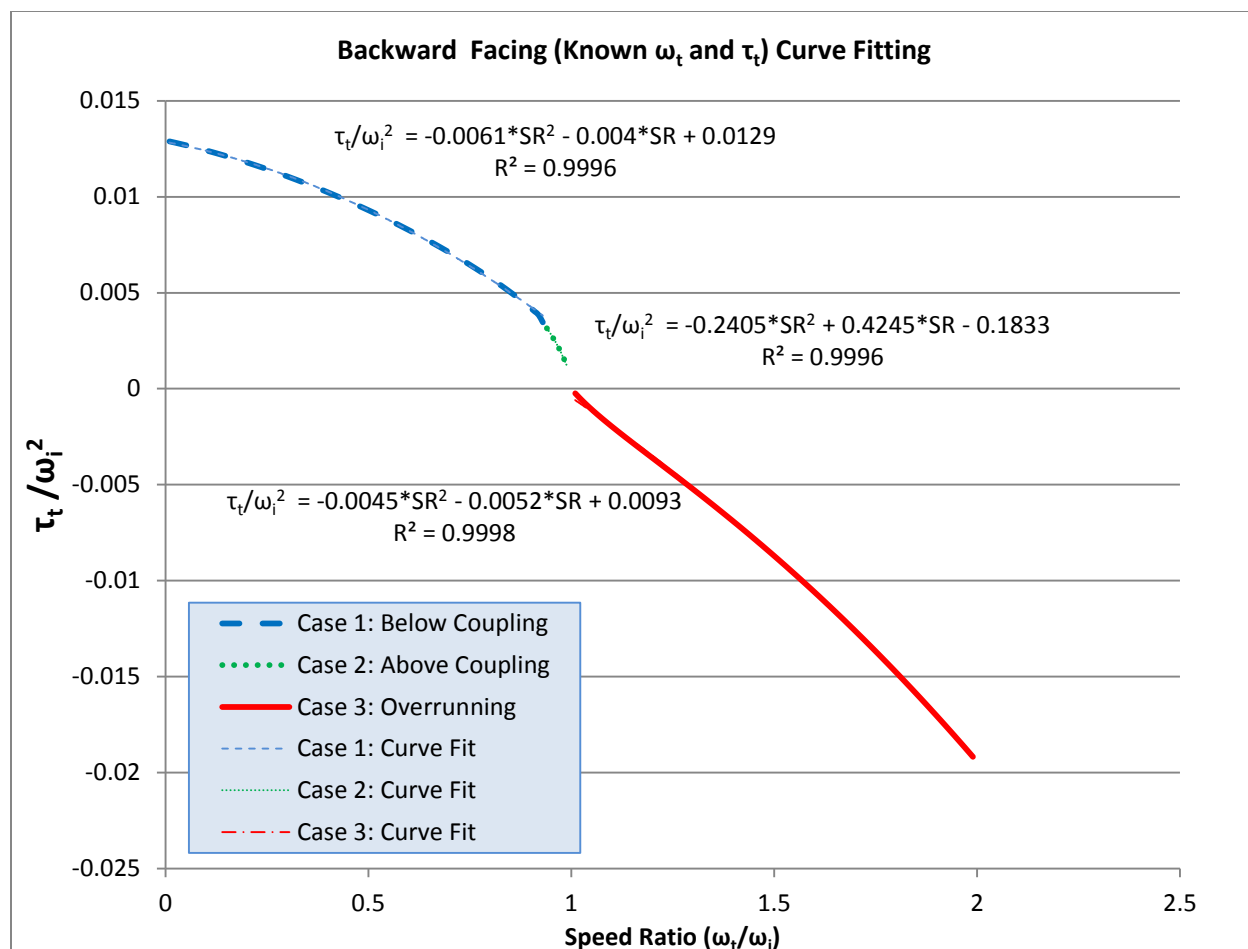
Figure 3-7, Torque Converter Performance Curve Fit for Case of Known Turbine Conditions

As shown in Figure 3-7, each of these curves has a well-fitting second order polynomial for the base curve with an R^2 value exceeding 99.9%. By knowing these curves, an algorithm was developed to determine the impeller speed and torque from the following process.

Table 3-3, Curve Fit Coefficients Developed for the Allison TC-210 Converter

Regime	a value	b value	c value	R^2
1	k_{1a}=-0.0068	k_{1b}=-0.0048	k_{1c}=0.0148	0.9998
2	k_{2a}=-0.1631	k_{2b}=0.2715	k_{2c}=-0.1070	0.9999
3	k_{3a}=-0.0064	k_{3b}=-0.0054	k_{3c}=0.0094	0.9996
torque	trf_a=-0.5017	trf_b=-0.6634	trf_c=2.0546	0.9999

In addition to determining the coefficients each case for speed ratio, a curve fit must be determined for the torque ratio for Regime 1 as torque is multiplied in this case. This curve fit is shown in Figure 3-8.
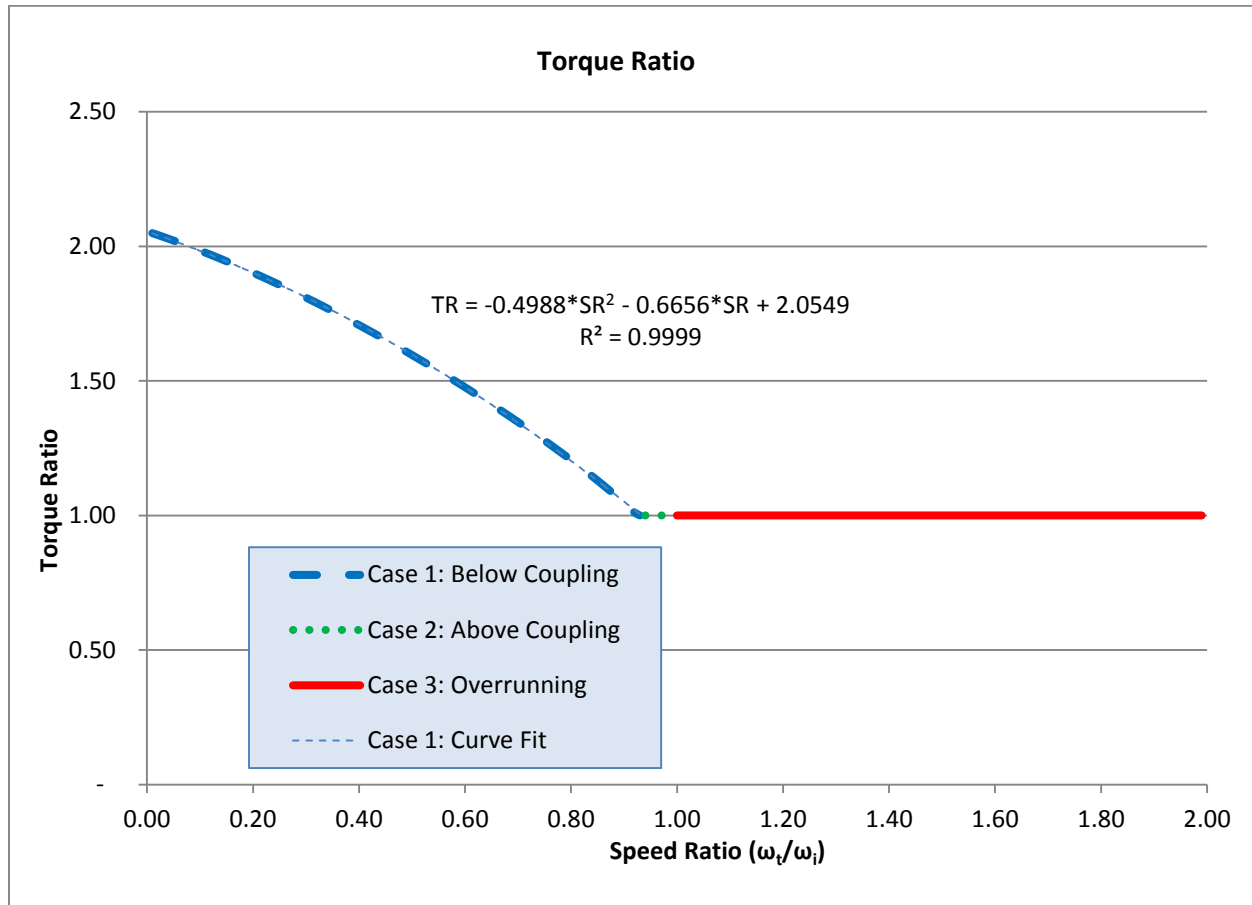

Figure 3-8, Torque Ratio Curve Fitting

Once these curve fits are established the following procedure must be followed:

1. Look at the sign of the torque, if it is negative, then move to step 10 for regime 3.

2. If the torque is positive, the converter must be in regimes 1 or 2.

3. Test first for ω_i assuming regime 1 by using equation 3.61.

$$\omega_i = \frac{-k_{1a}\omega_t + \sqrt{(k_{1b}\omega_t)^2 - 4k_{1c}(k_{1a}\omega_t^2 - \tau_t)}}{2k_{1a}} \tag{3.61}$$

4. Find the speed ratio (SR). If this speed ratio is greater than one, then skips steps 5, 6 and 7 and proceed to 8.

$$SR = \frac{\omega_t}{\omega_i} \tag{3.62}$$

5. Use the speed ratio to determine the torque by using equation 3.63.

$$\tau_i = \frac{\tau_t}{trf_a SR^2 + trf_b SR + trf_c} \tag{3.63}$$

6. Determine the torque ratio (TR)

$$TR = \frac{\tau_t}{\tau_i} \tag{3.64}$$

7. If the torque ratio is greater than one, then this is the correct torque and speed and the calculation is complete, otherwise the converter is coupled and proceed to step 8.

8. To determine the coupled speed, reevaluate the speed using the second regime curve fit.

$$\omega_i = \frac{-k_{2b}\omega_t + \sqrt{(k_{2b}\omega_t)^2 - 4k_{2c}(k_{2a}\omega_t^2 - \tau_t)}}{2k_{2c}} \tag{3.65}$$

9. Set the $\tau_t = \tau_i$ as the torque ratio is equal to one.

10. If SR is less than 1, the calculation is complete. If the torque was negative, then also set $\tau_t = \tau_i$ as the torque ratio is one. Determine the impeller speed with equation 3.66

$$\omega_i = \frac{-k_{3b}\omega_t + \sqrt{(k_{3b}\omega_t)^2 - 4k_{3c}(k_{3a}\omega_t^2 - \tau_t)}}{2k_{3c}} \qquad (3.66)$$

The impeller conditions are now established for all turbine torques and speeds and this procedure can be implemented in a modeling tool such as ADVISOR as will be shown later in sections of this study.

Figure 3-9, Known Turbine Conditions Model Results
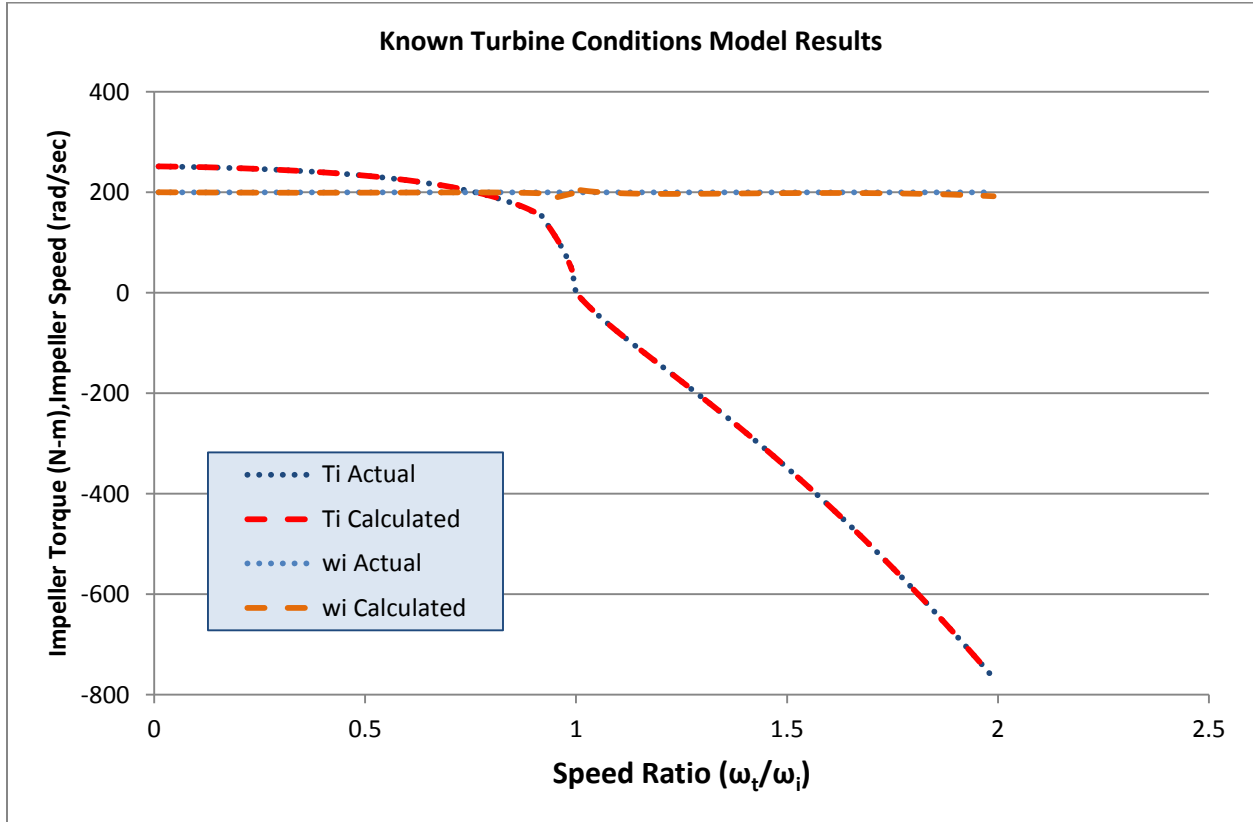
All models in this study are driven by speed ratio where the impeller speed is fixed and the turbine speed is varied to achieve a full spectrum of ratios. Results on other impeller speeds are similar. As shown in Figure 3-9 the calculated torques and speeds begin to deviate at the transitions from one regime to the next, but overall fit is well within expectations.

53

3.3.3. Known Impeller Conditions (forward facing models)

In the case of a forward facing model ω_i, τ_i are known and we need to develop relations for turbine speed and torque. Like the other cases three distinct curve fits are needed to determine the speed performance. In this case it is the function of the inverse of SR and τ_i/ω_t^2 as shown in Figure 3-10.
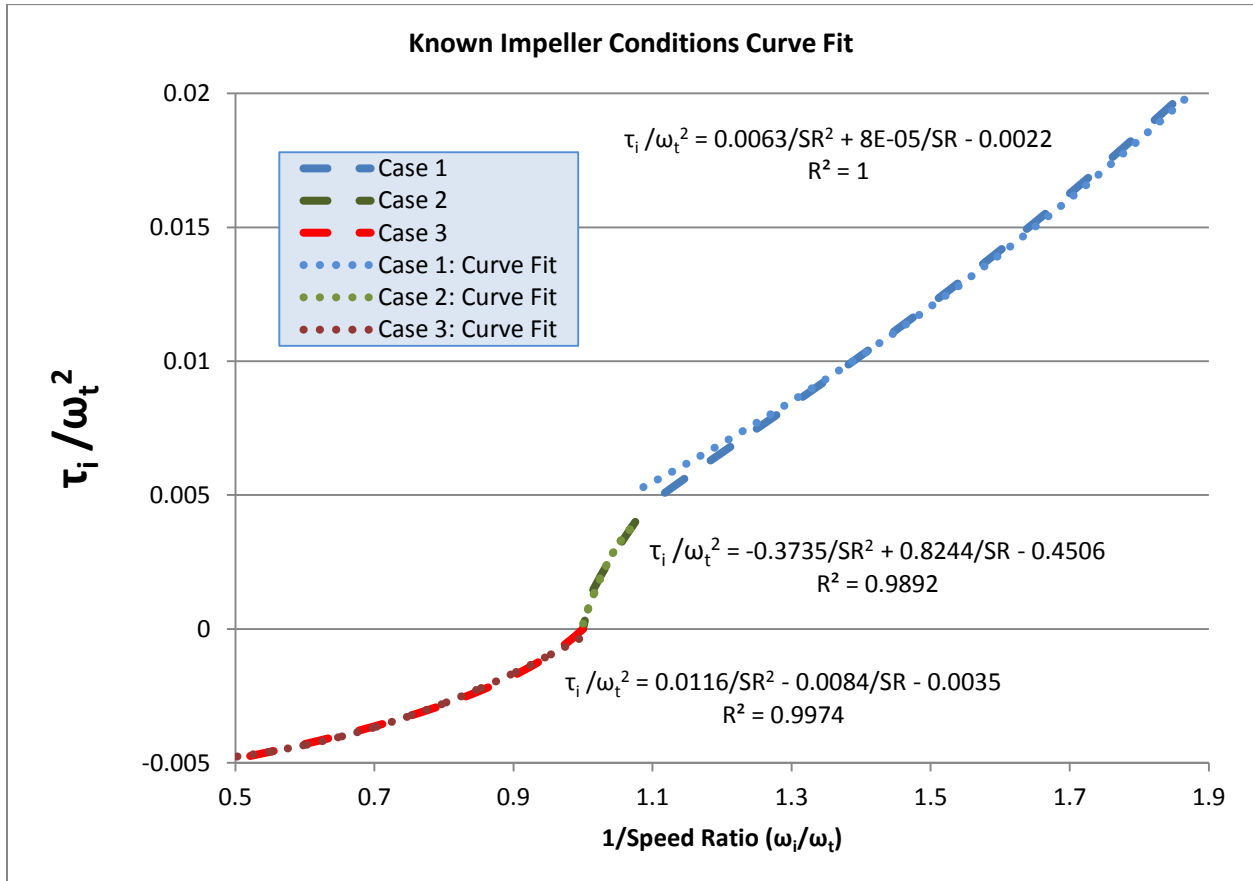

Figure 3-10, Forward Facing Curve Fits

The coefficients for the individual curve fits are presented in Table 3-4.

Table 3-4, Forward Facing Model Curve Fit Coefficients

Regime	a value	b value	c value	R^2
1	$k_{1a}=0.0063$	$k_{1b}=0.00008$	$k_{1c}=-0.0022$	0.9999
2	$k_{2a}=-0.3735$	$k_{2b}=0.8244$	$k_{2c}=-0.45$	0.9892
3	$k_{3a}=0.0116$	$k_{3b}=-0.0084$	$k_{3c}=-0.0035$	0.9974
1(torque)	$trf_a=-0.5017$	$trf_b=-0.6634$	$trf_c=2.0546$	0.9846

Much like the backward facing model, the following procedure can now be used to determine the turbine torque and speed.

1. Determine the direction of the torque, if negative, then move to step 6 for the Regime 3 approach.

2. For data where the torque is positive, assume Regime 1 and use the k_1 developed coefficients to determine the turbine speed according to 3.67

$$\omega_t = \frac{-k_{1b}\omega_i + \sqrt{(k_{1b}\omega_i)^2 - 4(k_{1a}\omega_i^2 - \tau_i)k_{1c}}}{2k_{1c}} \tag{3.67}$$

3. Knowing the turbine speed, determine the speed ratio

4. From the speed ratio, determine whether this is above the coupling point.

5. If the converter is determined to be above the coupling point, use the Regime 2 curve fit to determine speed.

$$\omega_t = \frac{-k_{2b}\omega_i + \sqrt{(k_{2b}\omega_i)^2 - 4(k_{2a}\omega_i^2 - \tau_i)k_{2c}}}{2k_{2c}} \tag{3.68}$$

6. For negative torque values, the speed can be calculated for Regime 3 by the following:

55

$$\omega_t = \frac{-k_{3b}\omega_i + \sqrt{(k_{3b}\omega_i)^2 - 4(k_{3a}\omega_i^2 - \tau_i)k_{3c}}}{2k_{3c}} \qquad (3.69)$$

7. The Speed Ratio can now be determined for each value using Equation 3.62

8. Using the determined SR, torque in each case can be determined using 3.70.

$$\tau_i = \frac{\tau_t}{trf_a SR^2 + trf_b SR + trf_c} \qquad (3.70)$$

With turbine torque and speed determined for any case the results of this approach are beneficial. As shown in Figure 3-11, these results are quite accurate for all conditions except for speed ratios in Regime 1 shortly before the transition to Regime 2.
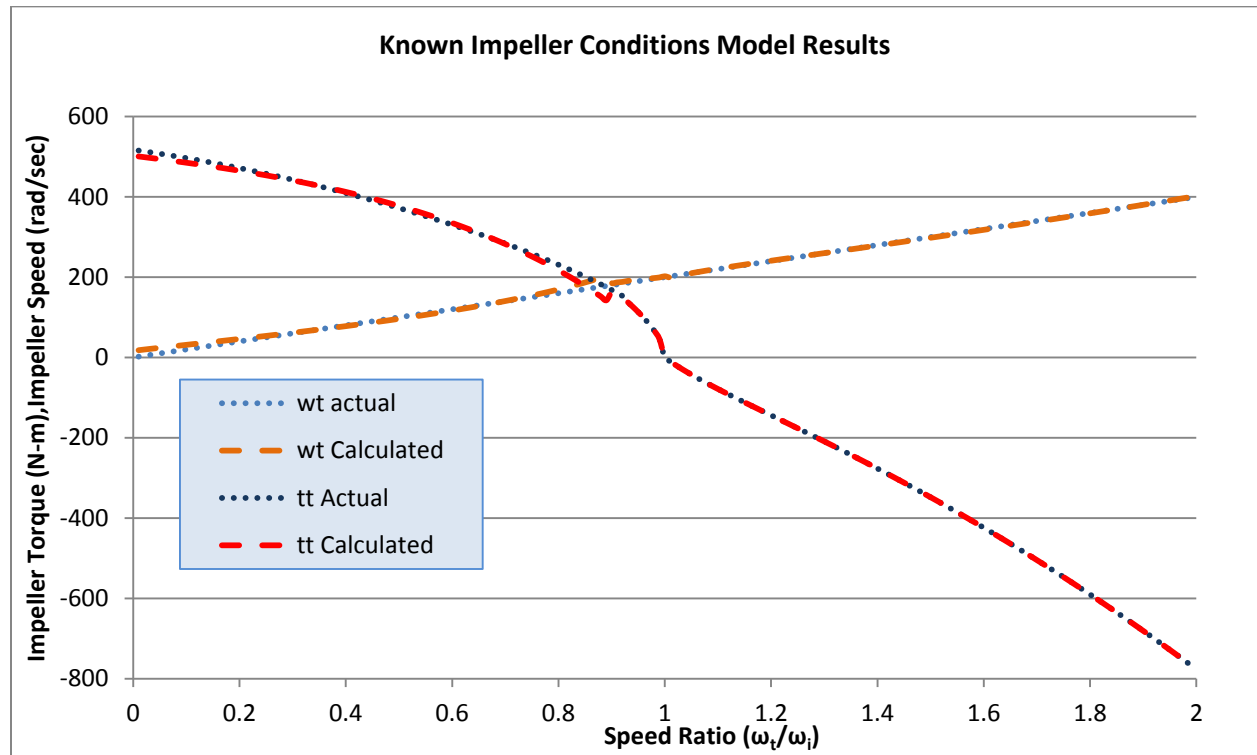
Figure 3-11, Known Impeller Conditions Results

3.3.4. Known Speeds

In the case of known speeds ω_i and ω_t are known and we need to develop relations for τ_i and τ_t. In this case, the speed ratio is also known. From this speed ratio, we can establish a series of curve fits for the flow rate Q. The flow rate curve fit and the already established torque can be used to determine the input and output torques.

Figure 3-12, Flow Rate Curve Fit

The determined coefficients from the curve fits are presented in Table 3-5.

Table 3-5, Flow Rate Curve Fit Coefficients

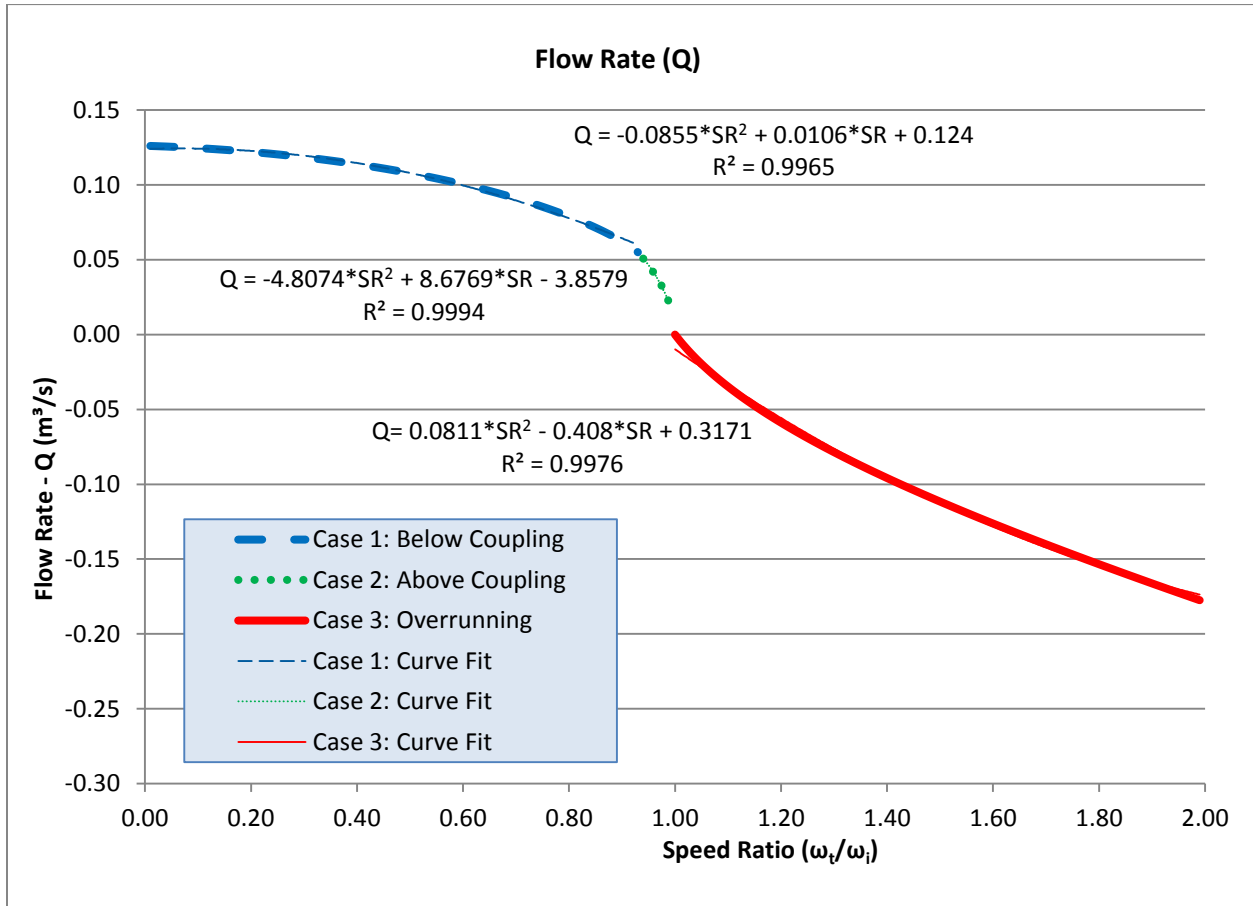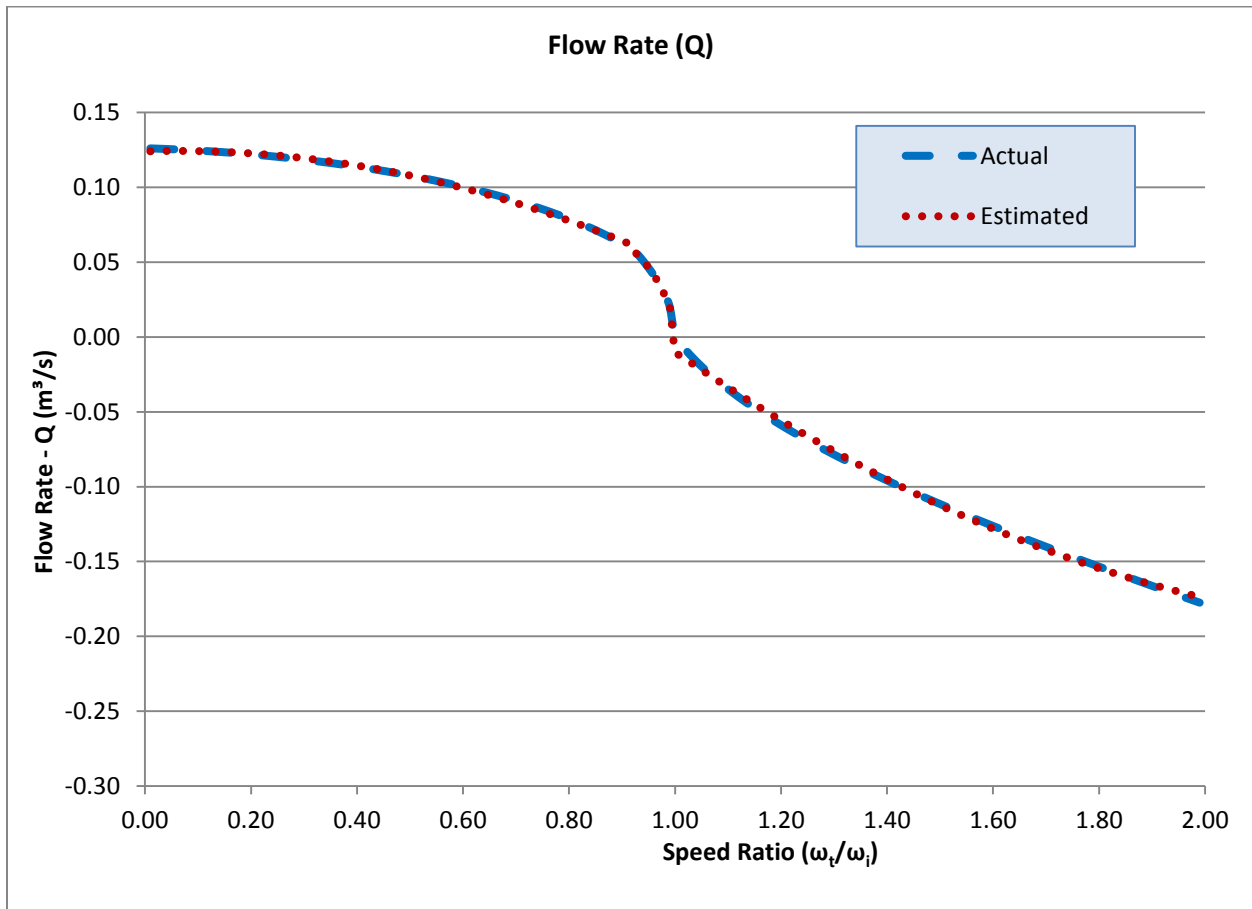| Regime	a value	b value	c value	R^2
1	k_{1a}=-0.0855	k_{1b}=0.0106	k_{1c}=0.124	0.9965
2	k_{2a}=-4.8074	k_{2b}=8.6769	k_{2c}=-3.8579	0.9994
3	k_{3a}=4.8074	k_{3b}=8.6769	k_{3c}=-3.8579	0.9976
1 (torque)	trf_a=-0.5017	trf_b=-0.6634	trf_c=2.0546	0.9846

Figure 3-13, Overall Flow Rate Curve Fit

Figure 3-13 shows that the overall estimated values for all three regimes. Note that the calculated curve fit flow rate has a high degree of accuracy across all Regimes.

58

The following procedure can now be used to determine the turbine and impeller speed.

1. Create a curve fit for all three Regimes of Q and the Regime 1 torque ratio. In this case, the values shown in Table 3-5 are used.

2. Determine the speed ratio and resulting regime.

3. Determine the torque ratio, for Regimes 2 and 3, TR=1. For regime 1, determine the torque ratio from Equation 3.71

$$TR = trf_a SR^2 + trf_b SR + trf_c \tag{3.71}$$

4. Determine Q from equation 3.72, where x is the regime determined.

$$Q = k_{xa} SR^2 + k_{xb} SR + k_{xc} \tag{3.72}$$

5. Determine impeller torque

$$\tau_{i1} = \rho Q(r_{ix}^2 \omega_i) + \rho Q^2 \left(\frac{r_{ix}\tan\alpha_{ix}}{A_{ix}} - \frac{r_{sx}\tan\alpha_{sx}}{A_{sx}} \right) \qquad \text{(regime 1)} \tag{3.73}$$

$$\tau_{i2} = \rho Q(r_{ix}^2 \omega_i - r_{tx}^2 \omega_t) + \rho Q^2 \left(\frac{r_{ix}\tan\alpha_{ix}}{A_{ix}} - \frac{r_{tx}\tan\alpha_{tx}}{A_{tx}} \right) \qquad \text{(regime 2)} \tag{3.74}$$

$$\tau_{i3} = \rho Q(\omega_i r'^2_{ix} - \omega_t r'^2_{tx}) + \rho Q^2 \left(\frac{r'_{ix}\tan\alpha_{ix'}}{A_{ix'}} - \frac{r_{tx'}\tan\alpha_{tx'}}{A_{tx'}} \right) \qquad \text{(regime 3)} \tag{3.75}$$

6. Turbine torque can now be found using the torque ratio

$$\tau_t = TR\tau_i \tag{3.76}$$

At this point we have determined the input and output torque of the converter based on the input and output speeds. Figure 3-14 shows the resulting calculation performance. The curve fits are determined to have a high degree of accuracy as shown in this Figure.
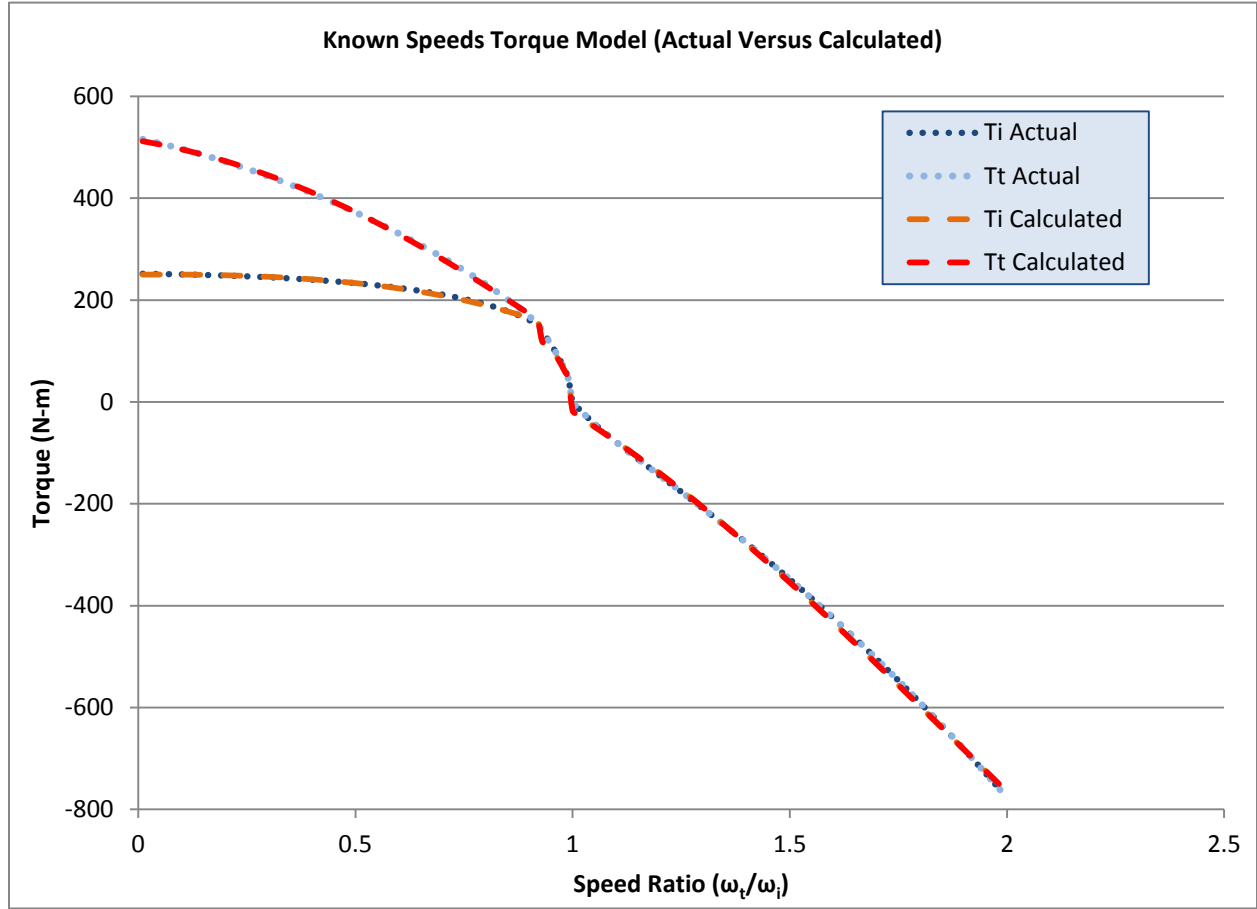
Figure 3-14, Determined Torques from a Known Speed Model

3.5. Model Implementation in ADVISOR

The primary intention of this work is to improve the accuracy of predictive models in the performance of plug-in hybrid school buses. As a result, these methods have been incorporated into ADVISOR to improve the accuracy of the system model. The original model created for the hybrid electric school buses was based on either pre-transmission hybrids, or manual post-transmission hybrids. A part of this work involved modifying the existing ADVISOR parallel driveline models to handle such a parallel post-transmission hybrid driveline with an automatic transmission and torque converter. shows the modified Simulink block. In this model, the manual parallel post transmission driveline was merged with the automatic standard driveline to create an automatic post transmission hybrid driveline.

As the changes to the driveline model also changed the model performance, two simultaneous models were run. One model is used as a control model with the same Simulink block and the as-built ADVISOR torque converter model and another with the newly modeled torque converter. The conventional ADVISOR blocks use lookup tables for the torque converter performance data. The lookup tables are populated from data tables provided by the user. The data studied here as a control unit is based on the standard data that is provided with ADVISOR. ADVISOR uses the torque converter data in two places; once for estimation of engine speed used for engine control and again for actual torque and speed fed from the transmission to the engine. Both blocksets, shown in Figure 3-16 and Figure 3-17, were modified in this study; the added torque converter model can be seen shaded. The contents of this block are included in the appendix.
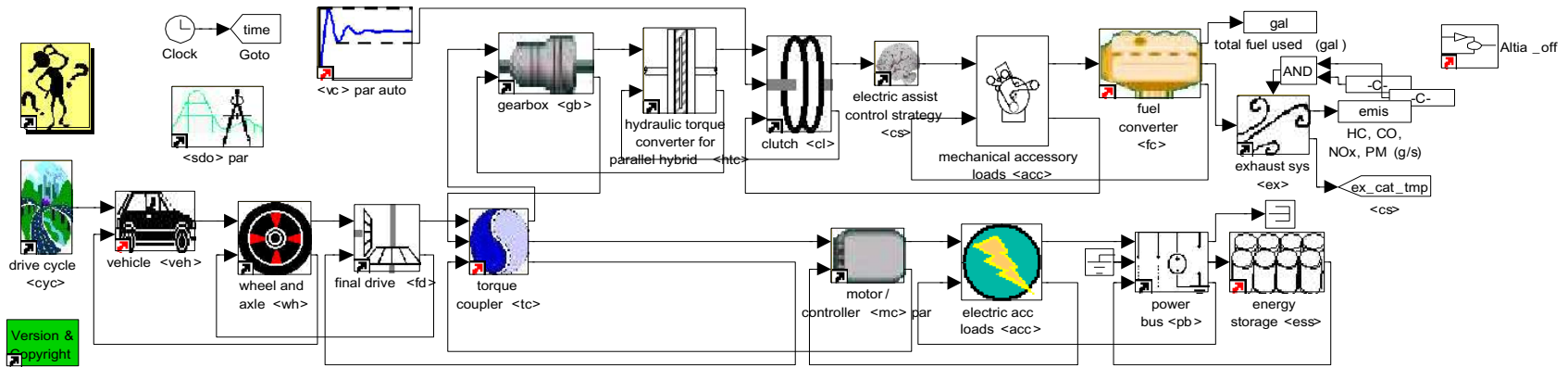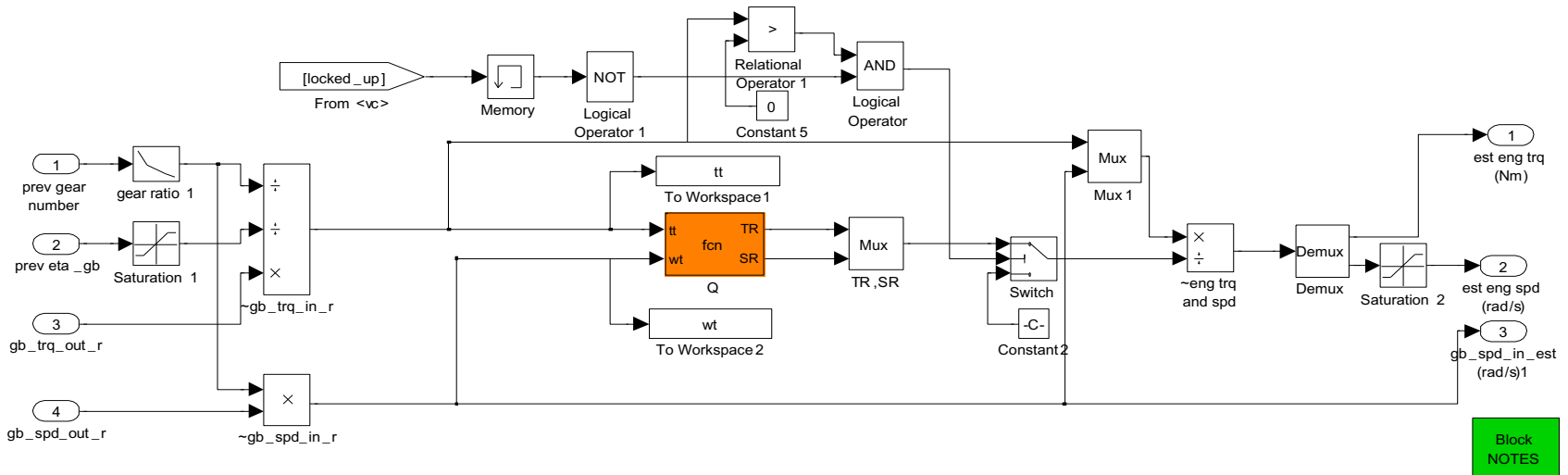
61

Figure 3-15, Modified ADVISOR Simulink Block

Figure 3-16, Engine Control Block in ADVISOR

62

www.manaraa.com
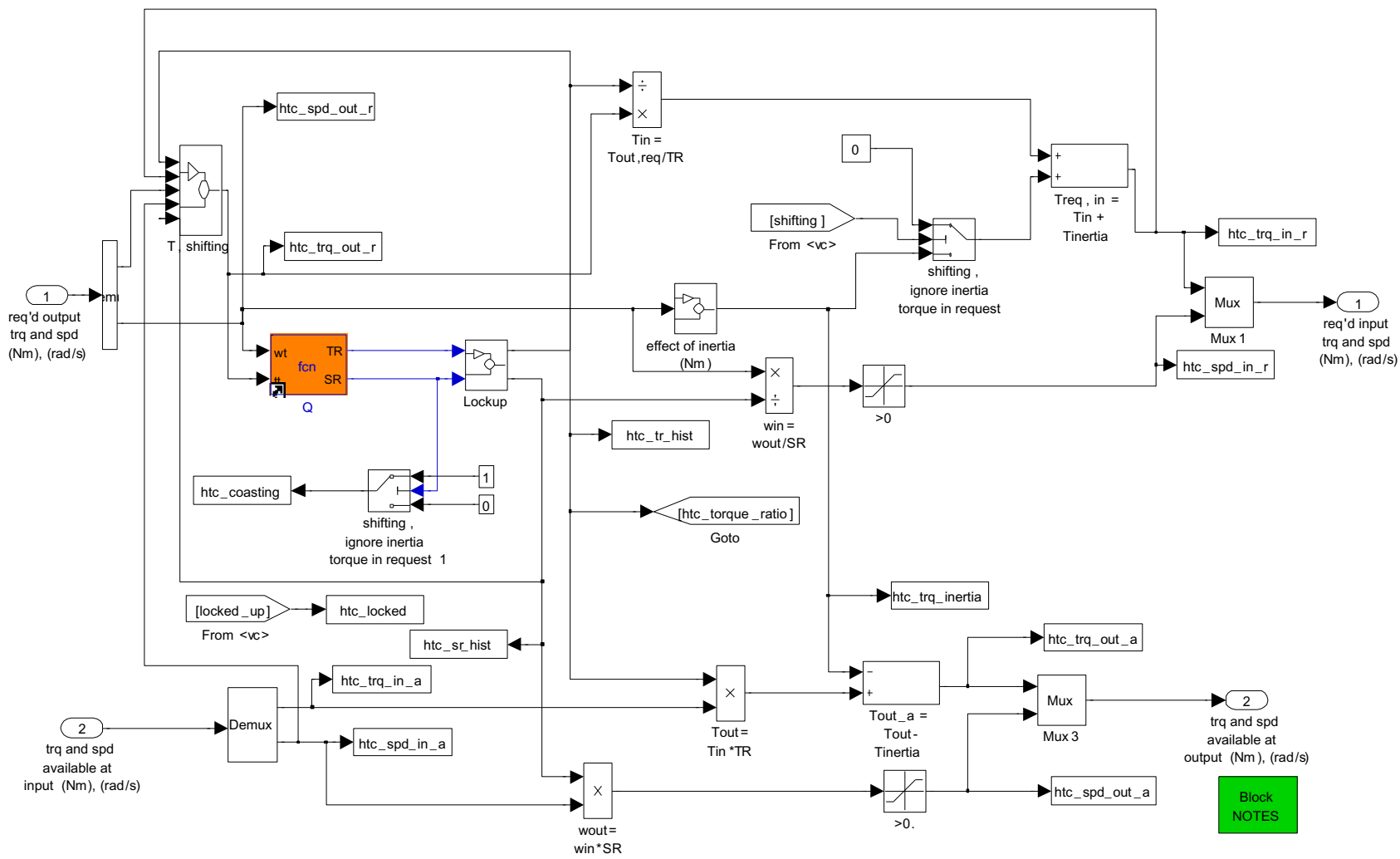
Figure 3-17, Modified ADVISOR Torque Converter Block

A basic algorithm for the torque converter function is as follows:

1. Set all of the k_1, k_2, k_3 and trf constants for the curve fits

2. Ensure that there are no negative turbine speeds

3. If the torque and speed are very low (vehicle is idling)

    a. Set the speed ratio (SR) to very low

    b. The torque ratio (TR) to maximum.

    This eliminates divide by zero errors in the code later.

4. If τ_t is greater than 0

    a. Assume it is in regime 1

    b. calculate impeller speed using the k_1 equation

    c. Determine SR by dividing ω_t / ω_i

    d. Determine TR from the TRF curve fit

    e. Calculate τ_i from TR and τ_t

    f. If τ_t is less that τ_i, then this is a coupled converter: use regime 2

        i. Use the k_2 equation to determine ω_i

        ii. Set $\tau_i = \tau_t$

5. Otherwise τ_t is less than zero

    a. Calculate ω_i from the k_3 equation

    b. Set $\tau_i = \tau_t$

6. Set the SR=ω_t/ω_i

7. Set the TR=τ_t / τ_i

8. Return SR and TR

Once the subroutine was written, the sub-block was inserted into the existing ADVISOR blocks which previously determined SR and TR. The ADVISOR code does not run if either of these values is zero. As a result, the code has a series of checks to ensure these values are never exactly zero. The ADVISOR models were used to compare the two torque converter models, lookup table versus the calculations developed here. The models were also compared with the real world hybrid system performance from dynamometer testing. The results from these comparisons are shown in later sections of this report.

4. Results

Using conservation of angular momentum and equating the pressure loss due to shock and flow losses to the pressure changes due to input and output torque, a set of equations is developed for each of the three distinct regimes. The final mathematical models are presented in section 3 in further detail. These models are based on similar modeling conducted by Hrovat and Tobler(Hrovat 1985), Kotwicki(Kotwicki 1982), and Ishihara and Emori(Ishihara and Emori 501). All of these studies present similar results, but with each there is a specific focus on a particular dynamic.

In the case presented here, a steady state model is sought which matches DOE's ADVISOR modeling package approach. Hrovat and Tobler(Hrovat 1985) present the beginnings of a negative flow regime, but this case includes transient and partial derivative terms. Hrovat and Tobler(Hrovat 1985) also make a series of geometric assumptions that are not sustained in the negative regime, namely the reverse flow angles being assumed to be the inverse of the positive flow angles. As was described in Section 3, the fluid approaches the back side of the blades, which are not symmetric and therefore this assumption is not valid. Kotwicki(Kotwicki 1982) presents an extension of Ishihara and Emori's(Ishihara and Emori 501) steady state base models. In this case the results match the Kotwicki(Kotwicki 1982) results for the regimes determined, regimes 1 and 2 assuming equal flow areas and radii are identical as assumed in their paper. In addition of the matching results, these data match similar published performance for positive

flow (Avallone et al.) (Stone and Ball 594) (Wikipedia contributors). Additionally, the published information that the torque ratio of a coupled torque converter is one provides further confirmation that the torque calculations are valid. This is due to the nature of the stator performance variables to drop out of the equation leaving only the impeller and stator torques remaining.

The mathematical relations that were developed were then used to develop effective methodologies for the various cases where one may need to determine particular outputs given particular inputs. The methods developed are:

- Determining impeller conditions from known turbine conditions
- Determining turbine conditions from known impeller conditions
- Determining component torques based on component speeds

The fourth possible scenario is based on known torques and determining component speeds. This scenario is indeterminate due to the singularity of torque ratio at all speed ratios in regimes two and three. This scenario is also the least likely to be required, as torque is often much more difficult to determine in a system due to complexity and cost. The algorithms developed here are presented in detail in chapter 3 of this report.

Validation of the individual methods was conducted by providing specific inputs although the outputs of each model were known. The calculated outputs of the model were then compared with the actual outputs. These results are shown in each individual regime during the model development. In most cases these results present a high degree of accuracy, although in the case

of known impeller results (Figure 3-11), the error in torque near the coupling point begins to rise from around 2% at 0.74 SR and increases to less than 10% at 0.84 SR and to nearly 19% at 0.89 SR. At this point the model shifts to Regime 2 with an average error of 0.8%. The average error for this entire dataset is 0.9%. Similarly the speed calculation has significant error in regimes of Regime 1 at the same points SR=0.86-0.89 and also at low speed ratios SR=0.01-0.23

In addition to validating the torque converter models themselves, the ADVISOR model was validated against both the ADVISOR Lookup model as well as the hybrid data logger from dynamometer testing. Figure 4-1 shows a speed trace of the three compared sources being run on the same drive cycle for comparison. The models run in ADVISOR show similar results to one another.

Vehicle Speed (MPH)
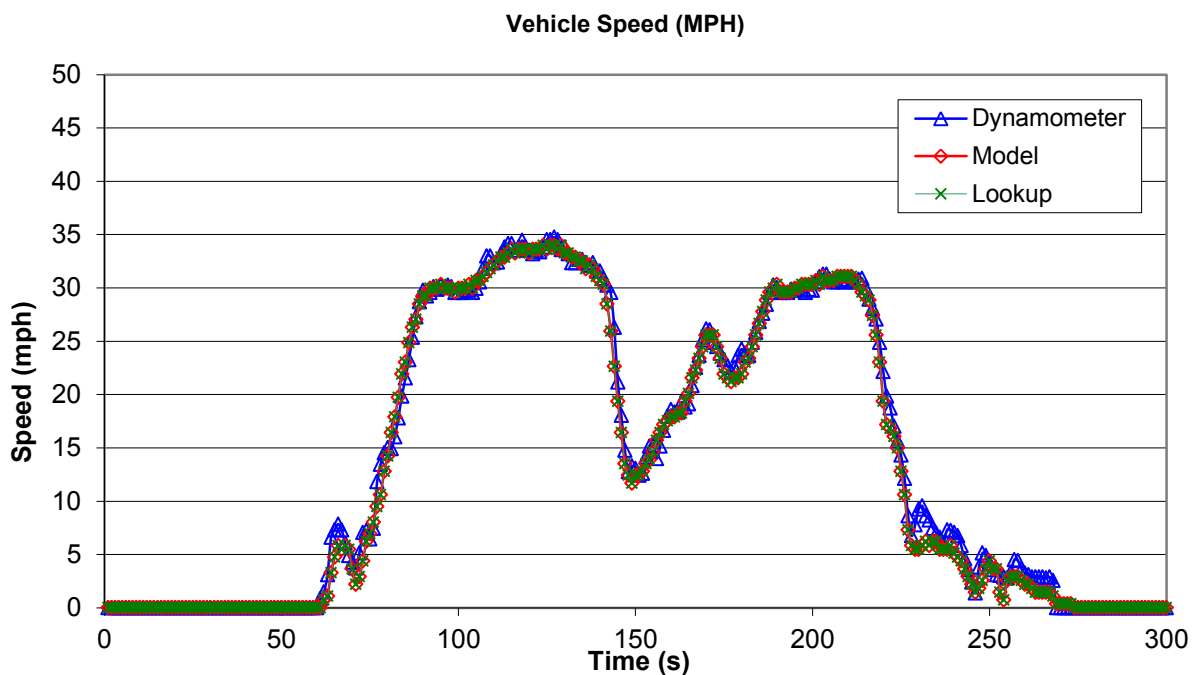
Figure 4-1, Test Drive Cycle Comparisons (WVUSub)

The overall torque converter performance is compared between the ADVISOR lookup table and the models created in this study as shown in Figure 4-2. This graph shows strong correlation between the ADVISOR lookup tables and the models created here. It is assumed that the lookup tables were created with a straight line fit from the input stall torque value of 2.05 and a standard geometry lookup table. The concave shape of the curve is also validated in Kotwicki(Kotwicki 1982).

Figure 4-2, Torque Converter Performance Comparison

The overall ADVISOR modeling provided significantly lower fuel economy results after being modified to model a parallel post transmission hybrid with a torque converter. The initial models

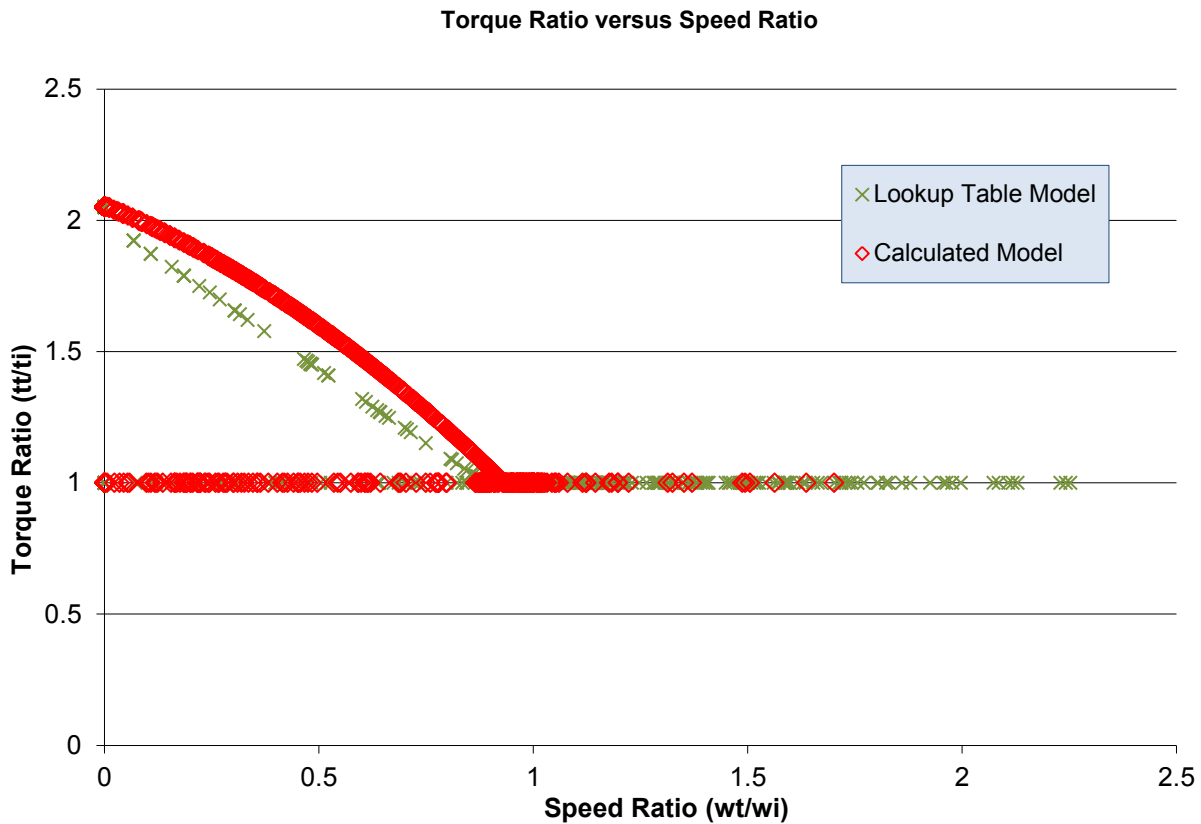showed 11.8 MPG, while the revised models showed 9.1 MPG for the lookup table model and 8.8 MPG for the modeled converter. These numbers are very close to the 8 to 9 miles per gallon being seen on average by school districts.   Additionally, late in 2009 NREL completed dynamometer testing of the buses (Gonder) and concluded that they achieve 8.8 MPG when run on the City Suburban Heavy Vehicle Cycle – Heavy Duty (CSHVC-HD) cycle. The CSHVC-HD is often considered a slightly more aggressive cycle than the WVU-Sub cycle.

While these data do not correlate well with the CaTTS dynamometer testing results of 13-16 MPG, the results of the CaTTS are not supported by other outside testing sources such as NREL(Gonder), Southwest Research Institute (SwRI), New York Power Authority (NYPA), and the many school districts driving the buses daily. Figures 4-3 and 4-4 show the results of the ADVISOR modeling for both the Lookup Table approach and the Modeled approach respectively.

70
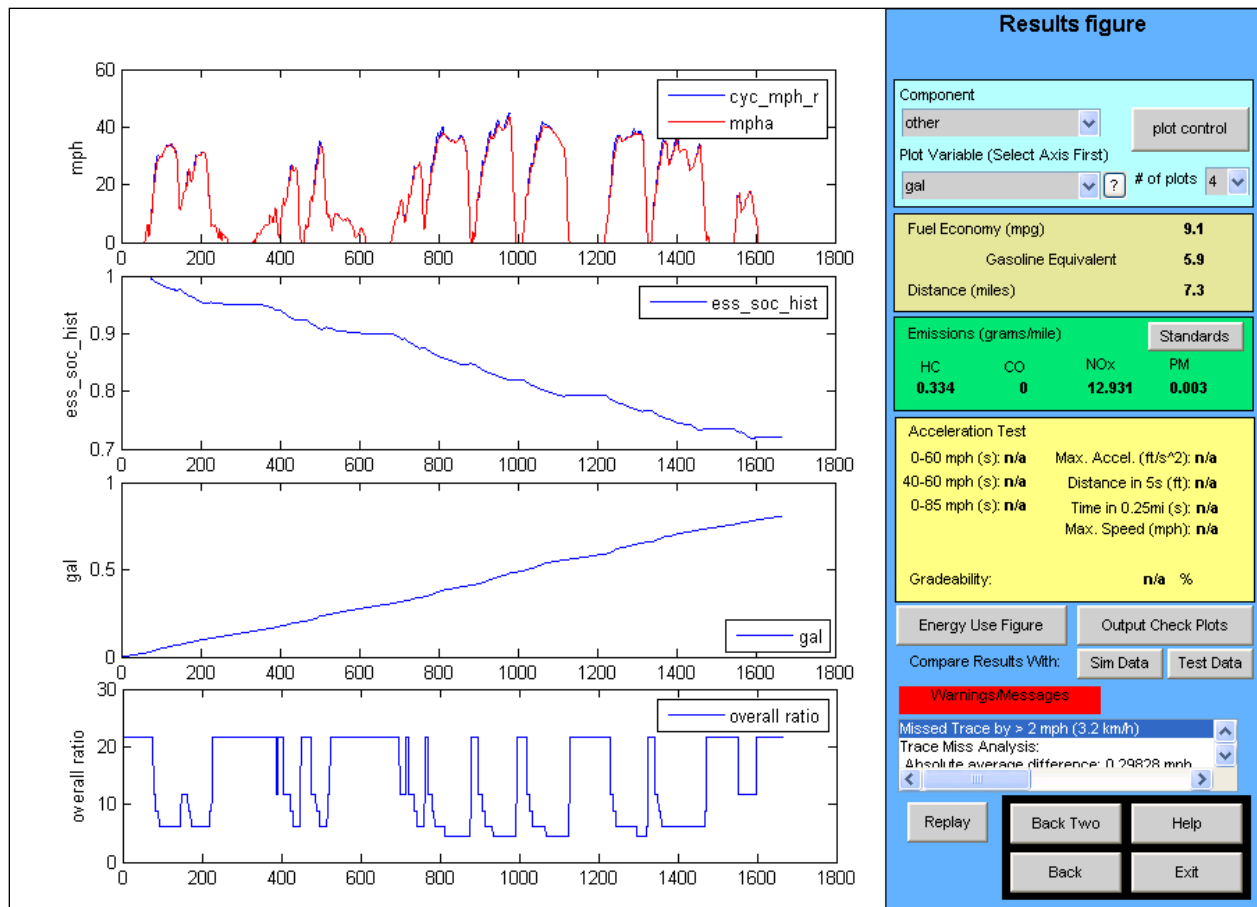
Figure 4-3, Advisor Results using the Lookup Tables
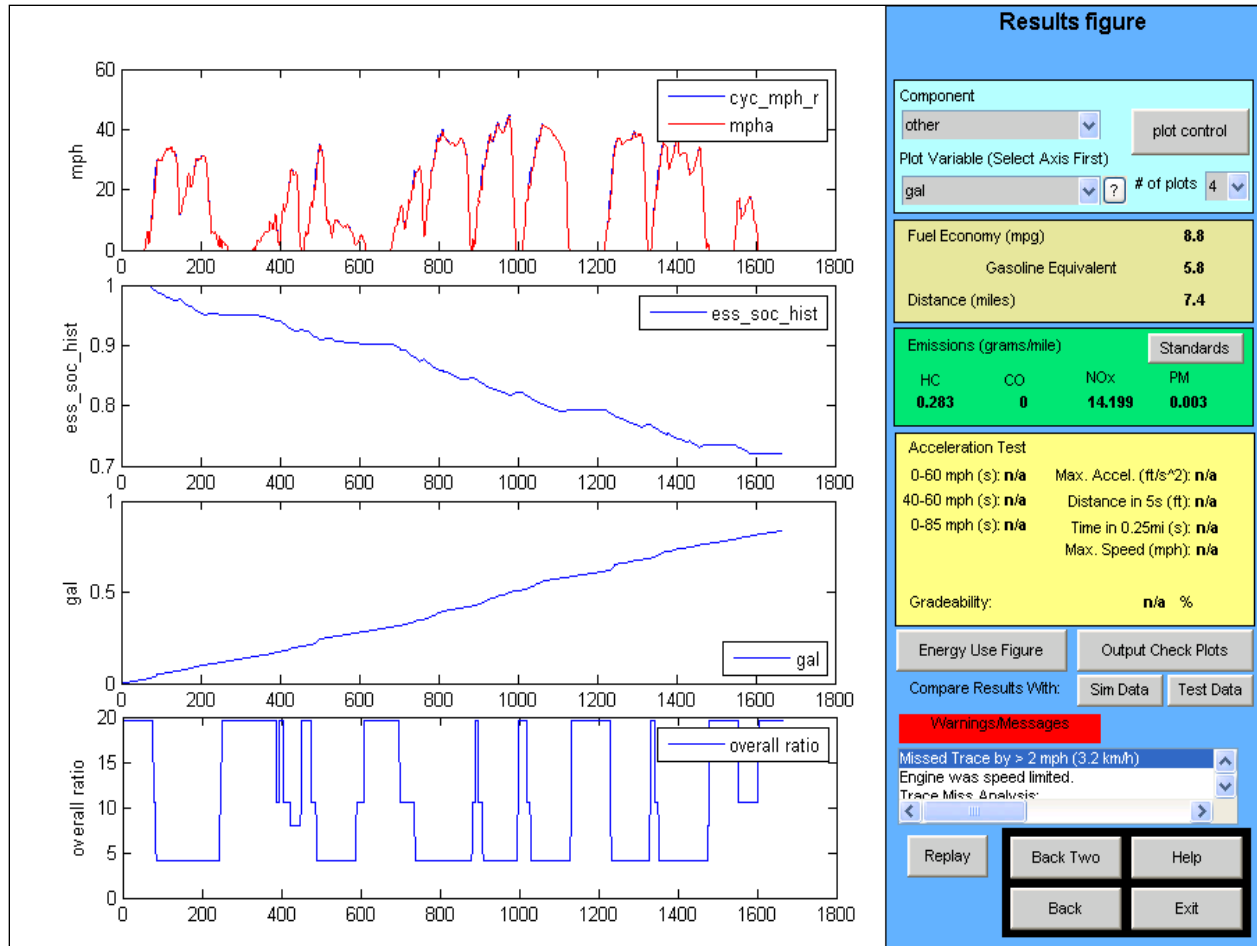
Figure 4-4, ADVISOR Results Using Torque Converter Model

By adding these characterizations to the ADVISOR models for hybrid vehicle performance, they present a clear argument indicating that significant losses can occur when an electric motor is applied downstream of the torque converter.

Figure 4-5 shows total energy losses resulting from two possible models of the torque converter. The model developed here is of two identical post transmission hybrid buses both driven on the West Virginia Suburban Cycle.
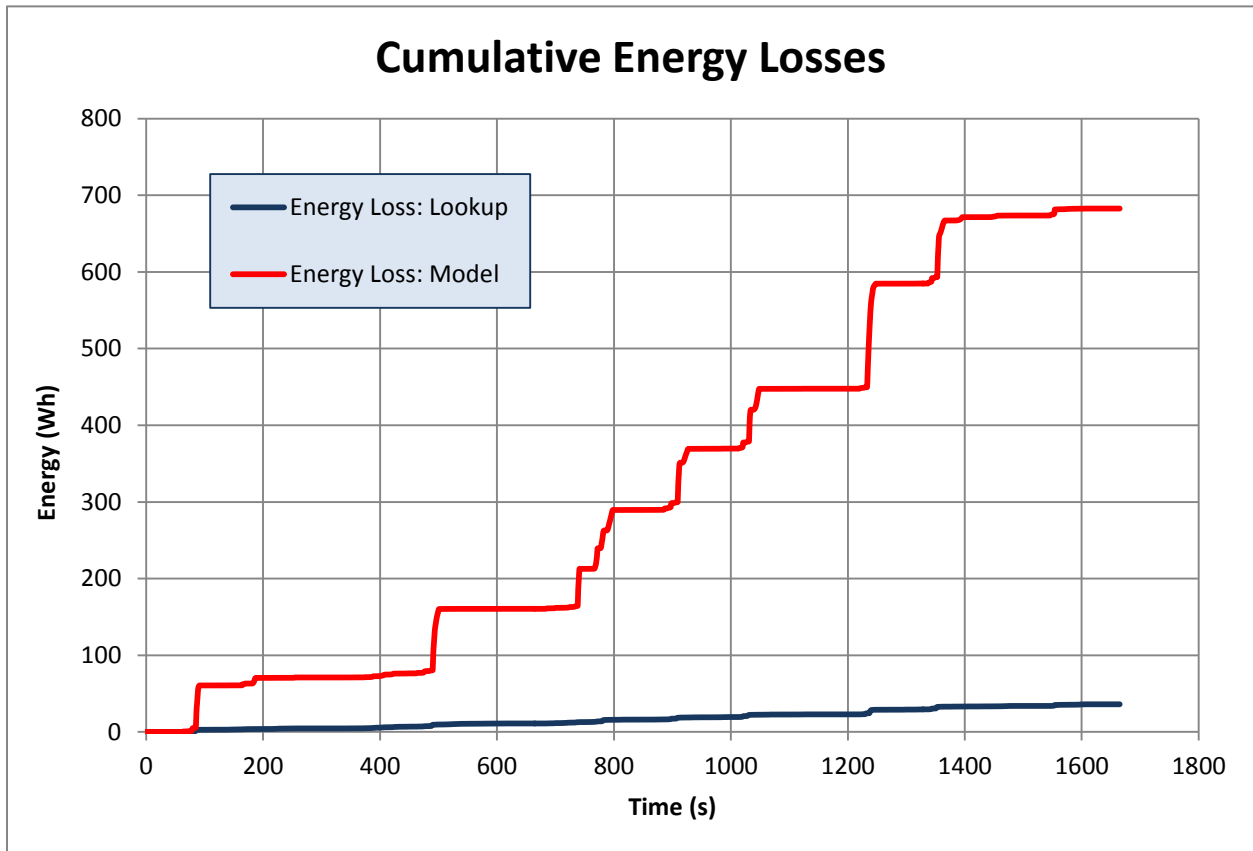
Figure 4-5, Cumulative Energy Losses from ADVISOR Vehicle Modeling

In the traditional ADVISOR model, the torque converter losses are reported as 36 W-h while the model developed in this case predicts a total loss of 683 W-h. The cumulative battery consumption in the model case of 11.4 kWh while in the lookup table case was only 11.0 kWh. These losses represent 6.2% of the total electrical consumption during the cycle versus 0.3% in

73

the lookup model case. The major losses in this case are occurring in specific bursts which line up with major acceleration events. A closer view of one of these bursts is shown in Figure 4.6.
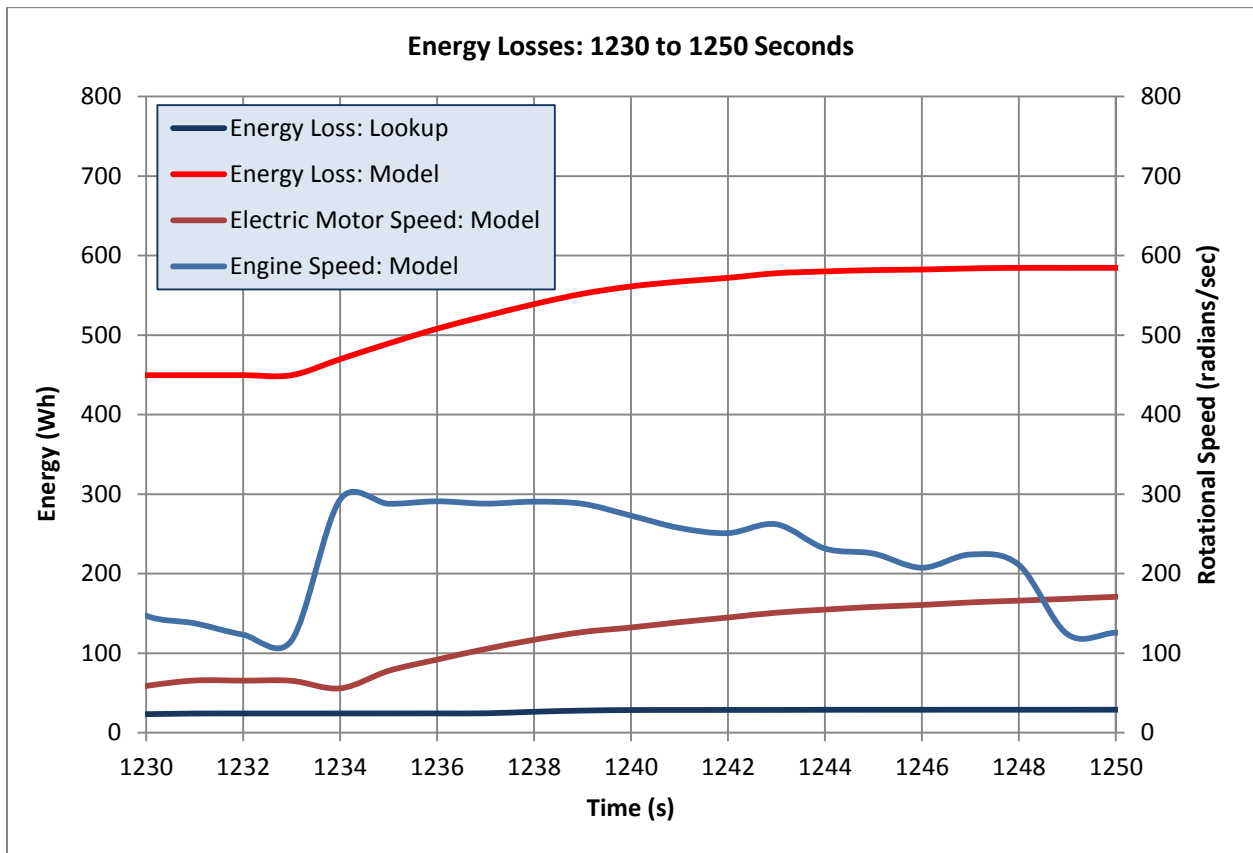
Figure 4-6, Torque Converter Energy Loss Burst

These bursts are occurring at times when the speed of the torque converter output is exceeding that of the engine or overrunning. It should be noted that the speed of the motor is also modified by the gear ratio which does not show on the chart.

5. Conclusions

This study was originated to determine the cause of the disparity between real world vehicle performance and ADVISOR modeling of plug-in post transmission hybrid school bus performance. Exhaustive searched showed that existing models do not appropriately account for the energy lost in the overrunning case of a torque converter. This case is more likely to occur in a parallel post transmission hybrid, and more importantly, the energy use to create the condition is intended to be used to drive the wheels. As a result, a methodology for performing steady-state calculations to determine the performance of a hydraulic torque converter in the overrunning regime was developed. Additionally, the more general case of different areas and radii within the converter in forward operating regimes was developed. The results for all regimes were then extended to a series of cases where particular variables are known to determine the remaining variables for use in modeling or control. Model derivations were based on sound methodology and applied in the new, or at least heretofore un-applied, negative flow condition. These models were validated against other published models in the positive flow regimes. This paper presents the newly formed set of equations for Regime 3 or negative flow.

The resulting models provided the basis to develop a set of systematic approaches to developing highly convenient models in three of the four possible known condition scenarios, as described below:

- Known Turbine Conditions – this applies to any backwards facing model such as ADVISOR or a system where the conditions are known downstream of the torque converter, such as wheel hub mounted torque sensors. The methodology developed here is highly accurate for all known turbine conditions.

- Known Impeller Conditions – This application is based on forward facing models, where the engine torque and speed are known such as PSAT or a control algorithm where the engine has been well documented and manifold absolute pressure is used to determine engine torque. The method developed here is very accurate for most speeds (<2% error) with the exception of Regime 1 when approaching the coupling point.

- Known Speeds – This case is more likely to exist in testing or controls where torque sensors are unavailable, but speeds are known. The method developed here is highly accurate.

- Known Torques – Although this is a possible scenario, there are few examples where torque is known and speed is not. The results of this were not developed here as Regimes 2 and 3 are indeterminate due to the singularity of torque ratio in these cases.

The systematic approach was developed here for each of the three determinate cases with relatively high accuracy in all cases.

The case of known turbine conditions was applied in a backwards facing modeling package (ADVISOR) to establish vehicle performance versus the traditional lookup table models. The resulting models predicted a significant increase in torque converter losses. In the specific case

of the ADVISOR models of the plug-in post transmission hybrid school buses tested on the West Virginia Suburban Cycle, the newly formed model showed a 683 Watt-hour predicted loss from the torque converter compared with the lookup table method which predicted a 36 Watt-hour loss. This 19 fold increase in predicted torque converter losses serves to confirm the concern that traditional vehicle models are underreporting the losses created by negative flow interaction with the torque converter, which happens in retrofit post transmission vehicles.

References

Allison Transmission. "specs_PTS.pdf." Allison Transmission. 7/25/2006 2006. 10/17/2010 <http://www.allisontransmission.com/documents/product/specs_PTS.pdf>.

Avallone, Eugene A., et al. Marks' Standard Handbook for Mechanical Engineers. 11th ed. New York: McGraw-Hill, 2007.

Gonder, Jeff. PHEV School Bus Testing. National Renewable Energy Laboratory, 2009.

Hrovat, D., and W. E. Tobler. "Bond Graph Modeling and Computer Simulation of Automotive Torque Converters." Journal of the Franklin Institute 319.1-2 (1985): 93-114.

Ishihara, T., and R. I. Emori. "Torque Converter as a Vibrator Damper and its Transient Characteristics." Society of Automotive Engineering (1966): 501.

Kotwicki, A. J. "Dynamic Models for Torque Converter Equipped Vehicles." International Congress & Exposition. Detroit, Michigan, February 22-26, 1982.

Pritchard, E., and R. R. Johnson. "Technical Performance Modeling of Hybrid and Plug-in Hybrid Electric School Buses using ADVISOR." International Mechanical Engineering Conference and Exhibition. Orlando, Florida, November 2005.

Stone, Richard, and Jeffrey K. Ball. Automotive Engineering Fundamentals. Warrendale, Pa.: SAE International, 2004.

Appendices

Appendix 1: Torque and Flow Calculations in Maple

Case 1: Torque and Flow Calculations

$$\tau_i := \rho \cdot Q \cdot \left(\varpi_i \cdot r_{ix}^2 - \varpi_s \cdot r_{sx}^2 \right) + \rho \cdot Q^2 \cdot \left(\frac{r_{ix} \cdot \tan\left(\alpha_{ix}\right)}{A_{ix}} - \frac{r_{sx} \cdot \tan\left(\alpha_{sx}\right)}{A_{sx}} \right)$$

$$\rho\, Q \left(\varpi_i\, r_{ix}^2 - \varpi_s\, r_{sx}^2 \right) + \rho\, Q^2 \left(\frac{r_{ix} \tan\left(\alpha_{ix}\right)}{A_{ix}} - \frac{r_{sx} \tan\left(\alpha_{sx}\right)}{A_{sx}} \right) \tag{1}$$

$$\tau_t := -\left(\rho \cdot Q \cdot \left(\varpi_t \cdot r_{tx}^2 - \varpi_i \cdot r_{ix}^2 \right) + \rho \cdot Q^2 \cdot \left(\frac{r_{tx} \cdot \tan\left(\alpha_{tx}\right)}{A_{tx}} - \frac{r_{ix} \cdot \tan\left(\alpha_{ix}\right)}{A_{ix}} \right) \right)$$

$$-\rho\, Q \left(\varpi_t\, r_{tx}^2 - \varpi_i\, r_{ix}^2 \right) - \rho\, Q^2 \left(\frac{r_{tx} \tan\left(\alpha_{tx}\right)}{A_{tx}} - \frac{r_{ix} \tan\left(\alpha_{ix}\right)}{A_{ix}} \right) \tag{2}$$

$$\tau_s := \rho \cdot Q \cdot \left(\varpi_s \cdot r_{sx}^2 + \varpi_t \cdot r_{tx}^2 \right) + \rho \cdot Q^2 \cdot \left(\frac{r_{sx} \cdot \tan\left(\alpha_{sx}\right)}{A_{sx}} - \frac{r_{tx} \cdot \tan\left(\alpha_{tx}\right)}{A_{tx}} \right)$$

$$\rho\, Q \left(\varpi_s\, r_{sx}^2 + \varpi_t\, r_{tx}^2 \right) + \rho\, Q^2 \left(\frac{r_{sx} \tan\left(\alpha_{sx}\right)}{A_{sx}} - \frac{r_{tx} \tan\left(\alpha_{tx}\right)}{A_{tx}} \right) \tag{3}$$

$$\varpi_s := 0$$

$$0 \tag{4}$$

$$dpi := \frac{\tau_i \cdot \varpi_i}{Q}$$

80

$$\frac{\left(\rho\, Q\, \varpi_i\, r_{ix}^2 + \rho\, Q^2 \left(\dfrac{r_{ix}\tan(\alpha_{ix})}{A_{ix}} - \dfrac{r_{sx}\tan(\alpha_{sx})}{A_{sx}}\right)\right)\varpi_i}{Q} \tag{5}$$

$$dpt := \frac{\tau_t \cdot \varpi_t}{Q}$$

$$\frac{\left(-\rho\, Q\left(\varpi_t\, r_{tx}^2 - \varpi_i\, r_{ix}^2\right) - \rho\, Q^2\left(\dfrac{r_{tx}\tan(\alpha_{tx})}{A_{tx}} - \dfrac{r_{ix}\tan(\alpha_{ix})}{A_{ix}}\right)\right)\varpi_t}{Q} \tag{6}$$

$$dps := \frac{\tau_s \cdot \varpi_s}{Q}$$

$$0 \tag{7}$$

$$dpslit := \frac{1}{2}\cdot\rho\cdot\left(Q\cdot\left(\frac{\tan(\alpha_{ix})}{A_{ix}} - \frac{\tan(\alpha_{te})}{A_{te}}\right) + \varpi_i\cdot r_{ix} - \varpi_t\cdot r_{te}\right)^2$$

$$\frac{1}{2}\,\rho\left(Q\left(\frac{\tan(\alpha_{ix})}{A_{ix}} - \frac{\tan(\alpha_{te})}{A_{te}}\right) + \varpi_i\, r_{ix} - \varpi_t\, r_{te}\right)^2 \tag{8}$$

$$dpslts := \frac{1}{2}\cdot\rho\cdot\left(Q\cdot\left(\frac{\tan(\alpha_{tx})}{A_{tx}} - \frac{\tan(\alpha_{se})}{A_{se}}\right) + \varpi_t\cdot r_{tx} - \varpi_s\cdot r_{se}\right)^2$$

$$\frac{1}{2}\,\rho\left(Q\left(\frac{\tan(\alpha_{tx})}{A_{tx}} - \frac{\tan(\alpha_{se})}{A_{se}}\right) + \varpi_t\, r_{tx}\right)^2 \tag{9}$$

$$dpslsi := \frac{1}{2}\cdot\rho\cdot\left(Q\cdot\left(\frac{\tan(\alpha_{sx})}{A_{sx}} - \frac{\tan(\alpha_{ie})}{A_{ie}}\right) + \varpi_s\cdot r_{sx} - \varpi_i\cdot r_{ie}\right)^2$$

$$\frac{1}{2}\,\rho\left(Q\left(\frac{\tan(\alpha_{sx})}{A_{sx}} - \frac{\tan(\alpha_{ie})}{A_{ie}}\right) - \varpi_i\, r_{ie}\right)^2 \tag{10}$$

$$dpfl := \frac{1}{2}\cdot\rho\cdot cf\cdot Q^2$$

$$\frac{1}{2}\,\rho\, cf\, Q^2 \tag{11}$$

$$compcase1 := dpslit + dpslts + dpslsi + dpfl - dpi - dpt$$

$$\frac{1}{2}\,\rho\left(Q\left(\frac{\tan(\alpha_{ix})}{A_{ix}} - \frac{\tan(\alpha_{te})}{A_{te}}\right) + \varpi_i\, r_{ix} - \varpi_t\, r_{te}\right)^2 + \frac{1}{2}\,\rho\left(Q\left(\frac{\tan(\alpha_{tx})}{A_{tx}} - \frac{\tan(\alpha_{se})}{A_{se}}\right) \tag{12}$$

$$+ \varpi_t\, r_{tx}\right)^2 + \frac{1}{2}\,\rho\left(Q\left(\frac{\tan(\alpha_{sx})}{A_{sx}} - \frac{\tan(\alpha_{ie})}{A_{ie}}\right) - \varpi_i\, r_{ie}\right)^2 + \frac{1}{2}\,\rho\, cf\, Q^2$$

81

$$-\frac{\left(\rho\, Q\, \varpi_i\, r_{ix}^2 + \rho\, Q^2 \left(\frac{r_{ix}\tan(\alpha_{ix})}{A_{ix}} - \frac{r_{sx}\tan(\alpha_{sx})}{A_{sx}}\right)\right)\varpi_i}{Q}$$

$$-\frac{\left(-\rho\, Q\left(\varpi_t\, r_{tx}^2 - \varpi_i\, r_{ix}^2\right) - \rho\, Q^2\left(\frac{r_{tx}\tan(\alpha_{tx})}{A_{tx}} - \frac{r_{ix}\tan(\alpha_{ix})}{A_{ix}}\right)\right)\varpi_t}{Q}$$

$collect(compcase1, Q)$

$$\left(\frac{1}{2}\rho\left(\frac{\tan(\alpha_{tx})}{A_{tx}} - \frac{\tan(\alpha_{se})}{A_{se}}\right)^2 + \frac{1}{2}\rho\left(\frac{\tan(\alpha_{ix})}{A_{ix}} - \frac{\tan(\alpha_{te})}{A_{te}}\right)^2 + \frac{1}{2}\rho\left(\frac{\tan(\alpha_{sx})}{A_{sx}}\right.\right. \tag{13}$$

$$\left.\left. - \frac{\tan(\alpha_{ie})}{A_{ie}}\right)^2 + \frac{1}{2}\rho\, cf\right)Q^2 + \left(\rho\left(\varpi_i\, r_{ix} - \varpi_t\, r_{te}\right)\left(\frac{\tan(\alpha_{ix})}{A_{ix}} - \frac{\tan(\alpha_{te})}{A_{te}}\right)\right.$$

$$+ \rho\left(\frac{r_{tx}\tan(\alpha_{tx})}{A_{tx}} - \frac{r_{ix}\tan(\alpha_{ix})}{A_{ix}}\right)\varpi_t - \rho\,\varpi_i\, r_{ie}\left(\frac{\tan(\alpha_{sx})}{A_{sx}} - \frac{\tan(\alpha_{ie})}{A_{ie}}\right)$$

$$+ \rho\,\varpi_t\, r_{tx}\left(\frac{\tan(\alpha_{tx})}{A_{tx}} - \frac{\tan(\alpha_{se})}{A_{se}}\right) - \rho\left(\frac{r_{ix}\tan(\alpha_{ix})}{A_{ix}} - \frac{r_{sx}\tan(\alpha_{sx})}{A_{sx}}\right)\varpi_i\right)Q$$

$$+ \frac{1}{2}\rho\left(\varpi_i\, r_{ix} - \varpi_t\, r_{te}\right)^2 + \frac{1}{2}\rho\,\varpi_i^2\, r_{ie}^2 + \frac{1}{2}\rho\,\varpi_t^2\, r_{tx}^2 + \rho\left(\varpi_t\, r_{tx}^2 - \varpi_i\, r_{ix}^2\right)\varpi_t - \rho\,\varpi_i^2\, r_{ix}^2$$

$Compatibility := 0 = collect(compcase1, Q)$

$$0 = \left(\frac{1}{2}\rho\left(\frac{\tan(\alpha_{tx})}{A_{tx}} - \frac{\tan(\alpha_{se})}{A_{se}}\right)^2 + \frac{1}{2}\rho\left(\frac{\tan(\alpha_{ix})}{A_{ix}} - \frac{\tan(\alpha_{te})}{A_{te}}\right)^2 + \frac{1}{2}\rho\left(\frac{\tan(\alpha_{sx})}{A_{sx}}\right.\right. \tag{14}$$

$$\left.\left. - \frac{\tan(\alpha_{ie})}{A_{ie}}\right)^2 + \frac{1}{2}\rho\, cf\right)Q^2 + \left(\rho\left(\varpi_i\, r_{ix} - \varpi_t\, r_{te}\right)\left(\frac{\tan(\alpha_{ix})}{A_{ix}} - \frac{\tan(\alpha_{te})}{A_{te}}\right)\right.$$

$$+ \rho\left(\frac{r_{tx}\tan(\alpha_{tx})}{A_{tx}} - \frac{r_{ix}\tan(\alpha_{ix})}{A_{ix}}\right)\varpi_t - \rho\,\varpi_i\, r_{ie}\left(\frac{\tan(\alpha_{sx})}{A_{sx}} - \frac{\tan(\alpha_{ie})}{A_{ie}}\right)$$

$$+ \rho\,\varpi_t\, r_{tx}\left(\frac{\tan(\alpha_{tx})}{A_{tx}} - \frac{\tan(\alpha_{se})}{A_{se}}\right) - \rho\left(\frac{r_{ix}\tan(\alpha_{ix})}{A_{ix}} - \frac{r_{sx}\tan(\alpha_{sx})}{A_{sx}}\right)\varpi_i\right)Q$$

$$+ \frac{1}{2}\rho\left(\varpi_i\, r_{ix} - \varpi_t\, r_{te}\right)^2 + \frac{1}{2}\rho\,\varpi_i^2\, r_{ie}^2 + \frac{1}{2}\rho\,\varpi_t^2\, r_{tx}^2 + \rho\left(\varpi_t\, r_{tx}^2 - \varpi_i\, r_{ix}^2\right)\varpi_t - \rho\,\varpi_i^2\, r_{ix}^2$$

$A_1 := coeff(compcase1, Q, 2)$

$$\frac{1}{2}\rho\left(\frac{\tan(\alpha_{tx})}{A_{tx}} - \frac{\tan(\alpha_{se})}{A_{se}}\right)^2 + \frac{1}{2}\rho\left(\frac{\tan(\alpha_{ix})}{A_{ix}} - \frac{\tan(\alpha_{te})}{A_{te}}\right)^2 + \frac{1}{2}\rho\left(\frac{\tan(\alpha_{sx})}{A_{sx}}\right. \tag{15}$$
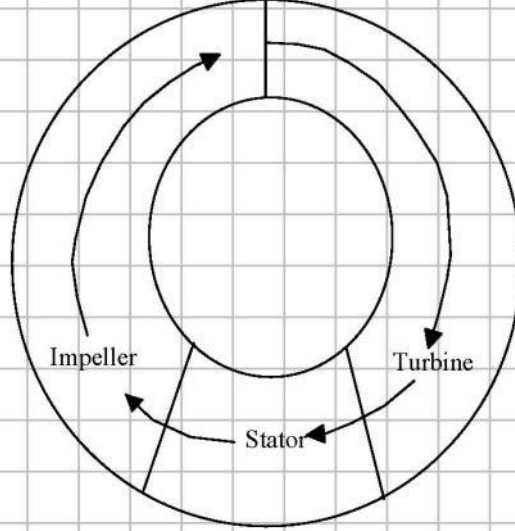
$$\left. - \frac{\tan(\alpha_{ie})}{A_{ie}}\right)^2 + \frac{1}{2}\rho\, cf$$

$B_1 := coeff(compcase1, Q, 1)$

82

$$\rho\left(\varpi_i\,r_{ix} - \varpi_t\,r_{te}\right)\left(\frac{\tan\left(\alpha_{ix}\right)}{A_{ix}} - \frac{\tan\left(\alpha_{te}\right)}{A_{te}}\right) + \rho\left(\frac{r_{tx}\tan\left(\alpha_{tx}\right)}{A_{tx}} - \frac{r_{ix}\tan\left(\alpha_{ix}\right)}{A_{ix}}\right)\varpi_t \qquad \textbf{(16)}$$

$$-\rho\,\varpi_i\,r_{ie}\left(\frac{\tan\left(\alpha_{sx}\right)}{A_{sx}} - \frac{\tan\left(\alpha_{ie}\right)}{A_{ie}}\right) + \rho\,\varpi_t\,r_{tx}\left(\frac{\tan\left(\alpha_{tx}\right)}{A_{tx}} - \frac{\tan\left(\alpha_{se}\right)}{A_{se}}\right)$$

$$-\rho\left(\frac{r_{ix}\tan\left(\alpha_{ix}\right)}{A_{ix}} - \frac{r_{sx}\tan\left(\alpha_{sx}\right)}{A_{sx}}\right)\varpi_i$$

$C_1 := coeff\left(compcase1, Q, 0\right)$

$$\frac{1}{2}\rho\left(\varpi_i\,r_{ix} - \varpi_t\,r_{te}\right)^2 + \frac{1}{2}\rho\,\varpi_i^2\,r_{ie}^2 + \frac{1}{2}\rho\,\varpi_t^2\,r_{tx}^2 + \rho\left(\varpi_t\,r_{tx}^2 - \varpi_i\,r_{ix}^2\right)\varpi_t - \rho\,\varpi_i^2\,r_{ix}^2 \qquad \textbf{(17)}$$

83

Case 2: Coupled Torque and Flow Calculations

Impeller Turbine Stator

$$\tau_i := \rho \cdot Q \cdot \left(\varpi_i \cdot r_{ix}^2 - \varpi_s \cdot r_{sx}^2 \right) + \rho \cdot Q^2 \cdot \left(\frac{r_{ix} \cdot \tan(\alpha_{ix})}{A_{ix}} - \frac{r_{sx} \cdot \tan(\alpha_{sx})}{A_{sx}} \right)$$

$$\rho \, Q \left(\varpi_i \, r_{ix}^2 - \varpi_s \, r_{sx}^2 \right) + \rho \, Q^2 \left(\frac{r_{ix} \cdot \tan(\alpha_{ix})}{A_{ix}} - \frac{r_{sx} \tan(\alpha_{sx})}{A_{sx}} \right) \tag{1}$$

$$\tau_t := -\left(\rho \cdot Q \cdot \left(\varpi_t \cdot r_{tx}^2 - \varpi_i \cdot r_{ix}^2 \right) + \rho \cdot Q^2 \cdot \left(\frac{r_{tx} \cdot \tan(\alpha_{tx})}{A_{tx}} - \frac{r_{ix} \cdot \tan(\alpha_{ix})}{A_{ix}} \right) \right)$$

$$-\rho \, Q \left(\varpi_t \, r_{tx}^2 - \varpi_i \, r_{ix}^2 \right) - \rho \, Q^2 \left(\frac{r_{tx} \tan(\alpha_{tx})}{A_{tx}} - \frac{r_{ix} \tan(\alpha_{ix})}{A_{ix}} \right) \tag{2}$$

$$t_s := 0; \; \varpi_s := \frac{Q \cdot \left(\frac{r_{sx} \cdot \tan(\alpha_{sx})}{A_{sx}} - \frac{r_{tx} \cdot \tan(\alpha_{tx})}{A_{tx}} \right) + \varpi_t \cdot r_{tx}^2}{r_{sx}^2}$$

$$0$$

$$\frac{Q \left(\frac{r_{sx} \tan(\alpha_{sx})}{A_{sx}} - \frac{r_{tx} \tan(\alpha_{tx})}{A_{tx}} \right) + \varpi_t \, r_{tx}^2}{r_{sx}^2} \tag{3}$$

$$dpi := \frac{\tau_i \cdot \varpi_i}{Q}$$

84

$$\frac{1}{Q}\left(\left(\rho\,Q\left(\varpi_i\,r_{ix}^2-Q\left(\frac{r_{sx}\tan\left(\alpha_{sx}\right)}{A_{sx}}-\frac{r_{tx}\tan\left(\alpha_{tx}\right)}{A_{tx}}\right)-\varpi_t\,r_{tx}^2\right)+\rho\,Q^2\left(\frac{r_{ix}\tan\left(\alpha_{ix}\right)}{A_{ix}}\right.\right.\right. \tag{4}$$
$$\left.\left.\left.-\frac{r_{sx}\tan\left(\alpha_{sx}\right)}{A_{sx}}\right)\right)\varpi_i\right)$$

$$dpt:=\frac{\tau_t\cdot\varpi_t}{Q}$$

$$\frac{\left(-\rho\,Q\left(\varpi_t\,r_{tx}^2-\varpi_i\,r_{ix}^2\right)-\rho\,Q^2\left(\frac{r_{tx}\tan\left(\alpha_{tx}\right)}{A_{tx}}-\frac{r_{ix}\tan\left(\alpha_{ix}\right)}{A_{ix}}\right)\right)\varpi_t}{Q} \tag{5}$$

$$dpslit:=\frac{1}{2}\cdot\rho\cdot\left(Q\cdot\left(\frac{\tan\left(\alpha_{ix}\right)}{A_{ix}}-\frac{\tan\left(\alpha_{te}\right)}{A_{te}}\right)+\varpi_i\cdot r_{ix}-\varpi_t\cdot r_{te}\right)^2$$

$$\frac{1}{2}\,\rho\left(Q\left(\frac{\tan\left(\alpha_{ix}\right)}{A_{ix}}-\frac{\tan\left(\alpha_{te}\right)}{A_{te}}\right)+\varpi_i\,r_{ix}-\varpi_t\,r_{te}\right)^2 \tag{6}$$

$$dpslts:=\frac{1}{2}\cdot\rho\cdot\left(Q\cdot\left(\frac{\tan\left(\alpha_{tx}\right)}{A_{tx}}-\frac{\tan\left(\alpha_{se}\right)}{A_{se}}\right)+\varpi_t\cdot r_{tx}-\varpi_s\cdot r_{se}\right)^2$$

$$\frac{1}{2}\,\rho\left(Q\left(\frac{\tan\left(\alpha_{tx}\right)}{A_{tx}}-\frac{\tan\left(\alpha_{se}\right)}{A_{se}}\right)+\varpi_t\,r_{tx}\right.$$
$$\left.-\frac{\left(Q\left(\frac{r_{sx}\tan\left(\alpha_{sx}\right)}{A_{sx}}-\frac{r_{tx}\tan\left(\alpha_{tx}\right)}{A_{tx}}\right)+\varpi_t\,r_{tx}^2\right)r_{se}}{r_{sx}^2}\right)^2 \tag{7}$$

$$dpslsi:=\frac{1}{2}\cdot\rho\cdot\left(Q\cdot\left(\frac{\tan\left(\alpha_{sx}\right)}{A_{sx}}-\frac{\tan\left(\alpha_{ie}\right)}{A_{ie}}\right)+\varpi_s\cdot r_{sx}-\varpi_i\cdot r_{ie}\right)^2$$

$$\frac{1}{2}\,\rho\left(Q\left(\frac{\tan\left(\alpha_{sx}\right)}{A_{sx}}-\frac{\tan\left(\alpha_{ie}\right)}{A_{ie}}\right)+\frac{Q\left(\frac{r_{sx}\tan\left(\alpha_{sx}\right)}{A_{sx}}-\frac{r_{tx}\tan\left(\alpha_{tx}\right)}{A_{tx}}\right)+\varpi_t\,r_{tx}^2}{r_{sx}}-\varpi_i\,r_{ie}\right)^2 \tag{8}$$

$$dpfl:=\frac{1}{2}\cdot\rho\cdot cf\cdot Q^2$$

$$\frac{1}{2}\,\rho\,cf\,Q^2 \tag{9}$$

$$compcase2:=dpslit+dpslts+dpslsi+dpfl-dpi-dpt$$

$$\frac{1}{2}\,\rho\left(Q\left(\frac{\tan(\alpha_{ix})}{A_{ix}}-\frac{\tan(\alpha_{te})}{A_{te}}\right)+\varpi_i\,r_{ix}-\varpi_t\,r_{te}\right)^2+\frac{1}{2}\,\rho\left(Q\left(\frac{\tan(\alpha_{tx})}{A_{tx}}-\frac{\tan(\alpha_{se})}{A_{se}}\right)\right.$$

$$+\varpi_t\,r_{tx}-\frac{\left(Q\left(\frac{r_{sx}\tan(\alpha_{sx})}{A_{sx}}-\frac{r_{tx}\tan(\alpha_{tx})}{A_{tx}}\right)+\varpi_t\,r_{tx}^2\right)r_{se}}{r_{sx}^2}\right)^2+\frac{1}{2}\,\rho\left(Q\left(\frac{\tan(\alpha_{sx})}{A_{sx}}\right.\right.$$

$$\left.-\frac{\tan(\alpha_{ie})}{A_{ie}}\right)+\frac{Q\left(\frac{r_{sx}\tan(\alpha_{sx})}{A_{sx}}-\frac{r_{tx}\tan(\alpha_{tx})}{A_{tx}}\right)+\varpi_t\,r_{tx}^2}{r_{sx}}-\varpi_i\,r_{ie}\right)^2+\frac{1}{2}\,\rho\,cf\,Q^2 \tag{10}$$

$$-\frac{1}{Q}\left(\left(\rho\,Q\left(\varpi_i\,r_{ix}^2-Q\left(\frac{r_{sx}\tan(\alpha_{sx})}{A_{sx}}-\frac{r_{tx}\tan(\alpha_{tx})}{A_{tx}}\right)-\varpi_t\,r_{tx}^2\right)+\rho\,Q^2\left(\frac{r_{ix}\tan(\alpha_{ix})}{A_{ix}}\right.\right.\right.$$

$$\left.\left.\left.-\frac{r_{sx}\tan(\alpha_{sx})}{A_{sx}}\right)\right)\varpi_i\right)$$

$$-\frac{\left(-\rho\,Q\left(\varpi_t\,r_{tx}^2-\varpi_i\,r_{ix}^2\right)-\rho\,Q^2\left(\frac{r_{tx}\tan(\alpha_{tx})}{A_{tx}}-\frac{r_{ix}\tan(\alpha_{ix})}{A_{ix}}\right)\right)\varpi_t}{Q}$$

collect(compcase2, Q)

$$\left(\frac{1}{2}\,\rho\left(\frac{\tan(\alpha_{tx})}{A_{tx}}-\frac{\tan(\alpha_{se})}{A_{se}}-\frac{\left(\frac{r_{sx}\tan(\alpha_{sx})}{A_{sx}}-\frac{r_{tx}\tan(\alpha_{tx})}{A_{tx}}\right)r_{se}}{r_{sx}^2}\right)^2+\frac{1}{2}\,\rho\left(\frac{\tan(\alpha_{ix})}{A_{ix}}\right.\right. \tag{11}$$

$$\left.-\frac{\tan(\alpha_{te})}{A_{te}}\right)^2+\frac{1}{2}\,\rho\left(\frac{\tan(\alpha_{sx})}{A_{sx}}-\frac{\tan(\alpha_{ie})}{A_{ie}}+\frac{\frac{r_{sx}\tan(\alpha_{sx})}{A_{sx}}-\frac{r_{tx}\tan(\alpha_{tx})}{A_{tx}}}{r_{sx}}\right)^2$$

$$\left.+\frac{1}{2}\,\rho\,cf\right)Q^2+\left(\rho\left(\varpi_i\,r_{ix}-\varpi_t\,r_{te}\right)\left(\frac{\tan(\alpha_{ix})}{A_{ix}}-\frac{\tan(\alpha_{te})}{A_{te}}\right)+\rho\left(\frac{r_{tx}\tan(\alpha_{tx})}{A_{tx}}\right.\right.$$

$$\left.-\frac{r_{ix}\tan(\alpha_{ix})}{A_{ix}}\right)\varpi_t+\rho\left(\frac{\varpi_t\,r_{tx}^2}{r_{sx}}-\varpi_i\,r_{ie}\right)\left(\frac{\tan(\alpha_{sx})}{A_{sx}}-\frac{\tan(\alpha_{ie})}{A_{ie}}\right.$$

$$\left.+\frac{\frac{r_{sx}\tan(\alpha_{sx})}{A_{sx}}-\frac{r_{tx}\tan(\alpha_{tx})}{A_{tx}}}{r_{sx}}\right)+\rho\left(\varpi_t\,r_{tx}-\frac{\varpi_t\,r_{tx}^2\,r_{se}}{r_{sx}^2}\right)\left(\frac{\tan(\alpha_{tx})}{A_{tx}}-\frac{\tan(\alpha_{se})}{A_{se}}\right.$$

$$- \frac{\left(\frac{r_{sx} \tan(\alpha_{sx})}{A_{sx}} - \frac{r_{tx} \tan(\alpha_{tx})}{A_{tx}} \right) r_{se}}{r_{sx}^2} \right] - \left(\rho \left(- \frac{r_{sx} \tan(\alpha_{sx})}{A_{sx}} + \frac{r_{tx} \tan(\alpha_{tx})}{A_{tx}} \right) \right.$$

$$+ \rho \left(\frac{r_{ix} \tan(\alpha_{ix})}{A_{ix}} - \frac{r_{sx} \tan(\alpha_{sx})}{A_{sx}} \right) \right) \varpi_i \Big) Q + \frac{1}{2} \rho \left(\varpi_i r_{ix} - \varpi_t r_{te} \right)^2 + \frac{1}{2} \rho \left(\frac{\varpi_t r_{tx}^2}{r_{sx}} \right.$$

$$\left. - \varpi_i r_{ie} \right)^2 + \frac{1}{2} \rho \left(\varpi_t r_{tx} - \frac{\varpi_t r_{tx}^2 r_{se}}{r_{sx}^2} \right)^2 + \rho \left(\varpi_t r_{tx}^2 - \varpi_i r_{ix}^2 \right) \varpi_t - \rho \left(\varpi_i r_{ix}^2 - \varpi_t r_{tx}^2 \right) \varpi_i$$
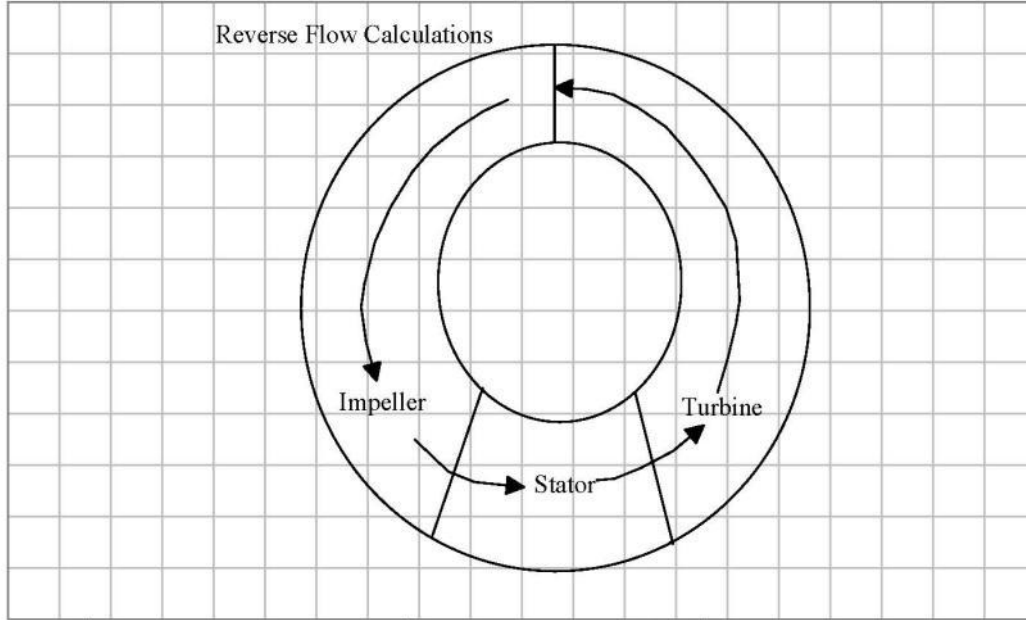
$A_2 = coeff\,(compcase2, Q, 2)$

$$A_2 = \frac{1}{2} \rho \left(\frac{\tan(\alpha_{tx})}{A_{tx}} - \frac{\tan(\alpha_{se})}{A_{se}} - \frac{\left(\frac{r_{sx} \tan(\alpha_{sx})}{A_{sx}} - \frac{r_{tx} \tan(\alpha_{tx})}{A_{tx}} \right) r_{se}}{r_{sx}^2} \right)^2 \tag{12}$$

$$+ \frac{1}{2} \rho \left(\frac{\tan(\alpha_{ix})}{A_{ix}} - \frac{\tan(\alpha_{te})}{A_{te}} \right)^2 + \frac{1}{2} \rho \left(\frac{\tan(\alpha_{sx})}{A_{sx}} - \frac{\tan(\alpha_{ie})}{A_{ie}} \right.$$

$$\left. + \frac{\frac{r_{sx} \tan(\alpha_{sx})}{A_{sx}} - \frac{r_{tx} \tan(\alpha_{tx})}{A_{tx}}}{r_{sx}} \right)^2 + \frac{1}{2} \rho \, cf$$

$B_2 = coeff\,(compcase2, Q, 1)$

$$B_2 = \rho \left(\varpi_i r_{ix} - \varpi_t r_{te} \right) \left(\frac{\tan(\alpha_{ix})}{A_{ix}} - \frac{\tan(\alpha_{te})}{A_{te}} \right) + \rho \left(\frac{r_{tx} \tan(\alpha_{tx})}{A_{tx}} - \frac{r_{ix} \tan(\alpha_{ix})}{A_{ix}} \right) \varpi_t \tag{13}$$

$$+ \rho \left(\frac{\varpi_t r_{tx}^2}{r_{sx}} - \varpi_i r_{ie} \right) \left(\frac{\tan(\alpha_{sx})}{A_{sx}} - \frac{\tan(\alpha_{ie})}{A_{ie}} + \frac{\frac{r_{sx} \tan(\alpha_{sx})}{A_{sx}} - \frac{r_{tx} \tan(\alpha_{tx})}{A_{tx}}}{r_{sx}} \right)$$

$$+ \rho \left(\varpi_t r_{tx} - \frac{\varpi_t r_{tx}^2 r_{se}}{r_{sx}^2} \right) \left(\frac{\tan(\alpha_{tx})}{A_{tx}} - \frac{\tan(\alpha_{se})}{A_{se}} \right.$$

$$\left. - \frac{\left(\frac{r_{sx} \tan(\alpha_{sx})}{A_{sx}} - \frac{r_{tx} \tan(\alpha_{tx})}{A_{tx}} \right) r_{se}}{r_{sx}^2} \right) - \left(\rho \left(- \frac{r_{sx} \tan(\alpha_{sx})}{A_{sx}} + \frac{r_{tx} \tan(\alpha_{tx})}{A_{tx}} \right) \right.$$

$$\left. + \rho \left(\frac{r_{ix} \tan(\alpha_{ix})}{A_{ix}} - \frac{r_{sx} \tan(\alpha_{sx})}{A_{sx}} \right) \right) \varpi_i$$

87

$C_2 = coeff\,(compcase2, Q, 0)$

$$C_2 = \frac{1}{2}\,\rho\,(\varpi_i\,r_{ix} - \varpi_t\,r_{te})^2 + \frac{1}{2}\,\rho\left(\frac{\varpi_t\,r_{tx}^2}{r_{sx}} - \varpi_i\,r_{ie}\right)^2 + \frac{1}{2}\,\rho\left(\varpi_t\,r_{tx} - \frac{\varpi_t\,r_{tx}^2\,r_{se}}{r_{sx}^2}\right)^2 + \rho\left(\varpi_t\,r_{tx}^2 \qquad \textbf{(14)}\right.$$
$$\left.- \varpi_i\,r_{ix}^2\right)\varpi_t - \rho\left(\varpi_i\,r_{ix}^2 - \varpi_t\,r_{tx}^2\right)\varpi_i$$

Reverse Flow Calculations

$$\tau_i := -\left(\rho \cdot Q \cdot \left(\varpi_i \cdot r_{ix}^2 - \varpi_t \cdot r_{tx}^2\right) + \rho \cdot Q^2 \cdot \left(\frac{r_{ix} \cdot \tan(\alpha_{ix})}{A_{ix}} - \frac{r_{tx} \cdot \tan(\alpha_{tx})}{A_{tx}}\right)\right)$$

$$-\rho\, Q\left(\varpi_i r_{ix}^2 - \varpi_t r_{tx}^2\right) - \rho\, Q^2 \left(\frac{r_{ix} \tan(\alpha_{ix})}{A_{ix}} - \frac{r_{tx} \tan(\alpha_{tx})}{A_{tx}}\right) \tag{1}$$

$$\tau_t := \rho \cdot Q \cdot \left(\varpi_t \cdot r_{tx}^2 - \varpi_s \cdot r_{sx}^2\right) + \rho \cdot Q^2 \cdot \left(\frac{r_{tx} \cdot \tan(\alpha_{tx})}{A_{tx}} - \frac{r_{sx} \cdot \tan(\alpha_{sx})}{A_{sx}}\right)$$

$$\rho\, Q\left(\varpi_t r_{tx}^2 - Q\left(\frac{r_{ix} \tan(\alpha_{ix})}{A_{ix}} - \frac{r_{sx} \tan(\alpha_{sx})}{A_{sx}}\right) - \varpi_i r_{ix}^2\right) + \rho\, Q^2 \left(\frac{r_{tx} \tan(\alpha_{tx})}{A_{tx}}\right. \tag{2}$$

$$\left. - \frac{r_{sx} \tan(\alpha_{sx})}{A_{sx}}\right)$$

$$\tau_s := -\left(\rho \cdot Q \cdot \left(\varpi_s \cdot r_{sx}^2 - \varpi_i \cdot r_{ix}^2\right) + \rho \cdot Q^2 \cdot \left(\frac{r_{sx} \cdot \tan(\alpha_{sx})}{A_{sx}} - \frac{r_{ix} \cdot \tan(\alpha_{ix})}{A_{ix}}\right)\right)$$

$$-\rho\, Q^2 \left(\frac{r_{ix} \tan(\alpha_{ix})}{A_{ix}} - \frac{r_{sx} \tan(\alpha_{sx})}{A_{sx}}\right) - \rho\, Q^2 \left(\frac{r_{sx} \tan(\alpha_{sx})}{A_{sx}} - \frac{r_{ix} \tan(\alpha_{ix})}{A_{ix}}\right) \tag{3}$$

$$\varpi_s := \frac{\left(Q \cdot \left(\frac{r_{ix} \cdot \tan(\alpha_{ix})}{A_{ix}} - \frac{r_{sx} \cdot \tan(\alpha_{sx})}{A_{sx}}\right) + \varpi_i r_{ix}^2\right)}{r_{sx}^2}$$

89

$$\frac{Q\left(\dfrac{r_{ix}\tan(\alpha_{ix})}{A_{ix}}-\dfrac{r_{sx}\tan(\alpha_{sx})}{A_{sx}}\right)+\varpi_i r_{ix}^2}{r_{sx}^2} \tag{4}$$

τ_t

$$\rho\,Q\left(\varpi_t r_{tx}^2-Q\left(\dfrac{r_{ix}\tan(\alpha_{ix})}{A_{ix}}-\dfrac{r_{sx}\tan(\alpha_{sx})}{A_{sx}}\right)-\varpi_i r_{ix}^2\right)+\rho\,Q^2\left(\dfrac{r_{tx}\tan(\alpha_{tx})}{A_{tx}}\right. \tag{5}$$
$$\left.-\dfrac{r_{sx}\tan(\alpha_{sx})}{A_{sx}}\right)$$

$$\tau_t := \rho\,Q\left(\varpi_t r_{tx}^2-\varpi_i r_{ix}^2\right)+\rho\,Q^2\left(\dfrac{r_{tx}\tan(\alpha_{tx})}{A_{tx}}-\dfrac{r_{ix}\tan(\alpha_{ix})}{A_{ix}}\right)$$

$$\rho\,Q\left(\varpi_t r_{tx}^2-\varpi_i r_{ix}^2\right)+\rho\,Q^2\left(\dfrac{r_{tx}\tan(\alpha_{tx})}{A_{tx}}-\dfrac{r_{ix}\tan(\alpha_{ix})}{A_{ix}}\right) \tag{6}$$

$$dpi := \frac{\tau_i\cdot\varpi_i}{Q}$$

$$\frac{\left(-\rho\,Q\left(\varpi_i r_{ix}^2-\varpi_t r_{tx}^2\right)-\rho\,Q^2\left(\dfrac{r_{ix}\tan(\alpha_{ix})}{A_{ix}}-\dfrac{r_{tx}\tan(\alpha_{tx})}{A_{tx}}\right)\right)\varpi_i}{Q} \tag{7}$$

$$dpt := \frac{\tau_t\cdot\varpi_t}{Q}$$

$$\frac{\left(\rho\,Q\left(\varpi_t r_{tx}^2-\varpi_i r_{ix}^2\right)+\rho\,Q^2\left(\dfrac{r_{tx}\tan(\alpha_{tx})}{A_{tx}}-\dfrac{r_{ix}\tan(\alpha_{ix})}{A_{ix}}\right)\right)\varpi_t}{Q} \tag{8}$$

$$dpslti := \frac{1}{2}\cdot\rho\cdot\left(Q\cdot\left(\dfrac{\tan(\alpha_{tx})}{A_{tx}}-\dfrac{\tan(\alpha_{ie})}{A_{ie}}\right)+\varpi_t\cdot r_{tx}-\varpi_i\cdot r_{ie}\right)^2$$

$$\frac{1}{2}\,\rho\left(Q\left(\dfrac{\tan(\alpha_{tx})}{A_{tx}}-\dfrac{\tan(\alpha_{ie})}{A_{ie}}\right)+\varpi_t r_{tx}-\varpi_i r_{ie}\right)^2 \tag{9}$$

$$dpslis := \frac{1}{2}\cdot\rho\cdot\left(Q\cdot\left(\dfrac{\tan(\alpha_{ix})}{A_{ix}}-\dfrac{\tan(\alpha_{se})}{A_{se}}\right)+\varpi_i\cdot r_{ix}-\varpi_s\cdot r_{se}\right)^2$$

$$\frac{1}{2}\,\rho\left(Q\left(\dfrac{\tan(\alpha_{ix})}{A_{ix}}-\dfrac{\tan(\alpha_{se})}{A_{se}}\right)+\varpi_i r_{ix}\right. \tag{10}$$

90

$$-\frac{\left(Q\left(\dfrac{r_{ix}\tan(\alpha_{ix})}{A_{ix}} - \dfrac{r_{sx}\tan(\alpha_{sx})}{A_{sx}}\right) + \varpi_i\, r_{ix}^2\right) r_{se}}{r_{sx}^2}\Bigg)^2$$

$$dpslst := \frac{1}{2}\cdot\rho\cdot\left(Q\cdot\left(\frac{\tan(\alpha_{sx})}{A_{sx}} - \frac{\tan(\alpha_{te})}{A_{te}}\right) + \varpi_s\cdot r_{sx} - \varpi_t\cdot r_{te}\right)^2$$

$$\frac{1}{2}\,\rho\left(Q\left(\frac{\tan(\alpha_{sx})}{A_{sx}} - \frac{\tan(\alpha_{te})}{A_{te}}\right) + \frac{Q\left(\dfrac{r_{ix}\tan(\alpha_{ix})}{A_{ix}} - \dfrac{r_{sx}\tan(\alpha_{sx})}{A_{sx}}\right) + \varpi_i\, r_{ix}^2}{r_{sx}} - \varpi_t\, r_{te}\right)^2 \qquad \textbf{(11)}$$

$$dpfl := \frac{1}{2}\cdot\rho\cdot cf\cdot Q^2$$

$$\frac{1}{2}\,\rho\, cf\, Q^2 \qquad \textbf{(12)}$$

$$compnegflow := dpslti + dpslis + dpslst + dpfl - dpi - dpt$$

$$\frac{1}{2}\,\rho\left(Q\left(\frac{\tan(\alpha_{tx})}{A_{tx}} - \frac{\tan(\alpha_{ie})}{A_{ie}}\right) + \varpi_t\, r_{tx} - \varpi_i\, r_{ie}\right)^2 + \frac{1}{2}\,\rho\Bigg(Q\left(\frac{\tan(\alpha_{ix})}{A_{ix}} - \frac{\tan(\alpha_{se})}{A_{se}}\right) \qquad \textbf{(13)}$$

$$+ \varpi_i\, r_{ix} - \frac{\left(Q\left(\dfrac{r_{ix}\tan(\alpha_{ix})}{A_{ix}} - \dfrac{r_{sx}\tan(\alpha_{sx})}{A_{sx}}\right) + \varpi_i\, r_{ix}^2\right) r_{se}}{r_{sx}^2}\Bigg)^2 + \frac{1}{2}\,\rho\Bigg(Q\Bigg(\frac{\tan(\alpha_{sx})}{A_{sx}}$$

$$- \frac{\tan(\alpha_{te})}{A_{te}}\Bigg) + \frac{Q\left(\dfrac{r_{ix}\tan(\alpha_{ix})}{A_{ix}} - \dfrac{r_{sx}\tan(\alpha_{sx})}{A_{sx}}\right) + \varpi_i\, r_{ix}^2}{r_{sx}} - \varpi_t\, r_{te}\Bigg)^2 + \frac{1}{2}\,\rho\, cf\, Q^2$$

$$- \frac{\left(-\rho\, Q\left(\varpi_i\, r_{ix}^2 - \varpi_t\, r_{tx}^2\right) - \rho\, Q^2\left(\dfrac{r_{ix}\tan(\alpha_{ix})}{A_{ix}} - \dfrac{r_{tx}\tan(\alpha_{tx})}{A_{tx}}\right)\right)\varpi_i}{Q}$$

$$- \frac{\left(\rho\, Q\left(\varpi_t\, r_{tx}^2 - \varpi_i\, r_{ix}^2\right) + \rho\, Q^2\left(\dfrac{r_{tx}\tan(\alpha_{tx})}{A_{tx}} - \dfrac{r_{ix}\tan(\alpha_{ix})}{A_{ix}}\right)\right)\varpi_t}{Q}$$

$$collect(compnegflow, Q)$$

$$\left(\frac{1}{2}\,\rho\left(\frac{\tan(\alpha_{ix})}{A_{ix}} - \frac{\tan(\alpha_{se})}{A_{se}} - \frac{\left(\dfrac{r_{ix}\tan(\alpha_{ix})}{A_{ix}} - \dfrac{r_{sx}\tan(\alpha_{sx})}{A_{sx}}\right) r_{se}}{r_{sx}^2}\right)^2 + \frac{1}{2}\,\rho\left(\frac{\tan(\alpha_{tx})}{A_{tx}}\right)\right. \qquad \textbf{(14)}$$

$$-\frac{\tan(\alpha_{ie})}{A_{ie}}\Bigg)^2+\frac{1}{2}\,\rho\left(\frac{\tan(\alpha_{sx})}{A_{sx}}-\frac{\tan(\alpha_{te})}{A_{te}}+\frac{\dfrac{r_{ix}\tan(\alpha_{ix})}{A_{ix}}-\dfrac{r_{sx}\tan(\alpha_{sx})}{A_{sx}}}{r_{sx}}\right)^2$$

$$+\frac{1}{2}\,\rho\,cf\Bigg]\,Q^2+\Bigg[\rho\left(\varpi_t\,r_{tx}-\varpi_i\,r_{ie}\right)\left(\frac{\tan(\alpha_{tx})}{A_{tx}}-\frac{\tan(\alpha_{ie})}{A_{ie}}\right)-\rho\left(\frac{r_{tx}\tan(\alpha_{tx})}{A_{tx}}\right.$$

$$\left.-\frac{r_{ix}\tan(\alpha_{ix})}{A_{ix}}\right)\varpi_t+\rho\left(\frac{\varpi_i\,r_{ix}^2}{r_{sx}}-\varpi_t\,r_{te}\right)\Bigg(\frac{\tan(\alpha_{sx})}{A_{sx}}-\frac{\tan(\alpha_{te})}{A_{te}}$$

$$+\frac{\dfrac{r_{ix}\tan(\alpha_{ix})}{A_{ix}}-\dfrac{r_{sx}\tan(\alpha_{sx})}{A_{sx}}}{r_{sx}}\Bigg)+\rho\left(\varpi_i\,r_{ix}-\frac{\varpi_i\,r_{ix}^2\,r_{se}}{r_{sx}^2}\right)\Bigg(\frac{\tan(\alpha_{ix})}{A_{ix}}-\frac{\tan(\alpha_{se})}{A_{se}}$$

$$-\frac{\left(\dfrac{r_{ix}\tan(\alpha_{ix})}{A_{ix}}-\dfrac{r_{sx}\tan(\alpha_{sx})}{A_{sx}}\right)r_{se}}{r_{sx}^2}\Bigg)+\rho\left(\frac{r_{ix}\tan(\alpha_{ix})}{A_{ix}}-\frac{r_{tx}\tan(\alpha_{tx})}{A_{tx}}\right)\varpi_i\Bigg]\,Q$$

$$+\frac{1}{2}\,\rho\left(\varpi_t\,r_{tx}-\varpi_i\,r_{ie}\right)^2+\frac{1}{2}\,\rho\left(\frac{\varpi_i\,r_{ix}^2}{r_{sx}}-\varpi_t\,r_{te}\right)^2+\frac{1}{2}\,\rho\left(\varpi_i\,r_{ix}-\frac{\varpi_i\,r_{ix}^2\,r_{se}}{r_{sx}^2}\right)^2-\rho\left(\varpi_t\right.$$

$$\left.r_{tx}^2-\varpi_i\,r_{ix}^2\right)\varpi_t+\rho\left(\varpi_i\,r_{ix}^2-\varpi_t\,r_{tx}^2\right)\varpi_i$$

$A_3=coeff\left(compnegflow,\,Q,\,2\right)$

$$A_3=\frac{1}{2}\,\rho\left(\frac{\tan(\alpha_{ix})}{A_{ix}}-\frac{\tan(\alpha_{se})}{A_{se}}-\frac{\left(\dfrac{r_{ix}\tan(\alpha_{ix})}{A_{ix}}-\dfrac{r_{sx}\tan(\alpha_{sx})}{A_{sx}}\right)r_{se}}{r_{sx}^2}\right)^2 \tag{15}$$

$$+\frac{1}{2}\,\rho\left(\frac{\tan(\alpha_{tx})}{A_{tx}}-\frac{\tan(\alpha_{ie})}{A_{ie}}\right)^2+\frac{1}{2}\,\rho\left(\frac{\tan(\alpha_{sx})}{A_{sx}}-\frac{\tan(\alpha_{te})}{A_{te}}\right.$$

$$\left.+\frac{\dfrac{r_{ix}\tan(\alpha_{ix})}{A_{ix}}-\dfrac{r_{sx}\tan(\alpha_{sx})}{A_{sx}}}{r_{sx}}\right)^2+\frac{1}{2}\,\rho\,cf$$

$B_3=coeff\left(compnegflow,\,Q,\,1\right)$

$$B_3=\rho\left(\varpi_t\,r_{tx}-\varpi_i\,r_{ie}\right)\left(\frac{\tan(\alpha_{tx})}{A_{tx}}-\frac{\tan(\alpha_{ie})}{A_{ie}}\right)-\rho\left(\frac{r_{tx}\tan(\alpha_{tx})}{A_{tx}}-\frac{r_{ix}\tan(\alpha_{ix})}{A_{ix}}\right)\varpi_t \tag{16}$$

$$+ \rho \left(\frac{\varpi_i r_{ix}^2}{r_{sx}} - \varpi_t r_{te} \right) \left[\frac{\tan(\alpha_{sx})}{A_{sx}} - \frac{\tan(\alpha_{te})}{A_{te}} + \frac{\dfrac{r_{ix} \tan(\alpha_{ix})}{A_{ix}} - \dfrac{r_{sx} \tan(\alpha_{sx})}{A_{sx}}}{r_{sx}} \right]$$

$$+ \rho \left(\varpi_i r_{ix} - \frac{\varpi_i r_{ix}^2 r_{se}}{r_{sx}^2} \right) \left[\frac{\tan(\alpha_{ix})}{A_{ix}} - \frac{\tan(\alpha_{se})}{A_{se}} \right.$$

$$\left. - \frac{\left(\dfrac{r_{ix} \tan(\alpha_{ix})}{A_{ix}} - \dfrac{r_{sx} \tan(\alpha_{sx})}{A_{sx}} \right) r_{se}}{r_{sx}^2} \right] + \rho \left(\frac{r_{ix} \tan(\alpha_{ix})}{A_{ix}} - \frac{r_{tx} \tan(\alpha_{tx})}{A_{tx}} \right) \varpi_i$$

$$C_3 = coeff \left(compnegflow, Q, 0 \right)$$

$$C_3 = \frac{1}{2} \rho \left(\varpi_t r_{tx} - \varpi_i r_{ie} \right)^2 + \frac{1}{2} \rho \left(\frac{\varpi_i r_{ix}^2}{r_{sx}} - \varpi_t r_{te} \right)^2 + \frac{1}{2} \rho \left(\varpi_i r_{ix} - \frac{\varpi_i r_{ix}^2 r_{se}}{r_{sx}^2} \right)^2 - \rho \left(\varpi_t r_{tx}^2 \right. \quad \textbf{(17)}$$

$$\left. - \varpi_i r_{ix}^2 \right) \varpi_t + \rho \left(\varpi_i r_{ix}^2 - \varpi_t r_{tx}^2 \right) \varpi_i$$

93

Appendix 2: Advisor Code For Known Turbine Conditions

```matlab
function [TR,SR] = fcn(tt,wt)

%  Torque Converter performance model - knowing wt and tt
%  Ewan Pritchard, Program Manager
%  Advanced Transportation Energy Center
%  10/1/2010
%  egpritch@ncsu.edu

idle=73.3038;
eps2=0.000001;

cp= 0.93;
K1=[-0.0068,-0.0048,0.0148]; %polynomial curve fit for regime 1 - Converter
K2=[-0.1631,0.2715,-0.1070]; %polynomial curve fit for regime 2 - Coupling
K3=[-0.0064,-0.0054,0.0094]; %polynomial curve fit for regime 3 - Overrun
TRF=[-0.5017,-0.6634,2.0546]; %polynomial curve fit for the TR in regime 1

wt=abs(wt); % in the incredibly odd case of reverse - should not happen.
%%%%%% This is for the no flow cases (no torque or velocity) %%%%%%%%
if (abs(tt)<eps2&&abs(wt)<eps2)
    SR=eps2;
    ti=tt/(TRF(1)*SR^2+TRF(2)*SR+TRF(3));

%%%%%% This is for the positive flow regime 1 %%%%%%%%%
% Regime 1, Converter - Regime 2, Coupling           %
% Flow will be positive if torque is positive        %
% torque should never be positive while the speed    %
% ratio is greater than one, this would be like      %
% water flowing uphill.                              %
%%%%%%%%%%%%%%%%%%%%%%%%%%%%%%%%%%%%%%%%%%%%%%%%%%%%%%%

elseif tt>=eps2 % Assuming Regime 1 first - initial calculation of wi
    wi=(-K1(2)*wt+sqrt((K1(2)*wt)^2-4*K1(3)*(K1(1)*wt^2-tt)))/(2*K1(3));
    if wi<idle
        wi=idle; % Because the engine cannot drop below idle speed
    end
    if abs(wt)<eps2
        wt=eps2;
    end
    SR=wt/wi;    % SR assuming we are below the coupling point
    ti=tt/(TRF(1)*SR^2+TRF(2)*SR+TRF(3)); %ti below the coupling point
%%%%%% This is for the positive flow regime 2 %%%%%%%%
% Regime 2, Overrun                                 %
% Calculated turbine torque in converter mode has   %
% dropped below the impeller, stopping the stator   %
% from holding torque and beginning to spin         %
%%%%%%%%%%%%%%%%%%%%%%%%%%%%%%%%%%%%%%%%%%%%%%%%%%%%%%
    if SR>cp     % Regime 2 - Modifiying the speed and setting ti=tt
```

94

```matlab
        if(((K2(2)*wt)^2-4*K2(3)*(K2(1)*wt^2-tt))>=0);
            wi=(-K2(2)*wt+sqrt((K2(2)*wt)^2-4*K2(3)*(K2(1)*wt^2-
tt)))/(2*K2(3));
        else
            wi=wt;
        end
        ti=tt;
        SR=wt/wi; %recalculate SR for accuracy
    end

%%%%% This is for the negative flow regimes %%%%%%%%%
% Regime 3, Overrun                                 %
% Flow will be negative if torque is negative       %
%                                                   %
%%%%%%%%%%%%%%%%%%%%%%%%%%%%%%%%%%%%%%%%%%%%%%%%%%%%%
else   %tt negative -> regen mode - use curve fit 3
    if((K3(2)*wt)^2-4*K3(3)*(K3(1)*wt^2-tt))<0
        wi=idle;
    else
        wi=(-K3(2)*wt+sqrt((K3(2)*wt)^2-4*K3(3)*(K3(1)*wt^2-tt)))/(2*K3(3));
    end
    ti=tt;
    if abs(wt)<eps2
        wt=eps2;
    end
    SR=wt/wi;
end
if abs(ti)<eps2
    ti=eps2/2.05;
end
if abs(tt)<eps2
    tt=eps2;
end
TR=tt/ti;
```